1 NANOCOMPOSITES

In this chapter the topic of the nanostructured composite materials is introduced, focusing on the two specific families of nanomaterials adopted as composite filler in the experimental activity: the carbon nanotubes and the nanofluids. After some brief general remarks on the field of nanoscience, these latter materials are presented and fully described in terms of their capability to improve the performances of the traditional composites. In the experimental section the production methods used to manufacture both kinds of nanocomposite materials are reported in details, as well as the results of their physical/chemical characterization analyses.

INDEX

1.1 Nanotechnology & Nanostructures

The term nanotechnology was coined in 1976 from Eric Drexler, who affirmed: "...a technology at molecular level that can let us set every atom where we want it to be. We call this ability 'nanotechnology', because it works on nanometric scale, one billionth of meter." Already Richard Feynman on 29 December 1959 in a lecture entitled "There's Plenty of Room at the Bottom", at the Californian Institute of Technology during the annual meeting of the American Physical Society, introduced such a concept. This can be considered the official birth of the nanotechnology: "What I want to talk about is the problem of manipulating and controlling things on a small scale. As soon as I mention this, people tell me about miniaturization, and how far it has progressed today. They tell me about electric motors that are the size of the nail on your small finger... But that's nothing; that's the most primitive, halting step in the direction I intend to discuss... In the year 2000, when they look back at this age, they will wonder why it was not until the year 1960 that anybody began seriously to move in this direction... But I am not afraid to consider the final question as to whether, ultimately, in the great future, we can arrange the atoms the way we want; the very atoms, all the way down!... The principles of physics, as far as I can see, do not speak against the possibility of building things atom by atom. It is not an attempt to violate any laws; it is something, in principle, that can be done; but in practice, it has not been done because we are too big...".

At more than fifty years of distance, this new discipline is still in an early experimental phase. It is possible however to observe some progress and the subsidies in such a circle are increased in a meaningful way. In Japan the government itself declares that nanotechnology will be the key of the next future and the same MITI (the office of industry and commerce) allocates large funds for the research in this field. In Europe the conferences on nanotechnologies are followed by the best scientists, and many universities are engaging in this research. In the United States many government agencies are subsidizing studies about nanotechnology: among these the NIH (National Institutes of Health), the NASA, the DARPA, the Department of Energy, the National Science Foundation and Defence Department. In short, it seems really that all the greatest human and technological resources of the planet are working united as never before to turn the goals of nanotechnology from a dream into reality.

The nano-prefix points at a mathematical magnitude equal to 10^{-9}; it concerns therefore a technology to atomic level, a scale where the applications of chemistry merge with those of physics, and genetic engineering goes hand in hand with quantum physics. In other terms, we can affirm that nanotechnologies are the focal point of different research areas that go from quantum mechanics, to chemistry, from material science to molecular biology, etc. Nanotechnologies require thus a revolutionary approach with the birth of new structures, corporate body of research and industries and the creation of new professional figures. The terms nanoscience and nanotechnology indicates the ability to study, to measure, to assemble, to manipulate and to characterize the matter on a

dimensional scale inferior to 100 nanometers, therefore to molecular level. Nevertheless nanotechnology are still in the initial phase of their development and they aim to exploit and apply the methods of nanosciences for the creation and use of materials, devices and systems with dimensions to molecular level. Operating in this sense it is possible to obtain products with characteristics greatly improved or with entirely new properties. In fact operating to nanometric level the matter offers different opportunities from those explored when operating on macro dimensions. In order to operate to nanometric level two ways are essentially followed. The first one refers to an approach of the type "top down" which, in few words, means to reduce the dimensions of the smallest structures toward nanometric levels with physical methods. The other way is denoted as "bottom up" meaning the process through which starting from components like molecules, one tries to control and assemble them in a such way as to use them as sort of "bricks", in order to realize nanostructures of organic and inorganic type. Numerous problems are found in this second way, but it seems to be a very promising approach. The fields of application of nanotechnology are very many, and they can influence quite many productive sectors such as, for example, the transportation means, telecommunications and information technologies, through the development and the application of new or improved materials; the pharmaceutical industry through the development of new drugs and new diagnostic systems and devices; the food industry and the cosmetic one; the sectors of the defence and the aerospace through the introduction of new products and materials that have characteristics and properties more and more developed.

Beside the large number of (possible) technological improvements own to specific nano-systems, the common feature usually pointed out when the nanoparticles are referred to is their property of an incredible increasing of the system exposition surface, typically referred to as 'surface area'. From a chemical point of view, the interaction between a material body and its surrounding environment is highly dependent on the body's surface characteristics, and, in turns, on the rate (i.e. the number) of the physical phenomena than can occur at the interfacial zones. As easy to realize, the rate between surface and bulk atoms/molecules of a nanoparticle is extremely high when compared to that of macro- and even micro-particles (see Fig.1.1): as a consequence, for the same quantity of nominally analogous materials (regarding the chemical composition), a tremendous increase in chemical reactivity is achieved only by reducing the system characteristic lengths from macro-/micro- to nano-scale. Hence, a (theoretically) infinite periodic table of chemical elements can be built by going to nano-size, since the physical and chemical behavior change considerably just for the scale reduction. Obviously, such great effectiveness can be exploited in the reverse direction, in order to obtain materials with typical properties but much more lightweight than the conventional ones. That is one of the substantial challenges of the nanocomposite materials: to reduce the weight of the usually adopted materials without lack (or, eventually, with some improvements) of the technical performances, thanks to the specific increasing of intrinsic efficacy due to large surface area nanoparticles employment.

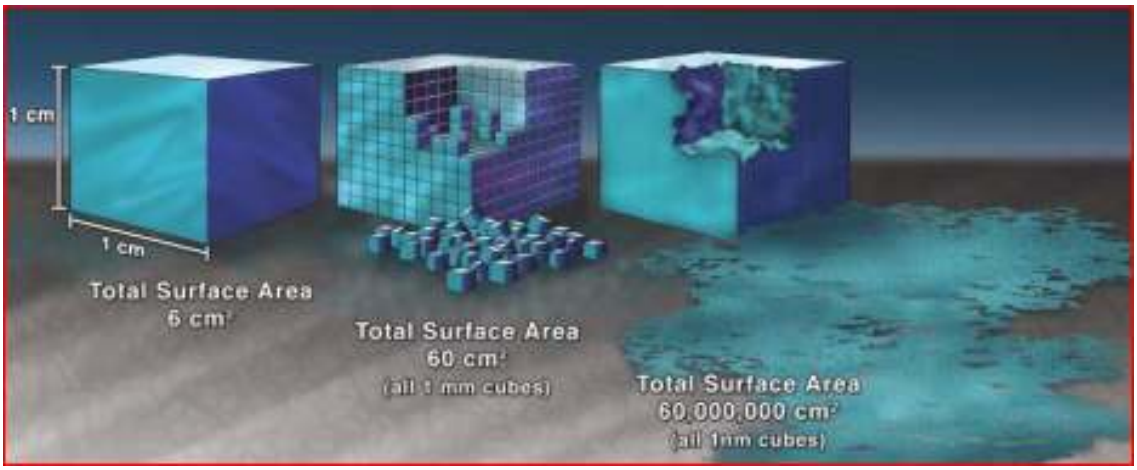

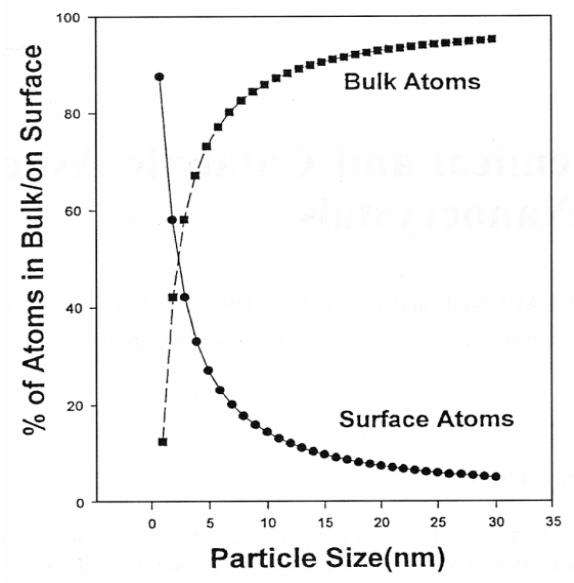

Fig.1.1. The morphological 'revolution' of the nanostructures: increasing of the surface area going to nano-size. On the top, a stylized comparison between ice-cubes of same weight but different base components size. On the left, schematic graphics showing the percentages of surface/bulk atoms dependance on the whole particle linear size. On the bottom, two same magnification SEM images (*SASLab TESCAN-Vega LSH,* Large Stage High Vacuum scanning electron microscope) highlight how different a carbon micro-fiber (left) can appear when compared to commercial carbon nano-fibers (right).

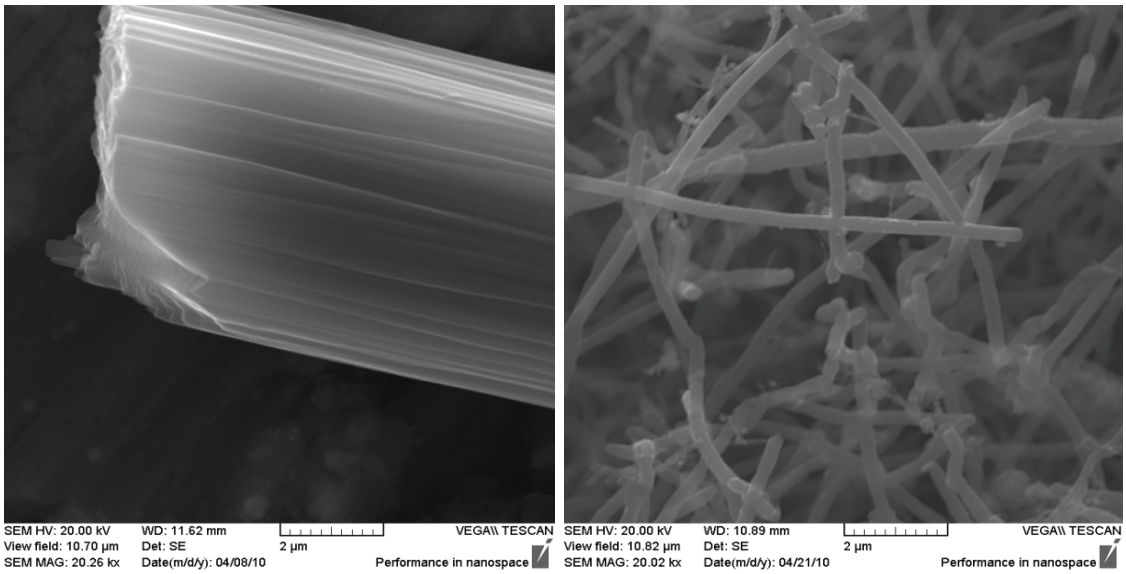

In what follows two of these fancy chemical species are presented, in order to introduce the experimental activities described in the later sections: the carbon nanotubes and the nanofluids. In Sect.1.1.1 the basic backgrounds of the physics of carbon nanotubes are provided. Inside the nanoscience, the study of carbon-nanostructures can be considered a large self-chapter: the importance of carbon in "macro-world" is evident since a lot of time, so it's easy to understand the big interest in developing carbon nanostructured materials. The carbon nanotubes are the smaller carbon fibers existing in nature, so their importance is strictly linked to the well known technological progress due to the development of the carbon fibers. The early history of carbon fibers was stimulated by needs for materials with special properties, both in the 19th century and more recently after World War II. The first carbon fiber was prepared by Thomas A. Edison to provide a filament for an early model of an electric light bulb. Specially selected Japanese Kyoto bamboo filaments were used to wind a spiral coil that was then pyrolyzed to produce a coiled carbon resistor, which could be heated ohmically to provide a satisfactory filament for use in an early model of an incandescent light bulb. Following this initial pioneering work by Edison, further research on carbon filaments proceeded more slowly, since carbon filaments were soon replaced by a more sturdy tungsten filament in the electric light bulb. Nevertheless research on carbon fibers and filaments proceeded steadily over a long time frame, through the work of Schützenberger, Pelabon, and others. Their efforts were mostly directed toward the study of vapor grown carbon filaments, showing filament growth from the thermal decomposition of hydrocarbons. The second applications-driven stimulus to carbon fiber research came in the 1950's from the needs of the space and aircraft industry for strong, stiff, light-weight fibers that could be used for building lightweight composite materials with superior mechanical properties. This stimulation led to great advances in the preparation of continuous carbon fibers based on polymer precursors, including rayon, polyacrylonitrile (PAN) and later mesophase pitch. The late 1950's and 1960's was a period of intense activity at the Union Carbide Corporation, the Aerospace Corporation and many other laboratories worldwide. This stimulation also led to the growth of carbon whiskers, which has become a benchmark for the discussion of the mechanical and elastic properties of carbon fibers. The growth of carbon whiskers was also inspired by the successful growth of single crystal whisker filaments at that time for many metals such as iron, non-metals such as Si, and oxides such as Al_2O_3, and by theoretical studies, showing superior mechanical properties for whisker structures. Parallel efforts to develop new bulk synthetic carbon materials with properties approaching single crystal graphite led to the development of highly oriented pyrolytic graphite (HOPG) in 1962 by Ubbelohde and co-workers, and HOPG has since been used as one of the benchmarks for the characterization of carbon fibers. While intense effort continued toward perfecting synthetic filamentary carbon materials, and great progress was indeed made in the early 60's, it was soon realized that long term effort would be needed to reduce fiber defects and to enhance structures resistive to crack propagation. New research directions were introduced because of the difficulty in improving the structure and microstructure of polymer-based carbon fibers for high strength and high modulus

applications, and in developing graphitizable carbons for ultra-high modulus fibers. Because of the desire to synthesize more crystalline filamentous carbons under more controlled conditions, synthesis of carbon fibers by a catalytic chemical vapor deposition (CVD) process proceeded, laying the scientific basis for the mechanism and thermodynamics for the vapor phase growth of carbon fibers in the 1960's and early 1970's [1]. In parallel to these scientific studies, other research studies focused on control of the process for the synthesis of vapor grown carbon fiber, leading to the more recent commercialization of vapor grown carbon fibers in the 1990's for various applications. Concurrently, polymer-based carbon fiber research has continued worldwide, mostly in industry, with emphasis on greater control of processing steps to achieve carbon fibers with ever-increasing modulus and strength, and on fibers with special characteristics, such as very high thermal conductivity, while decreasing costs of the commercial products.

As research on vapor grown carbon fibers (VGCF) on the micrometer scale proceeded, the growth of very small diameter filaments less than 10nm was occasionally observed and reported [2], but no detailed systematic studies of such thin filaments were carried out. An example of a very thin vapor grown nanofiber along with a multiwall nanotube is shown in the bright field TEM image reported in Fig.1.2. Reports of thin filaments below 10 nm inspired researchers to ask whether there was a minimum dimension for such filaments. Early work on VGCF, obtained by thickening filaments such as the fiber denoted by VGCF in Fig.1.2, showed very sharp lattice fringe images for the inner-most cylinders. Whereas the outermost layers of the fiber have properties associated with VGCF, there may be a continuum of behaviour of the tree rings as a function of diameter, with the innermost tree rings perhaps behaving like carbon nanotubes. Direct stimulus to study carbon filaments of very small diameters more systematically came from the discovery of fullerenes by Kroto and Smalley [3]. In December 1990 at a carbon-carbon composites workshop, papers were given on the status of fullerene research by Smalley, the discovery of a new synthesis method for the efficient production of fullerenes by Huffman, and a review of carbon fiber research by Dresselhaus. Discussions at the workshop stimulated Smalley to speculate about the existence of carbon nanofilament of dimensions comparable to C_{60} (see Fig.1.2). These conjectures were later followed up in August 1991 by discussions at a fullerene workshop in Philadelphia on the symmetry proposed for a hypothetical single-wall carbon nanotubes capped at either end by fullerene hemispheres, with suggestions on how 'zone folding' could be used to examine the electron and phonon dispersion relations of such structures. However, the real breakthrough on carbon nanotube research came with Iijima's report of experimental observation of carbon nanotubes using transmission electron microscopy [4]. It was this work which bridged the gap between experimental observation and the theoretical framework of carbon nanotubes in relation to fullerenes and as theoretical examples of 1D systems. Since the pioneering work of Iijima, the study of carbon nanotubes has progressed rapidly.

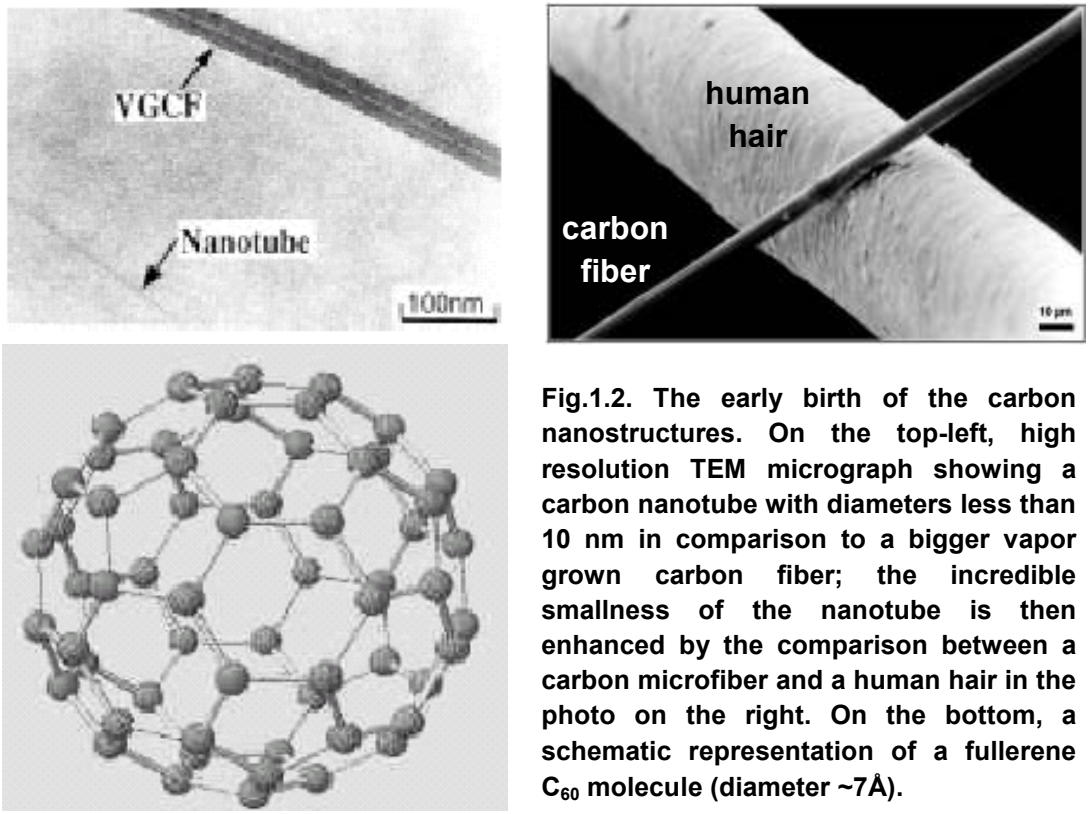

Fig.1.2. The early birth of the carbon nanostructures. On the top-left, high resolution TEM micrograph showing a carbon nanotube with diameters less than 10 nm in comparison to a bigger vapor grown carbon fiber; the incredible smallness of the nanotube is then enhanced by the comparison between a carbon microfiber and a human hair in the photo on the right. On the bottom, a schematic representation of a fullerene C_{60} molecule (diameter ~7Å).

In Sect.1.1.2 the intriguing issue of the nanofluids is presented. Nanofluids are a new class of solid-liquid composite materials consisting of solid nanoparticles (in the range of 1-100 nm), dispersed in a heat transfer fluid such as ethylene glycol, water or oil [5,8]. Engineers and scientists have been quite active over the past few decades in the search of novel ways to increase heat removal performances of various cooling devices. For example, recent technological advances in manufacturing have led to the miniaturization of many components in numerous applications. These include many electronic devices, such as microprocessors, where continually increasing power densities are requiring more innovative techniques of heat dissipation. One common heat removal technique is the use of radial flow cooling systems (i.e. impinging jet systems with or without confinement). Researchers have investigated the use of such cooling systems for various cutting-edge applications, including electronic equipment cooling (see for example [9,10]). Albeit now somewhat dated, Downs and James [11] made a good overview of impinging jet heat transfer. Projects have included the analysis of flow behavior and heat transfer characteristics of impinging jet systems with or without confinement, as well as fixed or rotating disks systems for various practical applications (see for example, [12,13]). Coolants used in such applications include air (or other gases), water, oil and other more recently developed cooling fluids such as FC-77 liquid. Considerable efforts have been made in studying the effects of various geometrical configurations on heat transfer characteristics of radial flow cooling systems. Although advances have been made, major improvements in heat transfer capabilities using traditional fluids have been limited due to the somewhat lackluster

heat transfer properties of traditional coolants. Aware of the limited heat transfer capabilities of these traditional coolants, engineers and researchers have long considered using small metallic particles in suspension in common fluids. It is well known that metals have much higher thermal conductivities than those of typical coolants. Therefore, it seems quite reasonable to assume that the resulting mixture will have enhanced heat removal capabilities, even with a small particle percentage. Published work on various mixtures using millimeter or micrometer sizes particles have started to appeared over a hundred years ago [14-17]. Other contributions on the performances of mixtures can be found for gas-solid particle mixtures [18-23] and liquid-solid particle mixtures [24-25]. Although considerable heat transfer enhancements were found with the use of two-phase mixtures, adverse effects such as channel clogging, increased pressure losses and pipeline erosion have generally halted practical application developments. Advances in manufacturing technologies have made the production of particles in the nanometre scale possible, thus researchers have looked into the possibility of using this new class of nanometer-sized particles for heat transfer enhancement capabilities of traditional coolants [26]. Initial research into these resulting mixtures, named nanofluids, seemed to indicate that the problems encountered with the inclusion of larger particles are considerably reduced with the use of nanoparticles [27,28]. Results have shown that oxide nanoparticles (for example Al_2O_3 and CuO, see Fig.1.3) have excellent dispersion properties in water, oil and ethylene glycol and form stable suspensions that even seem to behave more like single-phase fluids than two phase mixtures [29]. Furthermore, these initial results have shown that the thermal properties of nanofluids appear to be considerably higher than those of the base fluid alone. For example, increases of roughly 20% in the effective thermal conductivity were found experimentally for as little as 1-5% in particle volume fraction of the mixture [28-30]. It is for these reasons that it is believed that nanofluids have the potential of becoming interesting alternatives for leading-edge high efficiency cooling requirements. As one will easily notice, the majority of the available literature on the topic thus far, albeit very limited, is focused on their physical and thermal properties. Recent relevant reviews of work on nanofluids may be found in [31,32]. A few papers can be found on the determination of the effective thermal conductivities [26-30,33-36] and/or effective nanofluid viscosities of various nanofluids [27,30,37]. It is also noticed that, for a same type of nanofluid, results presented by different authors exhibit considerable dispersion. Possible reasons for this could be, amongst others, particle size/shape effects, temperature effects, particle-clustering, etc. These are all effects that are currently not very well understood and initial papers on their influences are just beginning to appear [27,38-41]. In the particular case of temperature effects on effective nanofluid properties, initial results presented in these papers clearly indicate, as could be expected, that thermal conductivities and viscosities of nanofluids are considerably influenced by mixture temperature. Recently, Koo and Kleinstreuer [40] and Chon et al. [41] have proposed new models for predicting nanofluid thermal conductivities taking into consideration both temperature and particle size effects. Although the relationships seem to perform satisfactorily when comparing to the available experimental data, it

appears, as mentioned in [40], that more data are required in order to improve models accuracy and versatility. Furthermore, to our knowledge, only a handful of published experimental results on the use of nanofluids in confined flow applications have surfaced so far [37,42]. These papers have provided the first empirical correlations for computing Nusselt numbers in laminar and turbulent tube flows using water-based nanofluids using Cu, TiO_2 and Al_2O_3 metallic nanoparticles. Results clearly show an increase in heat transfer performance with an increase in particle volume fraction for same Reynolds numbers. Numerical works by have also illustrated that the use of nanofluids can considerably enhance heat removal in two different confined-flow situations, namely tube flow [43,44] and radial flow between two disks [44,45]: in these papers, the single-phase fluid approach was considered. Also, physical and thermal properties were all assumed to be constant in the entire computational domain (temperature independent) and were specified using available data/relationships in recent literature. In both these configurations, heat transfer enhancements of approximately 60% were readily possible for Water/Al_2O_3 nanofluids with relatively low particle loadings. Associated increases in wall shear stress values were also noticed. Even though the available data provides interesting insight into nanofluid properties and heat transfer benefits, a considerable amount of work remains to be done on this fascinating subject. Indeed, to this day, no formulated theory has been advanced that could help predict the flow of a nanofluid by considering it as a multi-component fluid [46]. Although nanofluids are two-phase mixtures, it remains questionable whether the classical theories and correlations developed for two-phase flows can be applied in the case of nanofluids [29]. On a more practical note, the possible use of these new coolants in practical engineering applications, including radial flow cooling systems, also requires investigation.

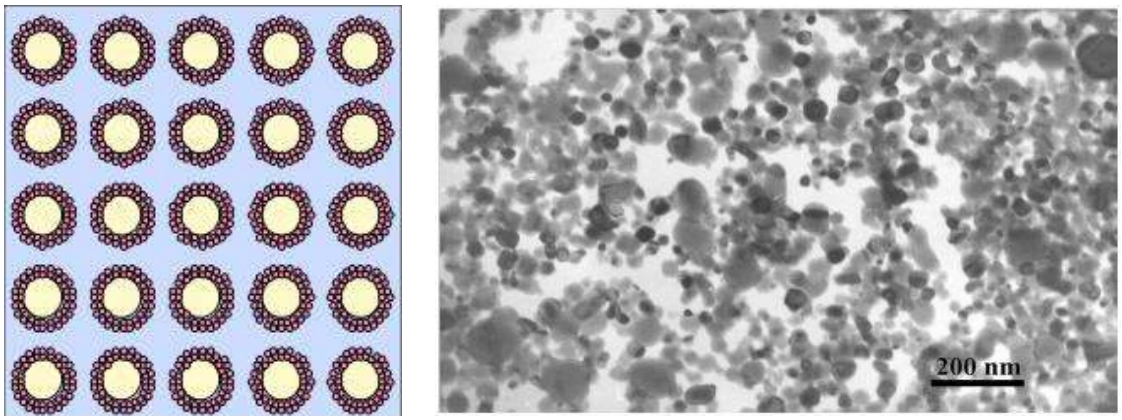

Fig.1.3. Nanofluid morphology. On the left, the schematic cross section of nanofluid structure consisting of nanoparticles, bulk liquid, and nanolayers at solid/liquid interface. On the right, TEM micrograph of CuO nanoparticles into ethylene glycol.

1.1.1 Carbon Nanotubes

Carbon nanotubes (CNTs) are unique nanostructures that can be considered conceptually as a prototype one-dimensional (1D) quantum wire. The fundamental building block of carbon nanotubes is the very long all-carbon cylindrical single wall carbon nanotube, one atom in wall thickness and tens of atoms around the circumference (typical diameter ~1.4 nm). Initially, carbon nanotubes aroused great interest in the research community because of their exotic electronic properties, and this interest continues as other remarkable properties are discovered and promises for practical applications develop.

Very small diameter (less than 10 nm) carbon filaments were prepared in the 1970's and 1980's through the synthesis of vapor grown carbon fibers by the decomposition of hydrocarbons at high temperatures in the presence of transition metal catalyst particles of <10nm diameter [2]. However, no detailed systematic studies of such very thin filaments were reported in these early years, and it was not until the observation of carbon nanotubes in 1991 by Iijima of the NEC Laboratory in Tsukuba, Japan (see Fig.1.4) using high resolution transmission electron microscopy [4] that the carbon nanotube field was seriously launched. Independently, and at about the same time (1992), Russian workers also reported the discovery of carbon nanotubes and nanotube bundles, but generally having a much smaller length to diameter ratio [47].

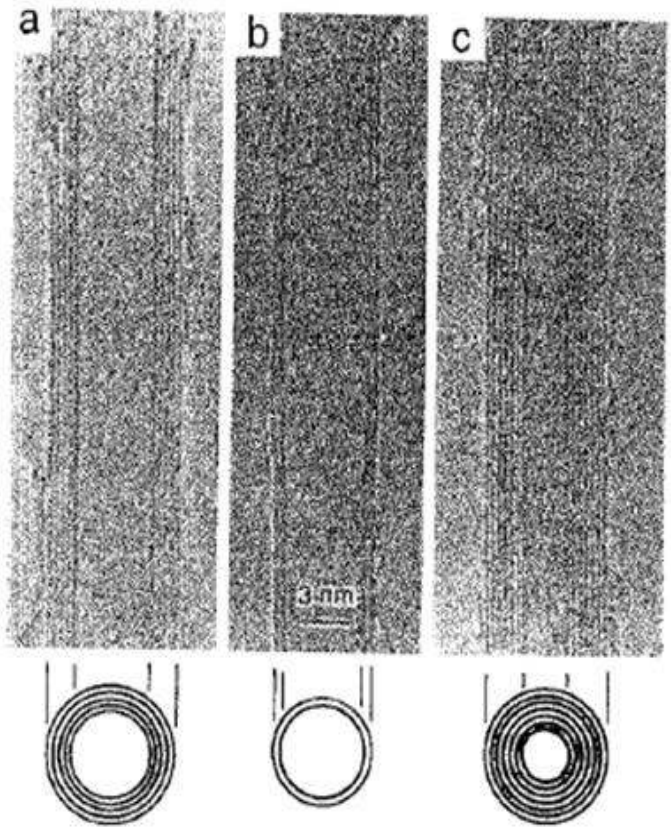

Fig.1.4. The observation by TEM of multi-wall coaxial nanotubes (see the schematic modelization below) with various inner and outer diameters, d_i and d_o, and numbers of cylindrical shells N reported by Iijima in 1991:
(a) N = 5, d_o = 67Å,
(b) N = 2, d_o = 55 Å,
(c) N = 7, d_i = 23 Å, d_o = 65 Å

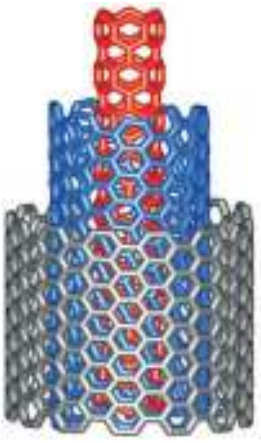

A direct stimulus to the systematic study of carbon filaments of very small diameters came from the discovery of fullerenes by Kroto, Smalley, Curl, and coworkers at Rice University [3]. In fact, Smalley and others speculated publically in these early years that a single wall carbon nanotube might be a limiting case of a fullerene molecule. The connection between carbon nanotubes and fullerenes was further promoted by the observation that the terminations of the carbon nanotubes were fullerene-like caps or hemispheres. It is curious that the smallest reported diameter for a carbon nanotube is the same as the diameter of the C_{60} molecule, which is the smallest fullerene to follow the isolated pentagon rule. This rule requires that no two pentagons be adjacent to one another, thereby lowering the strain energy of the fullerene cage. While there is not, as yet, a definite answer to a provocative question raised by Kubo and directed to Endo in 1977, regarding the minimum size of a carbon fiber, this question was important for identifying carbon fibers with very small diameters as carbon nanotubes, the one-dimensional limit of a fullerene molecule.

It was the Iijima observation of the multiwall carbon nanotubes in 1991 that heralded the entry of many scientists into the field of carbon nanotubes, stimulated at first by the remarkable one-dimensional (1D) quantum effects predicted for their electronic properties, and subsequently by the promise that the remarkable structure and properties of carbon nanotubes might give rise to some unique applications. Whereas the initial experimental Iijima observation was for multi-wall nanotubes (MWCNTs, Fig.1.4), it was less than two years before single-wall carbon nanotubes (SWCNTs) were discovered experimentally by Iijima and his group at the NEC Laboratory and by Bethune and coworkers at the IBM Almaden Laboratory [48,49]. These findings were especially important because the single wall nanotubes are more fundamental, and had been the basis for a large body of theoretical studies and predictions that preceded the experimental observation of single wall carbon nanotubes. The most striking of these theoretical developments was the prediction that carbon nanotubes could be either semiconducting or metallic depending on their geometrical characteristics, namely their diameter and the orientation of their hexagons with respect to the nanotube axis (chiral angle). Though predicted in 1992, it was not until 1998 that these predictions regarding their remarkable electronic properties were corroborated experimentally. A major breakthrough occurred in 1996 when Smalley and coworkers at Rice University successfully synthesized bundles of aligned single wall carbon nanotubes, with a small diameter distribution, thereby making it possible to carry out many sensitive experiments relevant to 1D quantum physics, which could not previously be undertaken. Of course, actual carbon nanotubes have finite length, contain defects, and interact with other nanotubes or with the substrate and these factors often complicate their behavior.

A great deal of progress has been made in characterizing carbon nanotubes and in understanding their unique properties since their "re-discovery" in 1991. The structure of carbon nanotubes has been explored early on by high resolution transmission electron microscopy (HRTEM) and scanning tunnelling microscopy (STM) techniques, yielding direct confirmation that the nanotubes are seamless cylinders derived from the

honeycomb lattice representing a single atomic layer of crystalline graphite, called a graphene sheet, represented by the hexagonal honeycomb lattice of Fig.1.5. The structure of a single-wall carbon nanotube is conveniently explained in terms of its 1D unit cell, defined by the vectors C_h and T in Fig.1.5a [50]. The circumference of any carbon nanotube is expressed in terms of the chiral vector $C_h = na_1 + ma_2$ which connects two crystallographically equivalent sites on a 2D graphene sheet. The construction in Fig.1.5a depends uniquely on the pair of integers (n; m) which specifies the chiral vector. Fig.1.5a shows the chiral angle θ between the chiral vector C_h and the "zigzag" direction (θ=0) and shows the unit vectors a_1 and a_2 of the hexagonal honeycomb lattice of the graphene sheet. Three types of nanotube structures can be generated by rolling up the graphene sheet into a cylinder (Fig.1.5) as described below and shown in Fig.1.6. The zigzag and armchair nanotubes, respectively, correspond to chiral angles of θ = 0° and 30°, and chiral nanotubes correspond to 0° < θ < 30°. The intersection of the vector OB (which is normal to C_h) with the first lattice point determines the fundamental 1D translation vector T. The unit cell of the 1D lattice is the rectangle defined by the vectors C_h and T. The cylinder connecting the two hemispherical caps of the carbon nanotube (see Fig.1.6) is formed by superimposing the two ends of the vector C_h and the cylinder joint is made along the two lines OB and AB' in Fig.1.5a. The lines OB and AB' are both perpendicular to the vector C_h at each end of C_h. In the (n; m) notation for C_h the vectors (n; 0) or (0; m) denote zigzag nanotubes and the vectors (n; n) denote armchair nanotubes. All other vectors (n; m) correspond to chiral nanotubes. The nanotube diameter d_t and the chiral angle θ are given by

$$d_t = \frac{\sqrt{3}a_{C-C}(m^2 + mn + n^2)^{1/2}}{\pi} = \frac{C_h}{\pi} \tag{1}$$

$$tg\theta = \frac{\sqrt{3}n}{(2m + n)} \tag{2}$$

where C_h is the length of C_h and $a_{C\text{-}C}$ is the C-C bond length (1.42Å). From Eq.(2) it follows that θ=30° for the (n; n) armchair nanotube and that the (n; 0) zigzag nanotube would have θ=60°, but limiting θ to be between 0 °≤ θ ≤ 30°, then by symmetry θ = 0° for a zigzag nanotube. Both armchair and zigzag nanotubes have a mirror plane and thus are considered as achiral. Differences in the nanotube diameter and chiral angle give rise to differences in the properties of the various carbon nanotubes. The number of hexagons (N), per unit cell of a chiral nanotube specified by integers (n; m), is given by

$$N = \frac{2(m^2 + mn + n^2)}{d_R} \tag{3}$$

where d_R=d if n-m is not a multiple of 3d or d_R=3d, if n-m is a multiple of 3d (d=gcd[n,m]). Each hexagon in the honeycomb lattice contains two carbon atoms. The unit cell area of the carbon nanotube is N times larger than that for a graphene layer and consequently the unit cell area for the nanotube in the reciprocal space is correspondingly 1/N times smaller.

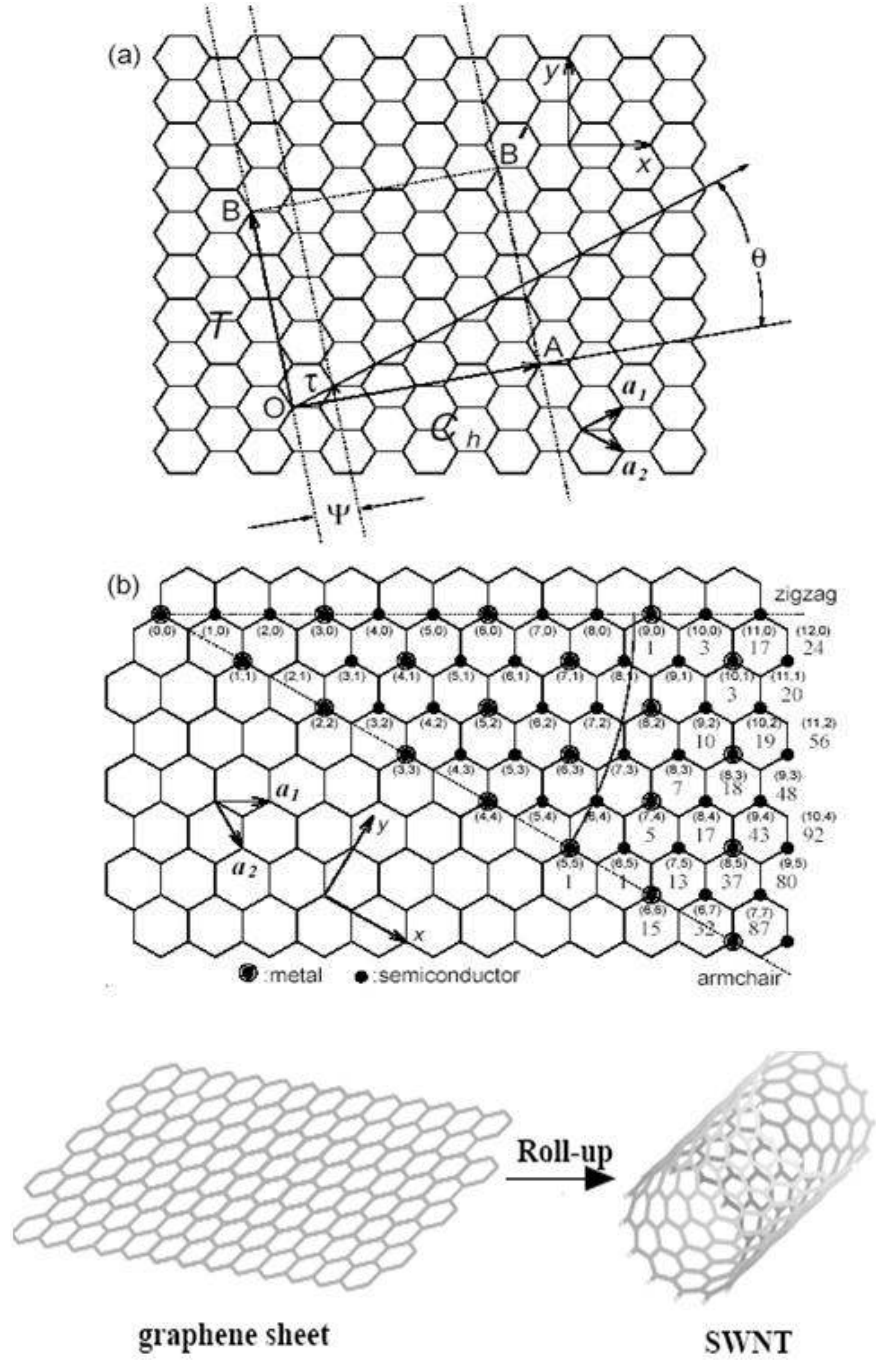

Fig.1.5. The construction of a SWCNT from a graphite layer. (a) The chiral vector OA or $C_h=na_1+ma_2$ is defined on the honeycomb lattice of carbon atoms by unit vectors a_1 and a_2 and the chiral angle θ with respect to the zigzag axis. Along the zigzag axis θ=0°. Also shown is the lattice vector OB = T of the 1D nanotube unit cell. The diagram is constructed for (n;m)=(4;2). (b) Possible vectors specified by the pairs of integers (n; m) for general CNTs, including zigzag, armchair, and chiral nanotubes. Below each pair of integers (n;m) is listed the number of distinct caps that can be joined continuously to the SWCNT denoted by (n; m). The encircled dots denote metallic nanotubes while the small dots are for semiconducting nanotubes.

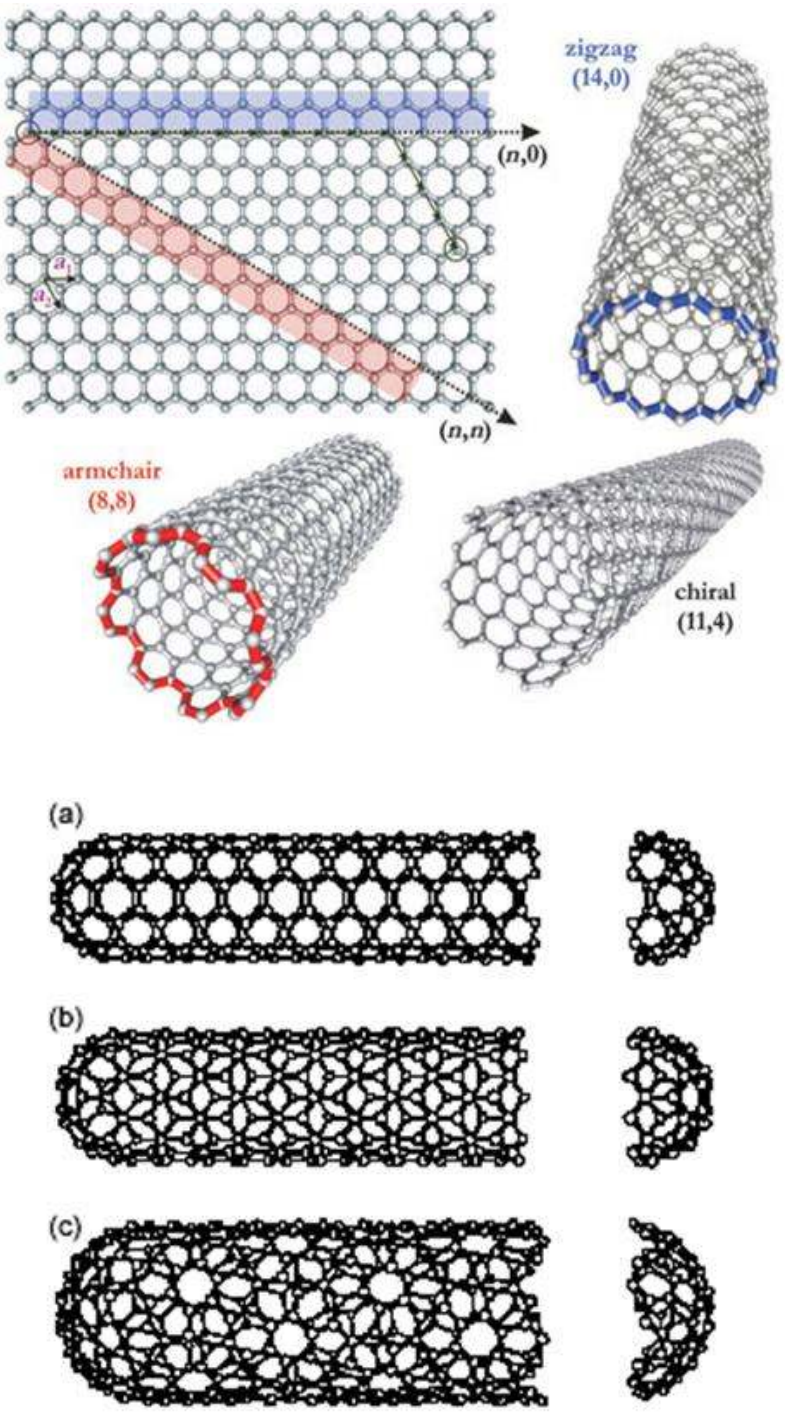

Fig.1.6. The different possible symmetries for a SWCNT. On the top, the construction directly guided from the hexagonal honeycomb graphene lattice. On the bottom, the schematic models for single-wall carbon nanotubes with the nanotube axis normal to the chiral vector which, in turn, is along: (a) the θ=30° direction [an "armchair" (n; n) nanotube], (b) the θ=0° direction [a "zigzag" (n; 0) nanotube], and (c) a general θ direction, such as OB (see Fig. 1.5), with 0 < θ < 30° [a "chiral" (n;m) nanotube]. The actual nanotubes shown here correspond to (n;m) values of: (a) (5,5), (b) (9,0), and (c) (10,5).

Fig.1.5b indicates the nanotubes that are semiconducting and those that are metallic, as well as the number of distinct fullerene caps that can be used to close the ends of an (n;m) nanotube, such that the fullerene cap satisfies the isolated pentagon rule.

The nanotube material produced by either the laser vaporization method or the carbon arc method appears in a scanning electron microscope (SEM) image as a mat of carbon "bundles" or "ropes" 10-20 nm in diameter and up to 100 μm or more in length. Under transmission electron microscope (TEM) examination, an individual carbon nanotube bundle can be imaged and shown to consist primarily of an array of single-wall carbon nanotubes aligned along a common axis (Fig.1.7). A collection of these intertwined bundles of single wall nanotubes is called a nanotube rope. This picture is corroborated by X-ray diffraction measurements (which view many ropes at once) and transmission electron microscopy (which views a single bundle). Typical diameters of the single-wall nanotubes are ~1.4 nm, very close to the diameter of an ideal (10,10) nanotube. X-ray diffraction measurements showed that these single-wall nanotubes form a 2D triangular lattice (see Fig.1.7). For carbon nanotubes synthesized by the laser vaporization method, the lattice constant for this triangular lattice is ~1.7 nm, with an inter-tube separation of 0.32 nm at closest approach between adjacent nanotubes within a single bundle. A MWCNT (see Fig.1.4) contain several coaxial cylinders, each cylinder being a single-wall carbon nanotube. Whereas multi-wall carbon nanotubes require no catalyst for their growth either by the laser vaporization or carbon arc methods, metal catalyst species such as the transition metals Fe, Co, or Ni are necessary for the growth of the SWCNTs. From an historical standpoint, the discovery in 1996 by the Rice group of a synthetic method involving laser vaporization of a graphite target that leads to high quality single-wall nanotubes gave a great boost to the field. The technique involves the laser vaporization of a target composed of Co-Ni/graphite at 1200°C. Subsequently, an efficient carbon arc method for making single-wall nanotubes with a diameter distribution similar to that of the Rice group was developed at Montpellier in France. These initial successes have triggered a worldwide effort to increase the yield and to narrow the diameter and chirality distribution of the nanotubes. The ability to synthesize nanotubes with a given chirality is particularly important in electronics applications since the electrical properties of the nanotubes depend on their chirality (see Fig.1.5b). Furthermore, for electronic applications, it is highly desirable to be able to grow a nanotube in a particular location and in a specified direction on a substrate. Progress in this direction was achieved by employing lithographic techniques to control the position of a metal catalyst particle and the use of the technique of chemical vapor phase deposition (CVD) to grow the nanotube at that location [51]. Along with the experimental efforts to improve the control and yield of the synthesis method, there are continuing theoretical efforts to interpret the experimental results and decipher the mechanism by which the nanotube structure is self-assembled from C atoms and small C clusters. Although the field is still very young, a tremendous amount of information has already been gathered on the structure and properties of both single- and multi-wall nanotubes and a multitude of applications have appeared on the horizon.

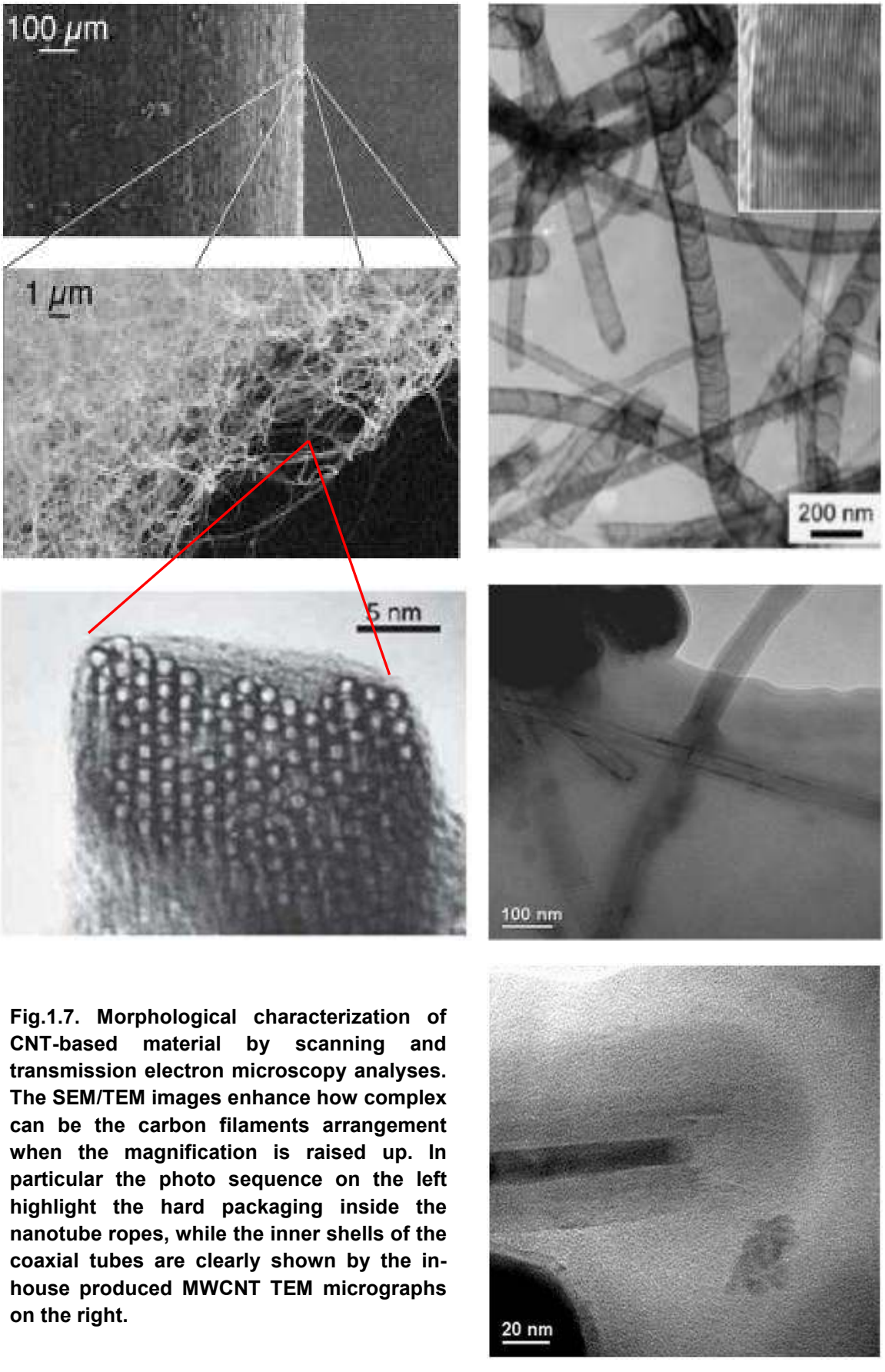

Fig.1.7. Morphological characterization of CNT-based material by scanning and transmission electron microscopy analyses. The SEM/TEM images enhance how complex can be the carbon filaments arrangement when the magnification is raised up. In particular the photo sequence on the left highlight the hard packaging inside the nanotube ropes, while the inner shells of the coaxial tubes are clearly shown by the in-house produced MWCNT TEM micrographs on the right.

Carbon nanotubes have attracted the fancy of many scientists worldwide. The small dimensions, strength and the remarkable physical properties of these structures make them a very unique material with a whole range of promising applications. The uniqueness of the nanotube arises from its structure and the inherent subtlety in the structure, which is the helicity in the arrangement of the carbon atoms in hexagonal arrays on their surface honeycomb lattices. The helicity (local symmetry), along with the diameter (which determines the size of the repeating structural unit) introduces significant changes in the electronic density of states, and hence provides a unique electronic character for the nanotubes. These novel electronic properties create a range of fascinating electronic device applications. The combination of size, structure and topology endows nanotubes with important mechanical (e.g., high stability, strength and stiffness, combined with low density and elastic deformability) and with special surface properties (selectivity, surface chemistry). In addition to the helical lattice structure and closed topology, topological defects in nanotubes, akin to those found in the fullerenes structures, result in local perturbations to their electronic structure; for example, the ends or caps of the nanotubes are more metallic than the cylinders, due to the concentration of pentagonal defects. These defects also enhance the reactivity of tube ends, giving the possibility of opening the tubes, functionalizing the tube ends and filling the tubes with foreign substances.

Since their discovery in 1991, several demonstrations have suggested potential applications of nanotubes. These include the use of nanotubes as electron field emitters for vacuum microelectronic devices, individual MWNTs and SWNTs attached to the end of an atomic force microscope (AFM) tip for use as nanoprobe, MWNTs as efficient supports in heterogeneous catalysis and as microelectrodes in electrochemical reactions, and SWNTs as good media for lithium and hydrogen storage. Some of these could become real marketable applications in the near future, but others need further modification and optimization. Areas where predicted or tested nanotube properties appear to be exceptionally promising are mechanical reinforcing and electronic device applications. The lack of availability of bulk amounts of well-defined samples and the lack of knowledge about organizing and manipulating objects such as nanotubes (due to their sub-micron sizes) have hindered progress in developing these applications. The last years, however, have seen important breakthroughs that have resulted in the availability of nearly uniform bulk samples. There still remains a strong need for better control in purifying and manipulating nanotubes, especially through generalized approaches such as chemistry. Development of functional devices/structures based on nanotubes will surely have a significant impact on future technology needs.

In the following several interesting applications of carbon nanotubes based on some of the remarkable materials properties of nanotubes are briefly described. Electron field emission characteristics of nanotubes and applications based on this, nanotubes as energy storage media, the potential of nanotubes as fillers in high performance polymer composites and nanotubes as novel probes and sensors are the major topics that are discussed.

Field emission is an attractive source for electrons compared to thermionic emission. It is a quantum effect. When subject to a sufficiently high electric field, electrons near the Fermi level can overcome the energy barrier to escape to the vacuum level. The basic physics of electron emission is well developed. The emission current from a metal surface depends on applied voltage, work function, and field enhancement factor. Electron field emission materials have been investigated extensively for technological applications, such as at panel displays, electron guns in electron microscopes, microwave amplifiers. For technological applications, electron emissive materials should have low threshold emission fields and should be stable at high current density. A current density of 1-10mA/cm^2 is required for displays and >500mA/cm^2 for a microwave amplifier. In order to minimize the electron emission threshold field, it is desirable to have emitters with a low work function and a large field enhancement factor. The work function is an intrinsic materials property. The field enhancement factor depends mostly on the geometry of the emitter and at first approximation is inversely proportional to the radius of the emitter tip. Tab.1.1 lists the threshold electrical field values for a 10mA/cm^2 current density for some typical materials.

Tab.1.1. Threshold electrical field values for different materials for a 10mA/cm^2 current density.

Material	Threshold electrical field (V/m)
Mo tips	50-100
Si tips	50-100
p-type semiconducting diamond	130
undoped defective CVD diamond	30-120
amorphous diamond	20-40
Cs-coated diamond	20-30
graphite powder (<1mm size)	17
nanostructured diamond [a]	3-5 (unstable > 30mA/cm^2)
carbon nanotubes [b]	1-3 (stable at 1A/cm^2)

[a] Heat-treated in H plasma - [b] random SWCN film

Carbon nanotubes have the right combination of properties - nanometer size diameter, structural integrity, high electrical conductivity, and chemical stability - that make good electron emitters. Electron field emission from carbon nanotubes was first demonstrated in 1995 [52,53], and has since been studied intensively on various carbon nanotube materials. Compared to conventional emitters, carbon nanotubes exhibit a lower threshold electric field, as illustrated in Tab.1.1. The current-carrying capability and emission stability of the various carbon nanotubes, however, vary considerably

depending on the fabrication process and synthesis conditions. Although carbon nanotube emitters show clear advantageous properties over conventional emitters in terms of threshold electrical field and current density, their emission site density (number of functioning emitters per unit area) is still too low for high resolution display applications. Films presently fabricated have typical emission site densities of 10^3-10^4/cm^2 at the turn-on field, and 10^6/cm^2 is typically required for high resolution display devices.

Carbon nanotubes are being considered for energy production and storage. Graphite, carbonaceous materials and carbon fiber electrodes have been used for decades in fuel cells, battery and several other electrochemical applications. Nanotubes are special because they have small dimensions, a smooth surface topology, and perfect surface specificness, since only the basal graphite planes are exposed in their structure. The rate of electron transfer at carbon electrodes ultimately determines the efficiency of fuel cells and this depends on various factors, such as the structure and morphology of the carbon material used in the electrodes. Several experiments have pointed out that compared to conventional carbon electrodes, the electron transfer kinetics take place fastest on nanotubes, following almost ideal behaviour. The area of hydrogen storage in carbon nanotubes remains active and controversial. Extraordinarily high and reversible hydrogen adsorption in SWNT-containing materials and graphite nanofibers (GNFs) has been reported and has attracted considerable interest in both academia and industry [54,55]. Tab.1.2 summarizes the gravimetric hydrogen storage capacity reported by various groups. However, many of these reports have not been independently verified. There is also a lack of understanding of the basic mechanism(s) of hydrogen storage in these materials. Materials with high hydrogen storage capacities are desirable for energy storage applications. Metal hydrides and cryo-adsorption are the two commonly used means to store hydrogen, typically at high pressure and/or low temperature. In metal hydrides, hydrogen is reversible stored in the interstitial sites of the host lattice. The electrical energy is produced by direct electrochemical conversion. Hydrogen can also be stored in the gas phase in the metal hydrides. The relatively low gravimetric energy density has limited the application of metal hydride batteries. Because of their cylindrical and hollow geometry, and nanometer-scale diameters, it has been predicted that the carbon nanotubes can store liquid and gas in the inner cores through a capillary effect. The potential of achieving/exceeding the benchmark of 6.5wt% H_2 to system weight ratio set by the Department of Energy has generated considerable research activities in universities, major automobile companies and national laboratories. At this point it is still not clear whether carbon nanotubes will have real technological applications in the hydrogen storage applications area. The values reported in the literature will need to be verified on well-characterized materials under controlled conditions. What is also lacking is a detailed understanding on the storage mechanism and the effect of materials processing on hydrogen storage. Perhaps the ongoing neutron scattering and proton nuclear magnetic resonance measurements will shed some light in this direction.

Material	Max. wt% H_2	T (K)	P (MPa)
SWCNTs (low purity)	5-10	133	0.040
SWCNTs (high purity)	~ 4	300	0.040
GNFs (tubular)	11.26	298	11.35
GNFs (herringbone)	67.55	298	11.35
graphite	4.52	298	11.35
GNFs	0.4	298-773	0.101
Li-GNFs	20	473-673	0.101
Li-graphite	14	473-673	0.101
K-GNFs	14	< 313	0.101
K-GNFs	5.0	< 313	0.101
SWCNTs (high purity)	8.25	80	7.18
SWCNTs (~50% pure)	4.2	300	10.1

Tab.1.2. Gravimetric storage of H_2 in various carbon materials.

The mechanical behaviour of carbon nanotubes is exciting since nanotubes are seen as the "ultimate" carbon fiber ever made. The traditional carbon fibers [1] have about fifty times the specific strength (strength/density) of steel and are excellent load-bearing reinforcements in composites. Nanotubes should then be ideal candidates for structural applications (see Fig.1.8). Carbon fibers have been used as reinforcements in high strength, lightweight, high performance composites; one can typically find these in a range of products ranging from expensive tennis rackets to spacecraft and aircraft body parts. NASA has recently invested large amounts of money in developing carbon nanotube-based composites for applications such as the futuristic Mars mission. Early theoretical work and recent experiments on individual nanotubes (mostly MWCNTs) have confirmed that nanotubes are one of the stiffest structures ever made [56,57]. Since carbon-carbon covalent bonds are one of the strongest in nature, a structure based on a perfect arrangement of these bonds oriented along the axis of nanotubes would produce an exceedingly strong material. Theoretical studies have suggested that SWNTs could have a Young's modulus as high as 1TPa, which is basically the in-plane value of defect free graphite. Although testing of individual nanotubes is challenging, and requires specially designed stages and nanosize loading devices, some clever experiments have provided valuable insights into the mechanical behaviour of nanotubes and have provided values for their modulus and strength. Early experiments have also used atomic force microscopy to bend nanotubes attached to substrates and thus obtain quantitative information about their mechanical properties. Most of the experiments done to date corroborate theoretical predictions suggesting the values of Young's modulus of nanotubes to be around 1Tpa. Although the theoretical estimate for the tensile strength of individual SWNTs is about 300GPa, the best experimental values (on MWNTs) are close to ~50GPa, which is still an order of magnitude higher than that of carbon fibers. The fracture and deformation behaviour of nanotubes is intriguing.

Simulations on SWNTs have suggested very interesting deformation behaviour; highly deformed nanotubes were seen to switch reversibly into different morphological patterns with abrupt releases of energy. Nanotubes gets twisted and buckled as they deform. They sustain large strains (40%) in tension without showing signs of fracture. The reversibility of deformations, such as buckling, has been recorded directly for MWNT, under TEM observations. Flexibility of MWNTs depends on the number of layers that make up the nanotube walls; tubes with thinner walls tend to twist more easily. This property is related to the in-plane ability of a planar graphene sheet and the ability for the carbon atoms to re-hybridize, with the degree of sp^2-sp^3 re-hybridization depending on the strain. Such behavior of nanotubes under mechanical loading is important for their potential application as nanoprobes, for example, for use as tips of scanning probe microscopes. The most important application of nanotubes based on their mechanical properties will be as reinforcements in composite materials. Although nanotube-filled polymer composites are an obvious materials application area, there have not been scaling-up successful experiments, which show the advantage of using nanotubes as fillers over traditional carbon fibers. The main problem is in creating a good interface between nanotubes and the polymer matrix and attaining good load transfer from the matrix to the nanotubes, during loading. The reason for this is essentially two-fold. First, nanotubes are atomically smooth and have nearly the same diameters and aspect ratios (length/diameter) as polymer chains. Second, nanotubes are almost always organized into aggregates which behave differently in response to a load, as compared to individual nanotubes. In addition, the surfaces of nanotubes have to be chemically modified (functionalized) to achieve strong interfaces between the surrounding polymer chains.

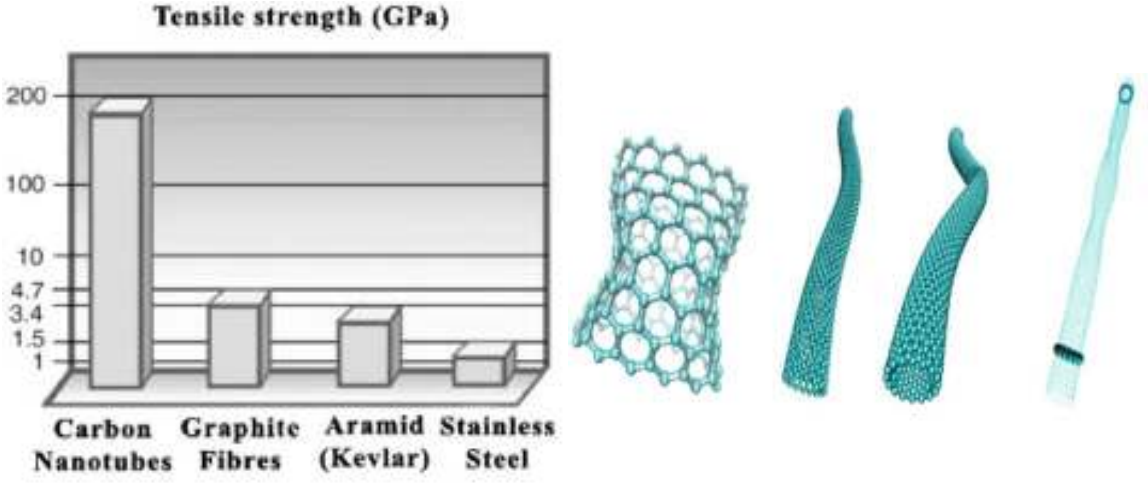

Fig.1.8. Mechanical properties of carbon nanotubes. Due to small densities (1.33 ÷ 1.40 g/cm^3 v.s. 2.7 g/cm^3 of aluminium alloys or 1.74 ÷ 1.94 g/cm^3 of carbon fibers) and to an incredible elasticity, with pliability up to very high angle without fracture (whereas metals and carbon fibers break over lower pliability angles), CNTs were claimed to have unbeatable efficiency: a tensile strength of 45 GPa (v.s. 2 GPa of high strength steels or 3.5 GPa of carbon fibers), and mostly a Young modulus of 1÷4 TPa (v.s. 0.23 ÷ 0.52 TPa of carbon fibers).

The small and uniform dimensions of the nanotubes produce some interesting applications. With extremely small sizes, high conductivity, high mechanical strength and exibility (ability to easily bend elastically), nanotubes may ultimately become indispensable in their use as nanoprobes. One could think of such probes as being used in a variety of applications, such as high resolution imaging, nano-lithography, nanoelectrodes, drug delivery, sensors and field emitters. The possibility of nanotube-based field emitting devices has been already discussed. Use of a single MWNT attached to the end of a scanning probe microscope tip for imaging has already been demonstrated [58,59]. Since MWNT tips are conducting, they can be used in STM, AFM instruments as well as other scanning probe instruments, such as an electrostatic force microscope. The advantage of the nanotube tip is its slenderness and the possibility to image features (such as very small, deep surface cracks), which are almost impossible to probe using the larger, blunter etched Si or metal tips. Biological molecules, such as DNA can also be imaged with higher resolution using nanotube tips, compared to conventional STM tips. In addition, due to the high elasticity of the nanotubes, the tips do not suffer from crashes on contact with the substrates. Any impact will cause buckling of the nanotube, which generally is reversible on retraction of the tip from the substrate. Attaching individual nanotubes to the conventional tips of scanning probe microscopes has been the real challenge. Bundles of nanotubes are typically pasted on to AFM tips and the ends are cleaved to expose individual nanotubes These tip attachments are not very controllable and will result in vibration problems and in instabilities during imaging, which decrease the image resolution. However, successful attempts have been made to grow individual nanotubes onto Si tips using CVD, in which case the nanotubes are firmly anchored to the probe tips. Due to the longitudinal (high aspect) design of nanotubes, nanotube vibration still will remain an issue, unless short segments of nanotubes can be controllably grown. In addition to the use of nanotube tips for high resolution imaging, it is also possible to use nanotubes as active tools for surface manipulation. It has been shown that if a pair of nanotubes can be positioned appropriately on an AFM tip, they can be controlled like tweezers to pick up and release nanoscale structures on surfaces; the dual nanotube tip acts as a perfect nano-manipulator in this case. It is also possible to use nanotube tips in AFM nano-lithography. Ten nanometer lines have been written on oxidized silicon substrates using nanotube tips at relatively high speeds, a feat that can only be achieved with tips as small as nanotubes. Since nanotube tips can be selectively modified chemically through the attachment of functional groups, nanotubes can also be used as molecular probes, with potential applications in chemistry and biology. Open nanotubes with the attachment of acidic functionalities have been used for chemical and biological discrimination on surface. Functionalized nanotubes were used as AFM tips to perform local chemistry, to measure binding forces between protein-ligand pairs and for imaging chemically patterned substrates. These experiments open up a whole range of applications, for example, as probes for drug delivery, molecular recognition, chemically sensitive imaging, and local chemical patterning, based on nanotube tips that can be chemically modified in a variety of ways.

1.1.2 Nanofluids

Nanofluids are a new class of solid-liquid composite materials consisting of solid nanoparticles (in the range of 1-100 nm), dispersed in a heat transfer fluid such as ethylene glycol, water or oil [6,7]. The Argonne National Laboratory (Illinois, U.S.A.) has pioneered the concept of nanofluids by applying nanotechnology to thermal engineering. Heating or cooling fluids are of great importance to many industrial fields, including electronics, heating, ventilating and air conditioning (HVAC), and transportation. The thermal conductivity of these fluids plays a vital role in the development of energy-efficient heat transfer equipment. Conventional heat transfer fluids have a relatively poor thermal conductivity compared to most solids [6,60]. The latter have 1÷3 orders of magnitude greater thermal conductivity than the former (see Fig.1.9). From Tab.1.3, the thermal conductivity of copper, for example, is 700 times that of water and 3000 times that of engine oil [61]. The orders of magnitude larger thermal conductivity of most solids compared with conventional cooling fluids such as water, ethylene glycol, and engine oil provided the original motivation to investigate the thermal transport properties of nanofluids [60].

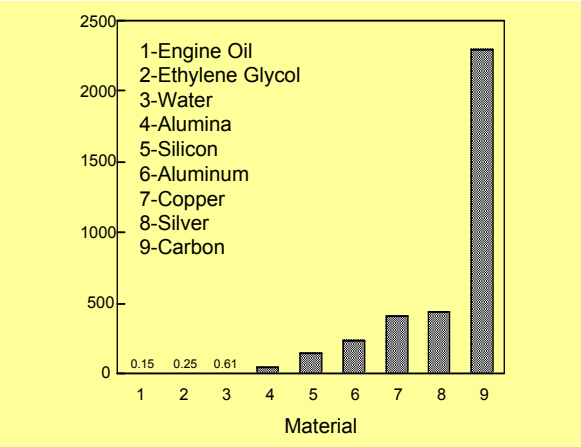

Fig.1.9. The orders of magnitude variations in the thermal conductivity between conventional solids and typical base fluids.

Tab.1.3. Thermal conductivity values for some solids and liquids at RT.

Material		Thermal conductivity (W/m-K)
Metallic solids	Silver	429
	Copper	401
	Aluminum	237
Non-metallic solids	Diamond	3300
	Carbon nanotubes	3000
	Silicon	148
	Alumina (Al_2O_3)	40
Metallic liquids	Sodium at 644 K	72.3
Non-metallic liquids	Water	0.613
	Ethylene glycol	0.253
	Engine oil	0.145

Nanofluids have received great attention given their reported gains in thermal conductivity (Fig.1.10). Yet the origin of these gains is highly debated. Critical comparisons are often lacking within a given study. Comparisons between studies introduces the attendant problem of different nanoadditives, concentrations, particle structure, potential or unknown aggregation, and surface chemistry [62]. In general, nanofluids contain organic or inorganic particles ranging in size from tens to hundreds of nanometers. With the burgeoning growth of nanomaterials, the number of formulations is nearly infinite. Unfortunately, as more nanofluids are tested for enhanced thermal conductivity, the range of values is also expanding. The effects seen in early results were attributed to Brownian motion [63]. Presumably nanoparticles with a higher heat capacity could transport heat more effectively than by liquid diffusion. However, by order of magnitude estimate, Keblinski showed that this occurred on too slow a timescale [64]. A parallel explanation was that the nanoparticles would enhance micro-convection, effectively promoting fluid mixing [65]. Recent calculations have also discounted this mechanism [66]. About the interfacial ordering-resistance, the interfacial layering refers to a phenomenon at the liquid-particle interface where liquid molecules are more ordered than those in the bulk liquid [67]. The ordered molecular layer would have a higher thermal conductivity than that of the random bulk. Interfacial ordering will be governed by the surface chemistry of the nano-additive. Functionalization affects the thermal interfacial resistance through its effect upon the molecular order in the interfacial solvation shell, which moderates the coupling between liquid and solid phonon coupling. If thermal energy (motion) is transported across a series of inhomogeneous liquid-particle interfaces, the interfacial thermal resistance will be critical to interfacial conductivity. The heat flux across an interface is dependent upon the temperature difference and the value of the Kapitza resistance. Molecular modeling has shown that this value is dependent upon the phonon-phonon coupling between the nanoparticles and the surrounding fluid [68]. Hence the molecular structure of the interface is key. Phonon frequencies in fluids are low while in solids they are high. An abrupt change in molecular structure between the liquid and particle will impose a mismatch between phonon modes and introduce a corresponding increase in Kapitza resistance. An ordered molecular interface could bridge this frequency gap. Ordered molecular interfaces can be formed by covalent bounds. Functional groups, e.g., hydroxyl, carbonyl, and carboxylic acid groups, can hydrogen bond with water molecules to increase local order. In solution, these oxygen functional groups would replace the surfactant, given the strong interaction of oxygen groups with the surrounding water and negligible interaction (actually repulsive) with the hydrophobic moiety of the amphiphilic surfactant. This ordered molecular interface would form shorter and more rigid molecular assemblies. These ordered assemblies with high frequency molecular bonds such as hydroxyl groups, O–H, would have less frequency mismatch with phonon modes associated with the MWNTs and thereby decrease the interfacial resistance. About the nanoparticle aggregation, also known as morphology, it refers to the shape of the nanoparticles and represents a method to simulate different extremes of nanoparticle aggregation as could occur in other systems. If intra-particle

thermal transport adds to the thermal conductivity, particles with higher aspect ratios will be far more advantageous than particles with a compact morphology [68,69]. Morphology variation can be accomplished by comparing CNTs with compact carbon black aggregates. About the ballistic transport, long-range phonon transport depends upon the particle internal structure (nanostructure). Given debate on the importance of intra-particle phonons accelerating thermal transport [66-68], it would be instructive to vary the particle crystalline structure. For carbonaceous particles, crystalline or noncrystalline material translates into graphitic or nongraphitic structure. Graphitic particles would be expected to possess thermal properties similar to ordered graphite, while non-graphitic particles would have correspondingly lower thermal transport given the myriad intraparticle junctions between lamellae, each imposing an interfacial resistance and perhaps acting as scattering centers. Graphitized versions of MWNTs and nano-onions present over a five-fold variation in nanostructure compared to their nascent counterparts, based on the lamellar length [70]. About the nanoparticle clustering, i.e. partial network formation, it refers to the development of a percolation network [71]. A minimum concentration is necessary to achieve long-range connectivity while lower concentrations can still form partial networks. In a solid matrix such a network is static, while in a fluid it can be dynamic, with connections actively forming, breaking, and reforming. Such partial networks can then provide an additional pathway for thermal energy transport by enhancing long-range phonon paths and decreasing the number of solid-liquid interfacial junctions without settling of the suspension. Even at lower concentrations than required to achieve a full percolation network, partial assemblies can contribute substantially to thermal transport, particularly given their extended aspect ratio, the magnitude of the contribution depending upon their contact resistance [68]. Moreover, functionalization can magnify this effect by virtue of the ordered molecular interface [68]. Particle clustering is considered as distinct from aggregation. It is synonymous with partial network formation or local percolation. The main rationale for this distinction is that aggregation, well known in colloids, will result in flocculation and precipitation. Suspension stability is lost and nanofluid property gains drop. If the partial network formation were static, it too might be considered to result in the same phase separation. Yet our fluids remained stable for months with no observable precipitation or other evidence of phase separation. Hence partial network formation is considered as dynamic. Dispersion of each material is important to achieving maximum enhancement for a given additive amount. Well before establishment of a percolation threshold, partial networks can form. Distinct from aggregation forming compact assemblies, clustering results in spatially distributed partial ‘networks’ consisting of a few contacting nanoparticles. Functionalization may aid the formation of such networks through hydrogen bonding. Such interparticle connections eliminate fluid-nanoparticle junctions and associated resistances while establishing instead particle-particle connections. The phonon transport through the solid-solid connection is expected to be much more facile, given matched phonon frequencies between the CNTs. As a result, nanoadditive concentrations below the percolation threshold can offer substantial gains in thermal conductivity via this

mechanism. Given that solid-state phonon transport as governed by nanoparticle nanostructure is not significant, the operative physical factor by which partial networking enhances thermal conductivity is reduction of interfacial resistance. Correspondingly higher concentrations are less effective as proportionally fewer nanoparticle-fluid interfaces are eliminated (in favor of more solid-solid connections). Establishment of extended networks (clusters), ultimately reaching a percolation network, may impose a practical limit on the nanocarbon additive concentration, given fluid viscosity constraints of practical cooling systems.

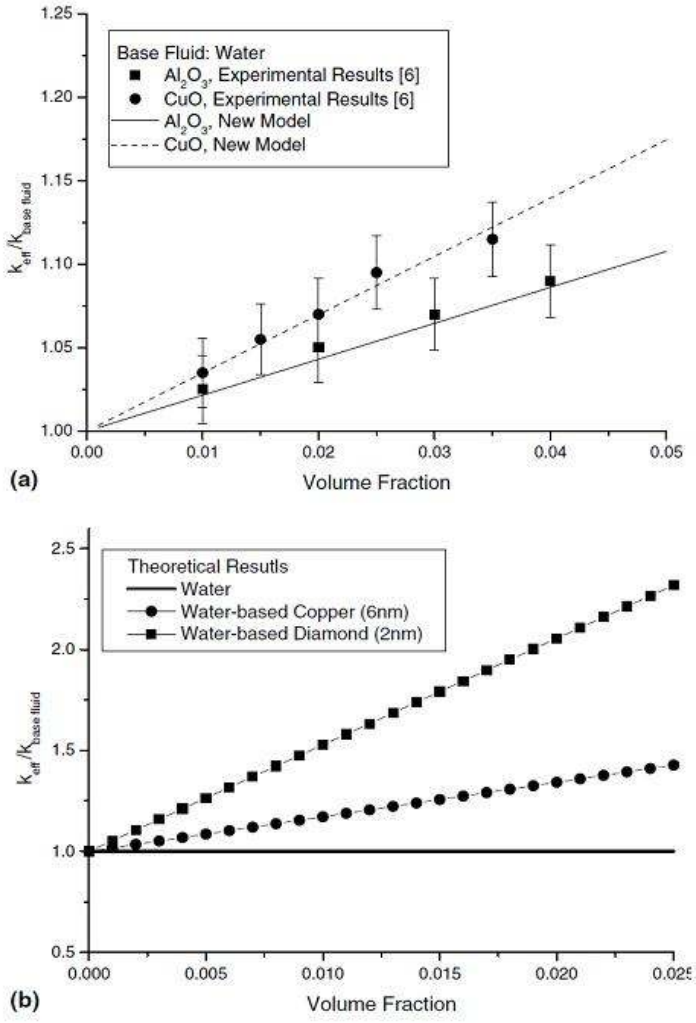

Fig.1.10.

Thermal conductivity of nanofluids normalized to that of the base fluid in dependence on the filler percentage, expressed as the volumetric fraction:

a) comparison between theoretical prediction and experimental data for water-based solution filled by CuO and Al nanoparticles;

b) theoretical predictions for water-based solution filled by Cu nanoparticles and nano-diamonds with linear dimensions from 2 to 6 nm.

Such considerations are strictly linked to the analysis of the rheological properties of nanofluids. Rheological properties play a very important role in fluid flow. During application of nanofluids they are likely to flow either by forced or natural convection and hence, the flow properties such as viscosity are therefore essential in the study of suspensions containing nanosized particles. All materials that show flow behavior are referred to as fluids. In all fluids, there are frictional forces between the molecules and, therefore, they display a certain flow resistance which can be measured as viscosity

[72]. Viscosity is a transport property which refers to the resistance of a material to flow. When dealing with nanofluids, one is often tempted to consider the dispersed medium under question as a homogeneous fluid characterized by properties such as density and viscosity which in turn will only require a single set of mass and momentum conservation equations. However, such a simple picture will not provide useful explanations for cases where the fluid is unsteady and non-uniform [73]. Isaac Newton found that the shear force acting on a liquid is proportional to the resulting flow velocity [74]. Hence, a fluid is said to be newtonian if the viscosity remains constant with an increase in shear rate. Newtonian flow behavior is observed in low molecular liquids such as water, mineral oils (without polymer additives) and solvents. However, more complex flow behaviour is expected for fluids containing suspended particles. Fluids, whose viscosity changes with an increase in shear rate, are referred to as non-newtonian. These fluids could be further classified according to their flow behavior. Shear-thinning and shear-thickening flow behavior is discussed in the following (see Fig.1.11). For samples that display shear-thinning behavior, the shear viscosity is dependent on the degree of shear load. Thus, the viscosity decreases with an increase in shear stress. In dispersions, shearing can cause the particles to orient in the flow direction and in the direction of the flow gradient. This can lead to disintegration of agglomerates or change in particle form. The interaction forces between particles may decrease during the process and cause a lowering in the flow resistance. Examples of shear-thinning materials include shampoos, paints and polymer solutions [72]. Similar to shear thinning fluids, the shear viscosity of samples displaying shear-thickening behavior is also dependent on the degree of shear load. However, the viscosity increases with an increase in shear stress. With highly concentrated suspensions, the probability of particle interaction is much higher and may result in particles becoming wedged together and thus increase the flow resistance. Particle shape plays an important role since during the shear process, particles rotate as they move. Cube-shape particles take up more volume when rotating than spherical particles and hence less free volume is available for the liquid between the particles. Compared to shear thinning materials, shear thickening materials are much less common in industrial practice. Examples of shear-thickening materials include dispersions with a high concentration of solids or polymers such as ceramic suspensions [72]. The yield point or yield stress refers to the external force required before a material will start to flow. A typical example is toothpaste; a certain amount of force must be applied before the toothpaste starts to flow. Materials with yield points tend to flow inhomogeneously.

Nanofluids containing metal nanoparticles were found to be Newtonian, whereas nanofluids containing metal oxides as well as carbon nanotubes showed non-Newtonian, shear thinning behaviour. Since the interaction forces between particles usually decrease during flow conditions, the flow resistance is also decreased. With no significant interaction forces between the particles, separation of the particles in the form of sedimentation may occur and therefore, rheological studies could possibly provide more information about the stability of the nanofluids and also the interactions between the particles and fluid molecules. The mechanism of heat transfer will also

remain a challenge for the future without the necessary theoretical background that is lacking in nanotechnology. However, experimental data from various research directions could eventually lead to a common basis towards understanding the heat transfer process.

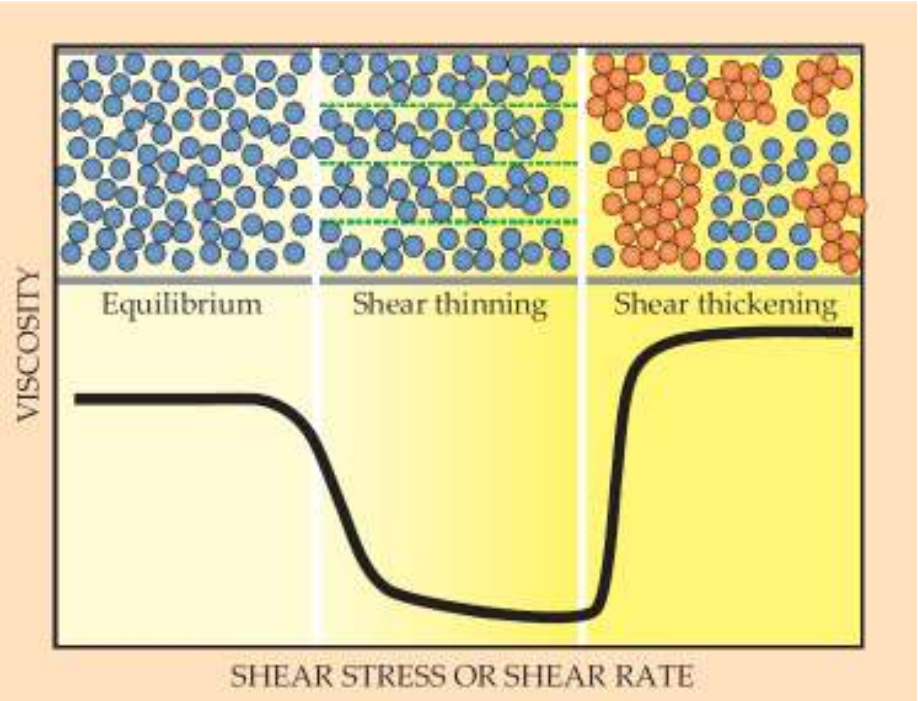

Fig.1.11. Typical behavior of viscosity v.s. shear rate for non-newtonian fluids, and schematic representation of particle-fluid interaction in the different range.

The technological barrier is that the preparation of nanofluids using current literature methods are expensive and therefore more research is necessary to produce cost-effective nanofluids which will be easy up scalable. To solve this problem, additional scientific study needs to be done on the influence of submicron and high aspect ratio particles on the physico-chemical properties of heat transfer fluids such as ethylene glycol, mineral oil and transformer oil. Until recently, there have been a limited number of studies on the characteristics of dispersion and rheological properties of nanofluids. Since nanofluids are expected to be used under flow conditions, the study of the rheological properties of the nanofluid is essential. Also, to understand the mechanism of heat transfer enhancement, it is crucial to have knowledge on the fluid-particle and particle-particle interactions within the fluid [73]. Stability of the suspensions is a crucial issue for both scientific research and practical applications. Particle aggregation and the formation of extended structures of linked nanoparticles will affect stability, and may be responsible for much of the disagreement between experimental results and the predictions of effective medium theory. Simultaneous studies of thermal conductivity and viscosity may give additional insight [6].

1.2 Nanostructured Composite Materials

In the last decades the research on composite materials have been acquiring importance due to the possibility of increasing the material mechanical performances while contemporary decreasing both mass and volume of the structures. Mass lowering is a "must" especially in military and space applications, since aircraft aerodynamic profile needs to be optimized and because of the high costs of launch and launcher and payload mass constraints [75]. The need to face up to the well know problem of the so called "space debris" has lead many aerospace researchers to look for advanced lightweight materials for ballistic applications. Among all innovative materials, a promising branch of such research focuses on the polymeric composite materials with inclusions of nanostructures [76].

Polymer nanocomposites are composites with a polymer matrix and a filler with at least one dimension less than 100 nm [77]. The fillers can be plate-like (clays), high aspect ratio nanotubes, and lower aspect ratio or equiaxed nanoparticles. While some nanofilled composites (carbon black [78] and fumed silica [79,80] - filled polymers) have been used for over a century, in recent years the dedicated research and development of nanofilled polymers has greatly increased. This is due to our increased ability to synthesize and manipulate a broad range of nanofillers and significant investment by government and industry in this field. Current interest in nanocomposites has been generated and maintained because nanoparticle and carbon nanotube-filled polymers exhibit unique combinations of properties not achievable with traditional composites. For example, the inclusion of equiaxed nanoparticles in thermoplastics, and particularly semicrystalline thermoplastics, increases the yield stress, the tensile strength, and Young's modulus [81] compared to pure polymer. Other examples include scratch-resistant transparent amorphous thermoplastic coatings [82]. These combinations of properties can be achieved because of the small size of the fillers, the large surface area the fillers provide, and in many cases the unique properties of the fillers themselves. As will be shown, in many cases these large changes in the material properties require small to modest nanofiller loadings. Unlike traditional micron-filled composites, these novel fillers often alter the properties of the entire polymer matrix while, at the same time, imparting new functionality because of their chemical composition and nanoscale size. In this section a general introduction to polymer nanocomposites is given, addressing what is unique to nanofillers compared to traditional micron-scale fillers, describing the nanofiller surface modification, and then providing specific examples of mechanical, electrical, and optical properties in nanoparticle-filled polymers.

The small size of nanofillers leads to several factors that distinguish nanocomposites from traditional composites. First of all, nanofillers are small mechanical, optical, and electrical defects compared to micron-scale fillers. This means that the addition of nanofillers to a polymer does not necessarily lead to a decrease in the ductility of the

polymer and in some cases can increase it [83,84]. It also means that below about 50 nm [85], many fillers do not scatter light significantly. Thus it is possible to make composites with altered electrical or mechanical properties that maintain their optical clarity. Finally, as small electrical defects, nanofillers do not concentrate electromagnetic fields as sharply as micron-scale fillers and indeed may act to trap charge and increase the electrical breakdown strength of polymers. Secondly, although many properties of a material are said to be intrinsic, they often depend upon matter being assembled above a critical length scale. When the nanoparticles decrease below this size, the properties of the particles can differ significantly from the bulk material; thus variations in melting temperature, color, magnetization, and charge capacity are often observed [86]. Third, the small size of the fillers leads to an exceptionally large interfacial area in the composites. Fig.1.12a shows the surface area per unit volume as a function of particle size for spherical particles that are ideally dispersed. If one compares the surface area of a 10mm carbon fiber to that of a 1nm single-walled nanotube for the same total volume of the two, the surface area increases by a factor of 10^4. In addition (Fig.1.12b), the inter-particle spacing decreases such that at small volume fractions of filler, the inter-particle spacing is similar to the radius of gyration of the polymer (100Å). The high surface area becomes even more significant when one considers that there is an interaction zone surrounding the filler. This is a region in which the structure and properties have been altered because of the presence of the filler. It could be a region of altered chemistry, polymer conformation, chain mobility, degree of cure, or crystallinity. This zone of affected polymer has been approximated to be between 2 and 9 nm thick [87], but may be much larger. If we assume that this interaction zone is about 10 nm in thickness, then at 2.5vol% of a 20 nm equiaxed nanoparticle well dispersed, 37% of the polymer has different properties from the bulk polymer. Therefore the interaction zone can be a significant portion, if not the entire bulk, of the matrix. Thus the nanofillers can alter the expected properties of the composite considerably. An example of the influence of the interaction zone on behavior can be seen by monitoring the glass transition temperature (T_g). The T_g of a bulk part can be raised and lowered with the addition of nanoparticles due to the immobilization of polymer chains by the particles or, conversely, an increase in polymer mobility due to noninteracting particles. Both increasing[88-90] and decreasing [91,92] T_g cases have been shown. The physical nature and extent of this interaction zone has recently been probed through some quite recent work on multiwalled carbon nanotubes [93], by a solvent processing method used to make MWCNT polymer nanocomposites. Upon observation of the composite fracture surface, a polymer layer was observed on the nanotubes (Fig.1.13) that had pulled out of the opposing side of the fracture. This ‘sheath’ was confirmed to be polymer from the matrix, but with obviously altered thermal and mechanical properties from the bulk. The thickness of this interfacial layer increased with chemical modification of the nanotubes. Nanoparticles can also influence the polymerization, curing, or crystallization aspects of polymer synthesis. For example, nanoparticles can serve as nucleation sites in semicrystalline polymers and result in changes in crystalline content and spherulite structure [94].

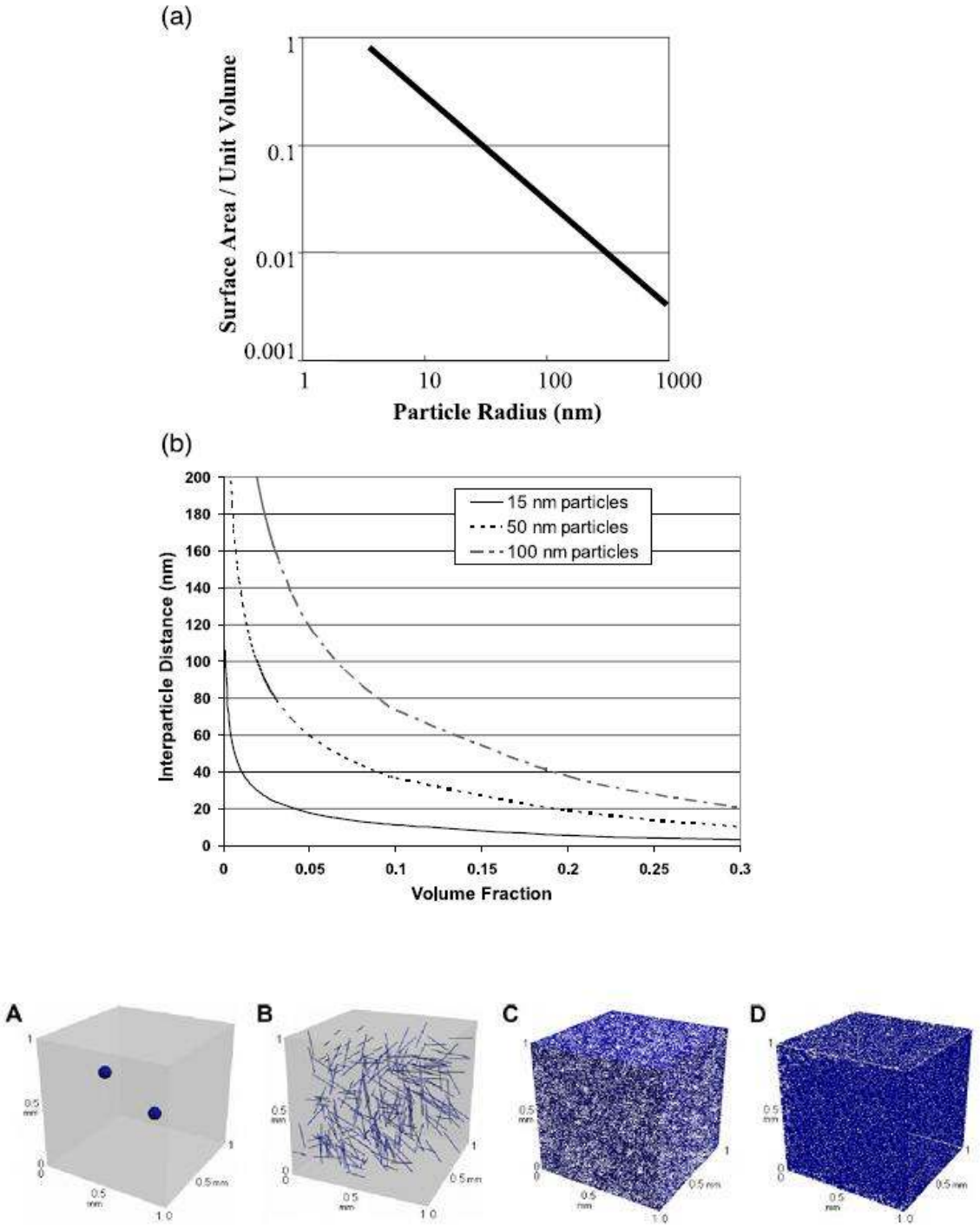

Fig.1.12. Nanocomposite v.s. micro-filled composite. (a) The surface area per unit volume as a function of particle size for spherical particles showing the large surface area in nanoparticles. (b) The interparticle spacing of nanoparticles arranged on a simple cubic lattice showing the variation with particle size (15, 50, and 100 nm diameter) and volume fraction. On the bottom, simulation for the distribution of micro- and nano-scale fillers of the same 0.1vol% in a reference volume of 1 mm^3 (A: Al_2O_3 particle; B: carbon fiber; C: graphite nanoparticles; D: carbon nanotubes).

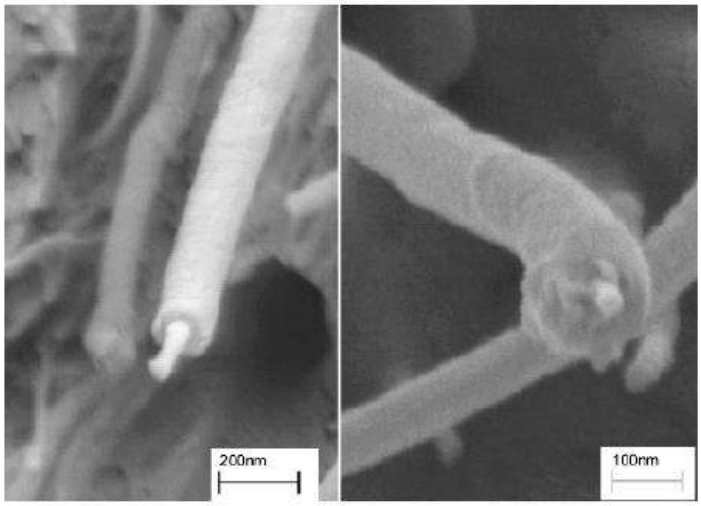

Fig.1.13. Polymer-coated nanotubes observed in the fracture surface of multi-walled carbon nanotubes reinforced polycarbonate composite.

The nanoscale sizes and subsequently higher surface energies of nanofillers lead to some unique challenges in the processing of these materials. The most critical of these challenges is dispersion of the nanofiller. Any agglomeration of the filler reduces the interfacial area in the composites and thus reduces the opportunity to take advantage of the unique nanofiller properties mentioned in the previous section. Thus aggregated nanoparticles are simply micron fillers. Controlling the size and degree of agglomeration of nanoparticles is difficult due to their large radius of curvature and subsequent increase in surface energy. As these high surface area fillers tend to aggregate, silanes and organotitanates are used extensively both to tailor the particle surface properties to mimic the surrounding matrix and to lower their surface energy and reduce their tendency to agglomerate [95-97]. Other methods to alter the surface properties of the nanoparticles include radiation grafting [98], chemical vapor deposition, and a host of complicated synthesis procedures that attempt to polymerize polymer chains off of initiating agents coupled to the surface [99-101] An excellent review by Caruso [102] provides an extensive background on the modification of nanoparticle surfaces. In addition to achieving better dispersion, these techniques control the nature of the interaction between the nanofillers and the polymer and thus the properties and size of the interaction zone.

Carbon nanotubes, for example, not only tend to agglomerate but are often prepared in a bundle-like structure, as mentioned in the previous section 1.1.1 (see Fig.1.7). In order to take advantage of their high surface area for interacting with the polymer, the bundles have to be separated into individual nanotubes. For MWCNT this can usually be accomplished with sonication [103,104] For SWCNT, exfoliation is a more difficult process but progress is being made [105-109]. The challenge is in exfoliating the bundles without shortening the SWCNT and introducing significant numbers of defects.

Once the nanotubes have been separated, it is important to disperse them uniformly in the polymer matrix, preventing their agglomeration. This is accomplished with functional groups which also mediates the interaction of the nanotubes with the polymer (see Fig.1.14). Non-covalent surface modification of carbon nanotubes includes all treatments that cause a change in the functional groups that face the solvent (or the polymer), without modifying the chemical nature of the nanotube. The advantage of the non-covalent surface modification is that the basic structure and hence the mechanical and electrical properties of the tubes are not affected due to the modification [110]. Non-covalent attachment is possible if there is a secondary bonding between these groups and the surface of the nanotube [111,112]. For example, wrapping of the nanotubes by polymer chains, in particular conjugated polymers, has been observed [111,113-115]. Covalent attachment of chemical groups to the outer wall of the nanotubes can occur particularly at defect sites. One example is the attack of the defect sites by concentrated nitric acid, in order to form carboxylic acid groups [116]. The reaction with nitric acid also eliminates the catalysts that are left from the nanotubes preparation process. This reaction has been applied on SWCNT and MWCNT. The resultant carboxylated nanotubes can then be further covalently modified by means of reactions based on the carboxylic acid groups [117,118]. There are also other variations of the chemical oxidation of carbon nanotubes (for example, applying a mixture of sulfuric acid and H_2O_2, [119]). The presence of carboxylic acid groups on the nanotube walls enables various reactions for the further attachment of functional groups [118,120-125]. Other types of covalent surface modification of carbon nanotubes are based on chemical reactions between the carbon-carbon bond structures and specific reagents such as fluorination [126] or on radical attachments [127,128]. These reactions and many others [129-133] enable tailoring of the nanofillers to the specific application and environment. The potential for using surface modification to improve the properties of nanotube-reinforced polymer composites has just begun to be explored.

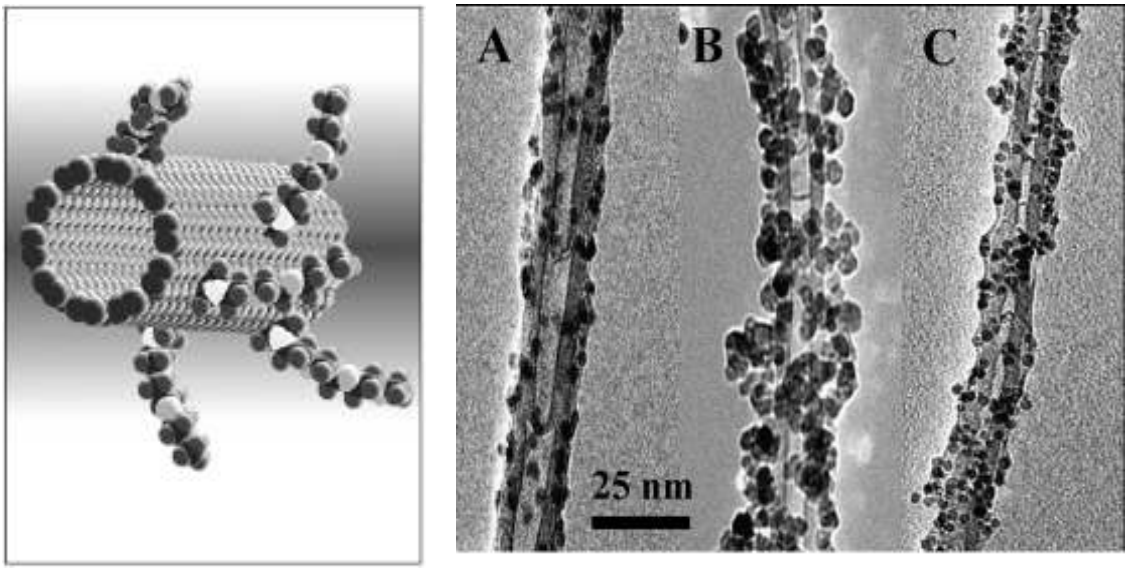

Fig.1.14. Introducing functional groups onto the surface helps to solubilize CNTs and facilitates their study. On the right, TEM images of bamboo-shaped MWCNTs functionalized by metallic nanoparticles (A:CdSe/ZnS, B: ZnO, C: Fe_2O_3)

Nanoparticle fillers are relatively equiaxed with diameters less than 100 nm (Fig.1.15). Nanoparticles (carbon black) have been used as fillers in polymers for the past century, but the advent of new particle synthesis techniques has made available industrial quantities of ceramic, piezoelectric, metal, and even polymer nanoparticles for use in polymer nanocomposite research. Synthesis of these nanoparticles is accomplished using a variety of methods, each with its own advantages and disadvantages [134]. One of the primary reasons for adding fillers to polymers is to improve mechanical performance. Traditional polymer composites filled with micron-size fillers often show improvements in stiffness and heat resistance in the form of increases in modulus, yield strength, and glass transition temperature [81,135]. In micron-filled composites, unfortunately, this often comes at the cost of a substantial reduction in ductility, and sometimes in impact strength, because of stress concentrations caused by the fillers. Well-dispersed nanofillers, on the other hand, are able to improve modulus and strength, and to maintain or even improve ductility because they are much smaller than the critical crack size for polymers and need not initiate failure. In addition, large amounts of traditional fillers are often required to achieve the desired properties, often diminishing the weight-savings gained in using low-density polymers. Polymer nanocomposites have been shown to provide unique combinations of mechanical and thermal properties often at very low filler weight fractions.

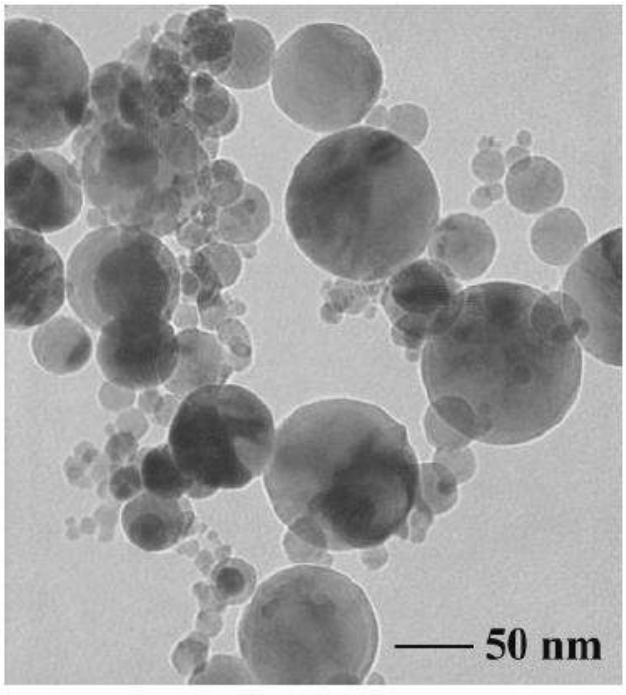

Fig.1.15. Typical poly-disperse oxide nanoparticles synthesized in a forced gas condensation process.

For example, dramatic improvements in the yield stress (30%) and Young's modulus (170%) have been shown in nanofilled polypropylene compared to micron-filled polypropylene [136]. These composites also showed no decrease in the strain-to-failure when filled with silica ranging from 7 to 40 nm in diameter. In addition, nylon filled with 50 nm silica particles displayed increases in tensile strength (15%), strain-to-failure (150%), Young's modulus (23%), and impact strength (78%), with only 5 wt% nanoparticles [137]. In a rubbery polyurethane elastomer, Petrovic and Zhang [138,139] found that a sixfold increase in the elongation-at-break and a threefold increase in the modulus were achievable with 40 wt% 12 nm silica compared to micron-size filler that embrittled the polymer. Furthermore, the nanocomposites showed no reduction in transparency even at these relatively high loadings unlike the micron-size filled systems. In attempting to modify an already two-phase system, Zhang et al.[140] filled high impact polystyrene with nanoparticles and showed increases in notched impact, tensile strength, and elastic modulus of the blend. In a study by Ash et al. [141], the mode of yielding in poly-methylmethacrylate, a brittle thermoplastic polymer, was changed from dilatational (craze) to shear by the incorporation of nanoparticles that showed no affinity for the matrix polymer. Extensions as high as 80% but averaging 30% were routinely seen and were accompanied by a necking phenomenon. The transition from crazing to shear yielding was hypothesized to be due to poorly bonded nanoparticles that are well dispersed in the polymer matrix. In this way, the polymer was hypothesized to detach from the nanoparticles and deform in response to the tensile stress, thus delocalizing the yield damage and preventing the typical craze-to-fracture brittle failure. The most dramatic increases in the modulus of nanocomposites occur in the region above the T_g. Often, these increases are much greater (4000%) than those that occur below T_g [91,142]. This is hypothesized to be due to the creation of cross-links, either temporary or permanent, between nanoparticles and polymer which serve to increase the plateau modulus. Indeed, the ability to strictly control the size and surface activity of nanoparticles in recent dynamic mechanical studies on silica/polyvinylacetate nanocomposites above the T_g has shed new light on the nonlinear reinforcement behavior of rubbery melts [143]. In this study, the modulus of the polymer nanocomposite melt is shown to vary depending on the imposition of a large or small amplitude strain. The corresponding hypothesis concludes that the nanoparticles act as centers for trapped, non-labile polymer chains that serve as temporary entanglements. In this work, the destruction and eventual recovery of the network offer an alternative to the particle filler networks widely believed to be responsible for the behavior known as the Payne effect [144]. Studies of the wear behavior of nanofilled polymer composites have also demonstrated encouraging results. In composites using micron-size fillers, the wear resistance increases, but often the coefficient of friction does as well. In silica/epoxy nanocomposites at low volume fractions (2 vol%), however, sliding wear tests showed that both the frictional coefficient and the specific wear rate were lower than either the unfilled epoxy or epoxy filled with micron-size fillers [145] This is significant because most filled systems display the decreased wear rate, but also show an increase in the friction coefficient. Nanoparticles are theorized to be able to

significantly reduce wear rates because the wear mechanism changes from severe abrasion wear to mild sliding wear. This is due to the reduction in the angularity of the filler particles and the fact that the transfer film, where abrasion is taking place, can be strengthened because the nanoparticles would have the capability of blending well with wear particles. In addition, the material removal of nanoparticulate composites is thought to be much milder than that of conventional composites because the fillers have the same size as the segments of the surrounding polymer chains [145]. The scratch resistance of nanocomposites is also improved over their micron counterparts [146]. Nano-TiO2-filled epoxy showed greater scratch resistance with the scratch track being much smoother than either the neat polymer or a micron-filled system [147]. In addition, the depth and width of the scratch track decreased in the nanofilled system. This behavior has also been seen in alumina/gelatin nanocomposites [148]. Nanoparticles have also been recently used to reinforce shape memory polymers for micro-electromechanical systems (MEMS) applications. Gall et al. [149] demonstrated that the microhardness and elastic modulus could be increased through the use of SiC nanoparticles. In this case, the small size of the MEMS devices necessitates the use of nanoparticles for incorporation into the device, but the nanoparticles actually increased the force of recovery from 300 mN for the unfilled resin to 450 mN for a 20wt% nanofilled composite. As with most mechanical systems, the property enhancements shown above experience an initial increase followed by a decrease usually in the 2-5 vol% range. The observation of a particular weight fraction at which mechanical behavior is optimized has been observed in other nanocomposite studies [91,136,140]. It is obvious that at lower particle loadings, there is generally not enough material altered by the presence of the particles to permit large-scale changes in material properties. Higher loadings induce agglomeration, which degrades the polymer performance through, for example, inclusion of voids that can act as preferential sites for crack initiation and failure. The thermal properties of polymers and their composites are important from a mechanical stability perspective as well as a processing perspective. Thus the ability to alter this behavior, either by increasing or decreasing the processing or service temperature, is highly important in finding new markets for polymer products. One of the most widely measured values to quantify thermal properties in polymers is the glass transition temperature. Changes in the glass transition temperature as a function of the filler content have been reported for a variety of polymer composites containing a wide variety of nanoscale fillers. Most researchers report an increase in the T_g as a function of filler content [87,91,150]; in fact, Avella and coworkers have shown a 35°C increase in the T_g of PMMA filled with just 6wt% $CaCO_3$ nanoparticles [151]. On the other hand, decreases in the nanocomposite T_g have also been reported [88,92]. The increases in T_g have been linked to the immobilization of the matrix within an interaction zone which hinders cooperative motion by raising the energy barrier for intermolecular chain movement [88,150]. However, attempts to relate the T_g reductions to existing theories of the glass transition have been limited. Becker et al. [88] reported that, over the range of filler volume fractions considered (0-10vol%), the T_g of their acetoxypropyl-trimethoxysilane-treated silica-filled copolymer system

decreased by 16°C, while the T_g of their composites prepared with as-received filler decreased by 9°C. This was contrasted with the increases in T_g observed for 10 nm silica coated with methacryloxypropyl-trimethoxysilane. In these latter specimens, the Tg increased by 10°C at 10vol% filler. However, the 100 nm silica used in the study produced no changes in the T_g with either coating at any filler concentration. Thus the increased surface area of the 10 nm silica and the interface between the coated particles and the polymer dramatically changed the polymer mobility in the bulk at fairly low volume fractions resulting in both increasing and decreasing T_g values. In some instances, the particle, the interaction zone, and the matrix have been modeled as a core-shell scheme to incorporate the interaction zone/low mobility region. If the volume fraction of the interaction zone is high enough, this model shows two T_g, while most researchers do not see this, there have been reports that show the additional relaxation mode corresponding to the restricted polymer network in contact with the nanofiller [152,153]. Recent work by Sternstein and Zhu [143] on silica/polyvinylacetate nanocomposites indicates that a greater far-field effect is at work in altering chain dynamics than simply a local immobilization of the polymer chain as has been previously suggested [153]. This far-field effect may have a very large effect on the glass transition as shown recently by Ash et al. [92] In this work, the T_g of alumina/PMMA nanocomposites at 1.0wt% filler drops by 25°C when compared to the neat polymer. Further additions of filler do not lead to additional T_g reductions. This novel thermal behavior is shown to vary with particle size, but this dependence can be normalized with respect to specific surface area. The nanocomposite T_g phenomenon is hypothesized to be due to non-adhering nanoparticles that act as well-dispersed internal void/polymer interfaces that break up the percolating structure of dynamically heterogeneous domains recently suggested by Long and Lequeux [154] to be responsible for the T_g reductions in polymer ultrathin films [155]. The results also point to a dramatically increased scope of the interaction zone and its far-field effect on the entire matrix.

A closely related topic in polymers and nanocomposites is the diffusivity of these materials. Studying gas transport of nanosilica-filled polymer by NMR permeativity increased with increasing filler content while retaining gas molecule size selectivity [156]. Similar results were shown using pulsed field gradient NMR techniques with an order of magnitude increase in translational diffusion seen at 30wt% silica in a random copolymer [157]. As stated above, the scattering of light by nanoscale particles is markedly reduced when the particle size is decreased less than 50 nm. Thus nanoparticles may be added to polymers to increase wear, toughness, etc., while maintaining the optical transparency that many organic materials possess. Apart from maintaining clarity in the visible wavelengths, adding nanoparticles can add interesting functionality in the form of UV absorption [158] and the alteration of the refractive index of the matrix polymer. The addition of TiO_2 nanoparticles to many polymers results in such a material where the particles act to absorb the UV radiation and increase the refractive index [146,159]. Indeed, nanocomposites of lead sulfide and polyethylene oxide now boast a refractive index of 3.9 [80,160], while gold nanoparticles contained

in gelatin have reduced the refractive index to about 1 [161]. Dichoric behavior has also been observed in nanoparticle-filled polymers that have been highly stretched, resulting in 'string of pearls'-type structures of fillers with very high aspect ratios. In these composites, the interaction with polarized light varies with the direction of both the incoming radiation and the orientation of the filler strands and results in both color [162] and intensity changes [163]. This type of composite response can be used in the liquid crystal displays [85] or in strain-based schemes for light-filtering devices. The opportunities to tune the electrical properties of polymers with nanocomposites extend beyond enhancing conductive polymers; superparamagnetism in magnetic materials [164,165] or tunable band gaps in quantum dot semiconductor arrays show promise when incorporated into polymers for additional functionality. In addition, the percolation threshold has been shown to be lower in nanocomposites than in traditional filled composites with values as low as 0.03vol% reported [166]. Hong et al. showed a lower percolation limit and a slower decrease in the resistivity with nanofiller concentration compared to conventional composite [167]. The dielectric breakdown strength of nanocomposites can also be enhanced over compositions with micron-scale fillers. In addition to traditional filler roles, organic-inorganic nanocomposites have found their way into etch resists used in semiconductor nanolithography. With line sizes in CMOS technology approaching 100 nm, adding silica nanoparticles to traditional organic resists, such as PMMA, have been shown to increase rigidity and display a higher glass transition temperature which enhances resist performance for nanometer pattern fabrication [168].

As far as ballistic properties are concerned, the fibre reinforced composite materials are increasingly used in the manufacturing of aerospace and automotive structures due to their high strength to weight ratios [169]. Every one of customers wishes good performance and mass production with low cost, but these properties are usually not possible all at once. The aviation industry normally entails components with a high design security without being mainly cost-effective. In the automotive industry the centre of attention is fairly diverse i.e., low cost mass production. The outstanding corrosion resistance of fibre reinforced polymer matrix-composites makes them predominantly attractive in this latter industry. Previous studies [170,171] presented an outline of these products. In the current research, a novel lighter armoured car-body manufactured from polymer-based composite materials bonded to an Al-substrate is examined as a substitute to the usual steel product. From a strategic point of view, the objective of this field of research is to improve or replace the heavy, steel Ballistic Protection Systems (BPS) system currently in use on special operations rotary wing aircraft by increasing the survivability of the aircraft, crew, and passengers while retaining a versatile and lightweight system, capable of sustaining multiple round impacts from small caliber weapons at variable ranges and angles of fire [172]. The aircraft must be able to operate in extreme weather and high altitude environments without a significant performance decrease during mission flights due to the presence of BPS. In recent history, research and development has led to great improvements in modern day BPS. Researchers are constantly in search of better materials and systems

with which to protect soldiers on the battlefield; whether it is body armor, aircraft or vehicular BPS. The natural human desire for self-preservation and the developments in munitions and threats have motivated individuals throughout history to search for better means of protection.The interest in developing advanced lightweight materials based on nanocomposites arise from the unconventional behavior of several nanomaterials in terms of impact energy dissipation. A rich and complex vibrational structure, in particular for acoustic phononic modes, gives to nanoparticles the possibility to withstand high external stresses without structural damages. Thanks to a suitable procedure of nanostructures intercalation within organic matrix, is thus possible to manufacture light composite materials with improved capabilities of ballistic protection, via energy spreading from local points over larger areas or by means of the well known shear thickening effect.

1.2.1 CNT-reinforced materials

Carbon nanotubes are in some ways the ideal fiber. The almost defect-free structure of the nanotubes results in mechanical properties that are comparable to those of a graphene sheet, as already discussed in Sect.1.1.1. Excellent studies have focused on the assessment of the mechanical properties of carbon nanotubes through both experiment and modeling (see Fig.1.16). The Young's modulus of these almost-perfect fibers has been predicted to be between 0.64 and 5.0 TPa for a SWCNT [173-179].The tensile strength of SWCNTs was calculated to range from 50 to 100 GPa depending on the type and number of defects present [180]. The nanometer-scale size of the nanotubes introduces technical difficulties in the experimental measurement of their mechanical properties. However, Yu and coworkers conducted tensile testing experiments on individual MWCNTs that were attached to opposing AFM tips on both ends [181]. They obtained values of 11-63 GPa for the tensile strength and 270-950 GPa for the elastic modulus of the MWNT. Yu and coworkers also conducted tensile tests on SWCNT bundles and obtained 320-1470 GPa for the elastic modulus [182]. Thus the strengths obtained by experimental measurements are lower than the calculated values, possibly due to intrinsic nanotube defects that cause premature mechanical failure or to other errors in the experimental methodology. Indirect measurements have yielded similar values for modulus and strength [183,184]. In addition to their unique mechanical properties, carbon nanotubes have a high aspect ratio, high thermal conductivity, high electrical conductivity, and low coefficient of thermal expansion [185]. In short, carbon nanotubes theoretically have the properties of an ideal graphite fiber. This alone makes them attractive for incorporation into polymers. In addition, their small size introduces the possibility of synthesizing transparent materials with low volume fractions of filler. Studies have been conducted in order to explore the mechanical properties of nanotube-reinforced polymer composites, keeping in mind the challenges to be addressed. MWNT-polystyrene films were prepared from solution in

toluene and tested in tension [103]: filling with 1wt% of MWCNT caused an increase of 36% in the elastic modulus, and 25% increase in strength. In another study, 5wt% MWCNT-epoxy samples were prepared and tested under tension and compression [186]. An increase of 20% in the tensile elastic modulus and the compression elastic modulus was observed. Insights into the mechanisms of load transfer were discussed for this system, because of the interesting behavior of the composites under tension and compression, as measured by Raman spectroscopy. In another study, carbon nanofiber reinforced poly(etherether)-ketone nanocomposites were prepared by twin-screw extrusion and tested by dynamic mechanical analysis and tensile tests [187]. A gradual increase in the elastic modulus as a function of nanofiber concentration was observed such that a loading of 15wt% nanofibers resulted in a 40% increase in the modulus. The effect of non-covalent modification of carbon nanotubes on the mechanical and thermal properties of nanotube-epoxy composite was investigated [112] using polyoxyethylene as a surfactant. In this work by Gong et al. an increase of 25°C in the glass transition temperature and a 30% increase in the elastic modulus, as measured by dynamic mechanical analysis, were observed with the incorporation of only 1wt% nanotubes. Using polyvinylidene fluoride, again as a non-covalent modifier, in MWCNT-polymethyl methacrylate (PMMA) nanocomposites [188] the dispersion of the nanotubes in the polymer was better, and the storage modulus, as measured by dynamic mechanical analysis, increased. In situ polymerization has been attempted also in the presence of carbon nanotubes, in order to achieve the participation of the nanotubes in the polymerization process and hence get a covalent attachment of the growing polymer chains to the nanotube surface. Such a study was conducted with methyl methacrylate polymerization and MWCNT [189]. Evidence for nanotube-polymer interactions was observed from the examination of the fracture surface of the composites. An increase in the heat deflection temperature was also observed with the incorporation of nanotubes. This in situ polymerization procedure was also used in a SWCNT-polyimide system [190]. In this research the electrical conductivity of the nanocomposite increased by ten orders of magnitude at 0.2wt% SWCNT loading while the mechanical properties also improved. Fluorinated MWCNT-reinforced polyvinyl alcohol composites were also prepared and mechanically tested [191]. A 400% increase in the storage modulus (as measured by dynamic mechanical analysis) was obtained for 4wt% functionalized MWCNT composite as compared to pure polyvinyl alcohol. From a mechanical properties viewpoint, the characteristic bending and looping of SWCNTs is problematic if the maximum reinforcement is to be obtained. Therefore research has been conducted to align the nanotubes by magnetic fields [192] and by melt spinning [193]. In both cases nanocomposites with anisotropic properties were obtained with increases in the elastic modulus realized in the alignment orientation. Few if any of the nanotube-filled polymer composites reported in the literature have achieved the properties expected by their high modulus and strength. This is because of three closely related factors: dispersion, load transfer, and volume fraction. For example, SWCNTs are synthesized in bundles. In the bundle form, the load-bearing portion of the bundle is only the outermost tubes. The tubes inside the bundle slide are relative to the others and

do not carry significant load. To solve this problem, the SWCNT must be separated from the bundles and as mentioned earlier progress is being made in this area. MWCNTs on the other hand, can be separated from their bundles. MWNTs however, are concentric tubes with poor bonding between the carbon layers. Therefore even if the outermost tube of a MWCNT is carrying load, the inner layers may not be. This also reduces their efficiency. Finally, the high surface area of the nanotubes makes it difficult to process composites with high volume fractions of fillers because the viscosity of the nanotube/matrix mixture is prohibitively high.

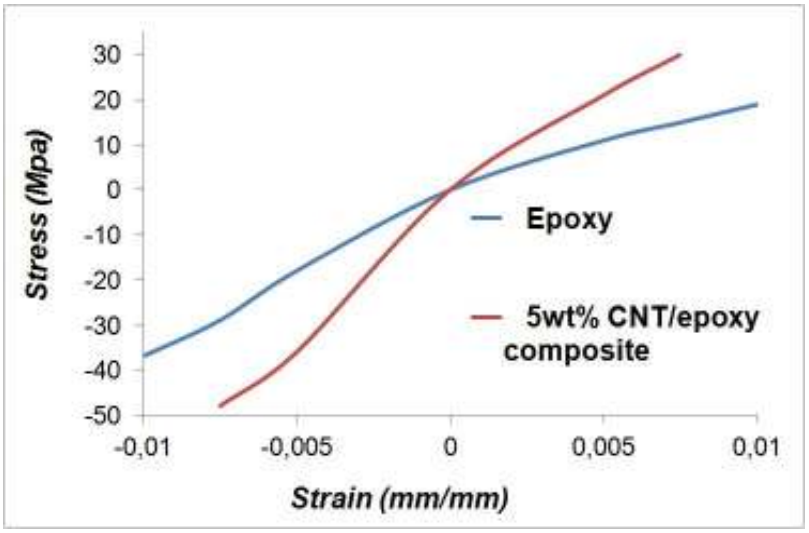

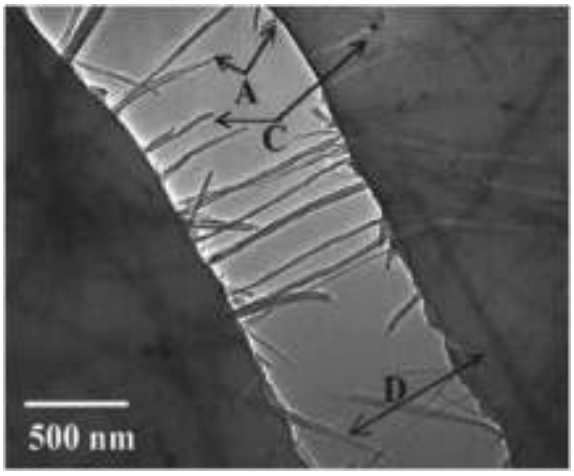

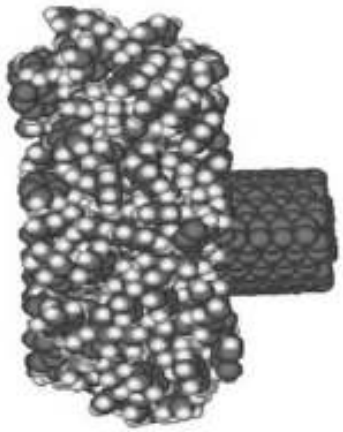

Fig.1.16. CNT-reinforced polymeric composite properties: the improvement of mechanical behavior by means of self-organization, high deformation and 'no' bond-breaking after relatively low wt% addition. On the top, the stress-strain relationship observed during the tension/compression testing of the nanotube-epoxy (5wt% MWCNTs) composite: it can be seen that the load transfer to the nanotube is higher during the compression cycle, because in tension the individual layers of the nanotubes slide with respect to each other, as visible in the SEM images of fracture surface on the left. On the right, a simulation of the interaction modality between a CNT inside the polymeric matrix.

Taken together, the following physical events all contribution to CNT-polymer interactions at the nanometer scale [194]: under no chemical bonding between CNT-polymer, the origins of CNT-polymer interactions are electrostatic and van der Waals forces; local non-uniformity of a CNT embedded in polymer matrix may result in nano-mechanical interlocking, an effect similar to the clench of gears; mismatch in CTEs is a significant factor contributing to both non-bond interactions and mechanical interlocking, because compressive thermal residual stress may increases the true 'contact' area between CNT and the surrounding polymers. From previous experimental studies and results of molecular modeling, it has been suggested that the interfacial shear stress of CNT/polymer systems is at least an order of magnitude higher that micro fiber reinforced composites. It is believed that the high CNT-polymer interfacial shear stress from molecular simulation is attributed, to a large extent, to the intimate contact between CNT and the polymer matrix at the nanometer scale. CNTs offer a much smooth contact surface deprived of local cavities for polymer adsorption, as contrast to polymer-micro fiber interface which might be full of local irregularities that are prone for micro crack development under applied load.

It is well established, from decades of research on micro fiber reinforced composites, that fiber-matrix interfacial shear stress is a critical parameter controlling the efficiency of stress transfer and hence some of the important mechanical properties of the composite such as elastic modulus, tensile strength, fracture toughness, as well as their long-term behavior. Current interests in using CNTs and anticipated potential applications for CNT reinforced polymer composites demand a better understanding of the CNT-matrix interfacial characteristics. However, the physics of interactions between CNT and its surrounding matrix material in such nano-composites has yet to be elucidated, and methods for determining the parameters controlling interfacial characteristics such as interfacial shear stress, is still challenging. Previous studies on CNT-polymer composite systems suggested that chemical bonding between CNT and the polymer matrix may or may not exist, and adhesion between CNT and certain polymer systems are strong, although there are also contrasting views. Upon close examination of the fracture surface of a MWNT/polyhydroxyaminoether composite, Bower et al. observed contact and adherence of the polymer to most of the nanotubes, and in some cases the entire surface of the nanotube was covered with a layer of polymer [195]. Chang et al. also observed CNT was well coated by polypyrroles in a CNT/polypyrroles composite produced by in situ polymerization. Raman scattering and X-ray diffraction data suggested there is no chemical reaction between CNT and the polymer [196]. In a study by Jia et al. [197], CNT was used as a reinforcement for PMMA, also by an in situ polymerization process. Chemical bonding between CNT and PMMA was confirmed using infrared transmission spectra. It was proposed that π-bond of CNT was opened due to the initiation of 2,2′-azobisisobutyronitrile and linked to each other, thus producing a stronger CNT-PMMA interface. From mechanics point of view, available literatures to date also offered evidence of strong CNT-polymer interactions. Lourie and Wagner first showed CNT fragmentation in epoxy matrix, implying that force was transmitted to the CNT from the surrounding matrix [198,199].

From fragmentation experiments, these authors estimated that the CNT-matrix stress transfer ability is at least one order of magnitude larger than that measured in conventional micro fiber-based composites. Compared to CNT-polymer interface, they attribute the lower interfacial strength of conventional micro fiber-polymer interface to larger defects that facilitate interfacial crack propagation [198]. Furthermore, Qian et al. [200] showed that tensile load can be transferred effectively from the polystyrene matrix to the CNT, resulting in high elastic modulus increase (42%) using just 1wt% CNT. Similar results were also shown by Xu et al. [201], using CNT/epoxy thin film composite system. Using an expanded form of Kelly-Tyson approach, Wagner [202] showed that high interfacial shear strength between CNT and polymers is possible, in agreement with results from molecular mechanics simulation of CNT pullout [203,204]. More recently, Cooper et al. [205] showed that interfacial shear strength between MWNT and epoxy ranged from 35-376 MPa, from pullout experiments using atomic force microscope. Despite these positive evidences of strong CNT-polymer interactions, that CNT-polymer interface only offers poor stress transfer was also reported. Based on evidence of micro Raman spectroscopy, Schadler et al. [206,207] showed that load transfer between CNT-epoxy was poor. Although these studies have provided some insights into the nature of CNT-polymer interactions at the interface, the physics of CNT-polymer interactions still await further elucidation, both qualitatively and quantitatively.

1.2.2 Nanofluid-reinforced materials

An intriguing issue of nanoscience research for aerospace applications is to produce a new thin, flexible, lightweight and inexpensive material that have an equivalent or even better ballistic properties than the existing Kevlar fabric [208]. A shear thickening fluid (STF) is a material with remarkable properties. STF are very deformable materials in the ordinary conditions and flow like a liquid as long as no force is applied. However they turn into a very rigid solid-like material at high shear rates. Shear thickening is a non-Newtonian fluid behavior defined as the increase of viscosity with the increase in the applied shear rate [209]. This phenomenon can occur in micro/nano colloidal dispersions. More concentrated colloidal suspensions have been shown to exhibit reversible shear thickening resulting in large, sometimes discontinuous increases in viscosity above a critical shear rate. Two main causes of reversible shear thickening have been proposed: the order–disorder transition [210-214] and the 'hydrocluster' mechanism [215-220]. This transition from a flowing liquid to a solid-like material is due to the formation and percolation of shear induced transient aggregates, or hydroclusters, that dramatically increase the viscosity of the fluid. Support for this hydrocluster mechanism has been demonstrated experimentally through rheological,

rheo-optics and flow-SANS experiments [215-221] as well as computer simulation [222]. It has been reported in the literature that shear thickening has been observed for a wide variety of suspensions such as clay-water, calcium carbonate-water, polystyrene spheres in silicon oil, iron particles in carbon tetrachloride, titanium dioxide-resin, silica-polypropylene glycol, and silica-ethylene glycol [223-229]. The phenomenon of shear thickening of suspensions in general has no useful applications in industrial production. Recently Wegner's group and U.S. Army research lab developed a body armor (see Fig.1.17) using shear thickening fluid and Kevlar fabric [229]. These research results demonstrate that ballistic penetration resistance of Kevlar fabric is enhanced by impregnation of the fabric with a colloidal shear thickening fluid (see Fig.1.18). Impregnated STF/fabric composites are shown to provide superior ballistic protection as compared with simple stacks of neat fabric and STF. Comparisons with fabrics impregnated with non-shear thickening fluids show that the shear thickening effect is critical to achieving enhanced performance.

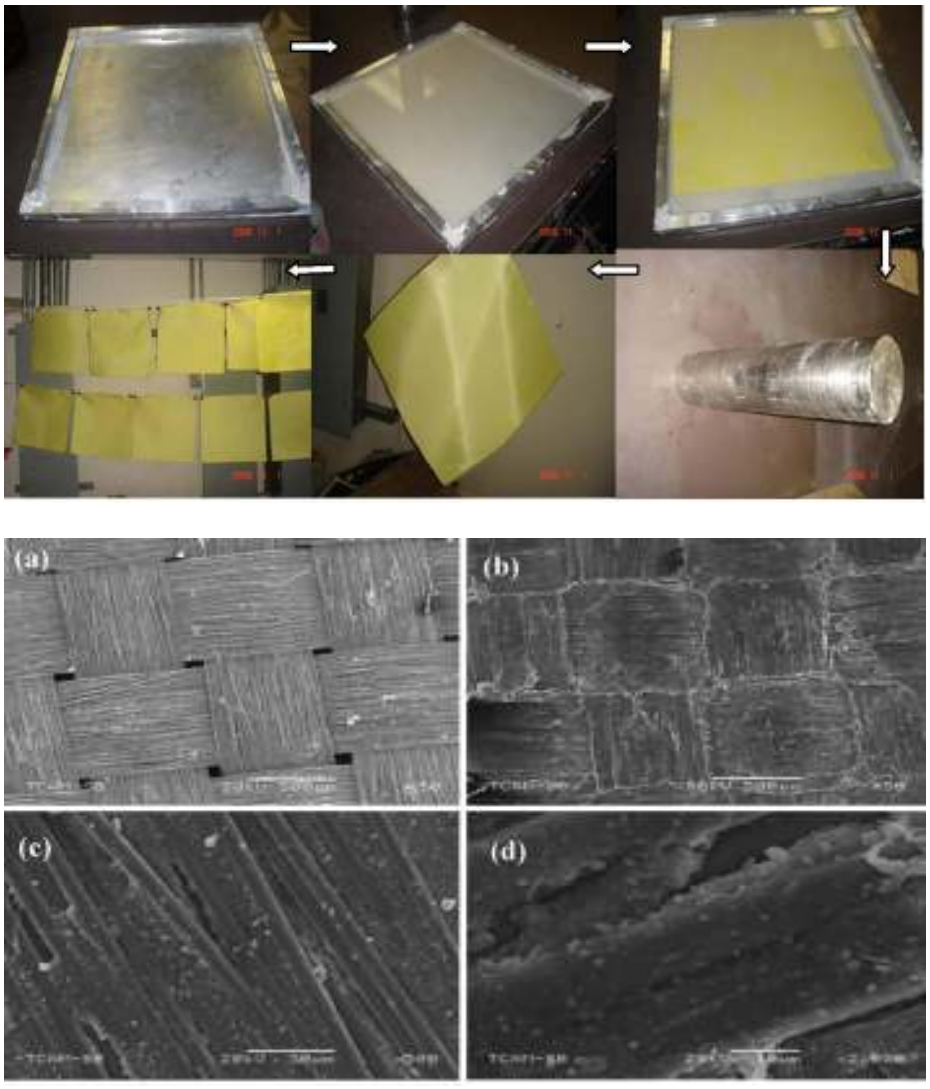

Fig.1.17. STF-reinforced Kevlar-based fabric realization. Above some pictures taken during the different step of the fabric impregnation procedure, below SEM images for (a) neat Kevlar fabrics and (b)-(d) STF/Kevlar composites [REF STF1].

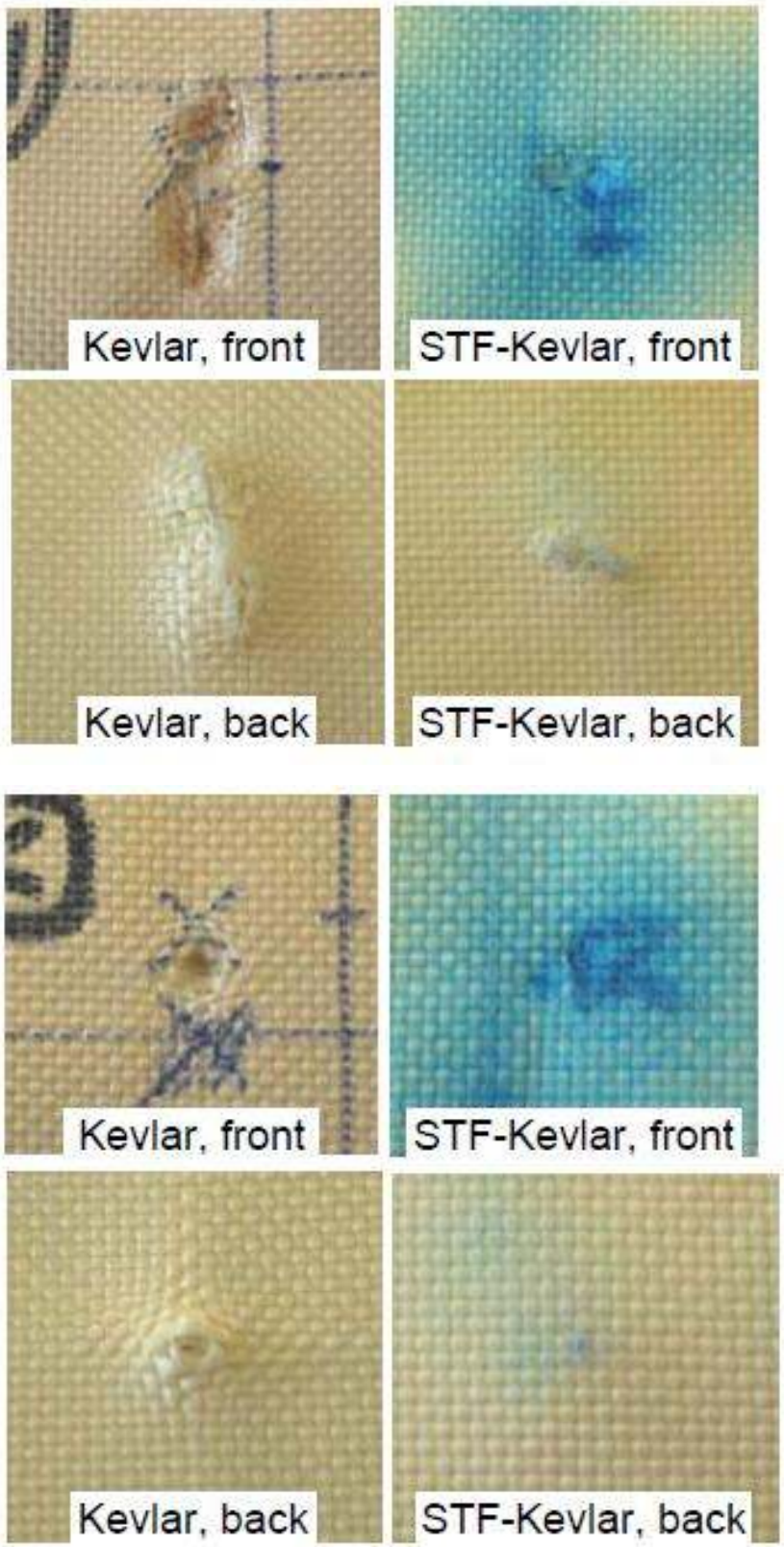

Fig.1.18. STF-reinforced Kevlar-based fabric resistance upon impact. From the pictures of front and back surfaces it's easy to appreciate the good improvements provided by the treatment of Kevlar fabric with silica-based nanofluid for both knife (above) and spike (below) low impact energy (~17J) tests.

The ballistic impact characteristics of Kevlar woven fabrics impregnated with a colloidal shear thickening fluid (see Fig.1.19) has been also studied [230-231]. The STF was prepared from 466 nm spherical colloidal silica particles and ethylene glycol. The synthesis procedure started with 3h of centrifugation for the colloidal solution at 3900rpm to separate the silica particles from the aqueous-based supernatant. The silica sediment was then crushed using a spatula and re-suspended in ethylene glycol using a vortex mixer. This process was repeated four times in order to minimize the amount of residual aqueous supernatant present within the samples. Ballistic impact results of Kevlar fabrics impregnated with this STF sample showed significant enhancements in ballistic penetration resistance of the STF impregnated fabrics compared to neat Kevlar due to the addition of STF without any loss in material flexibility. They have also prepared the STF from solvent exchange method. In this method colloidal silica was heated to evaporate water from colloidal solution and the evaporated amount of water was replaced with an equivalent amount of ethylene glycol. This process continued until all the water was replaced with 57% or 62% of ethylene glycol by volume. The rheological measurements of these samples also showed a shear thickening behavior [232,233]. Recently high-power ultrasound irradiation has been extensively used in the dispersion of nanoparticles in liquids [234,235] and it is also considered as one of the efficient techniques to disperse nanoparticles into materials [236,237]. Intense ultrasound waves traveling in liquids generate growing cavities. When the cavity attains a critical size it implodes, generating extreme conditions of intense heat and tremendous pressure that provide an unusual chemical environment for chemical reactions. The formation, growth, and implosive collapse of bubbles in a liquid irradiated with ultrasound are the physical phenomenon responsible for most of the sonochemistry. Ultrasound is produced in liquids by means of piezoelectric or magnetostrictive materials: materials that expand or contract when they are placed in electromagnetic fields. Exposing such materials to a field alternating at an ultrasonic frequency produces ultrasound [238-242]. In a recent investigation [230] a high intensity ultrasonic irradiation technique for synthesis of STF was adopted. PEG was used as suspending liquid phase because of its non-toxicity, thermal stability, easy to handle and easily available in bulk quantities which make it useful for bulk production. In this technique ethanol has been as a solvent because its sonochemical effects have been well studied [243,244] and also it was used as a solvent in the impregnation process of STF on Kevlar and nylon fabric for body armor applications.

Many researchers have used various techniques to prepare the shear thickening fluid [208]. Acoustic cavitations technique is one of the efficient ways to disperse nanoparticles into the liquid polymers. In this case, the application of alternating acoustic pressure above the cavitations threshold creates numerous cavities in the liquid. Some of these cavities oscillate at a frequency of the applied field (usually 20 kHz) while the gas content inside these cavities remains constant. However, some other cavities grow intensely under tensile stresses while yet another portion of these cavities, which are not completely filled with gas, start to collapse under the compression stresses of the sound wave. In the latter case, the collapsing cavity generates tiny

particles of ‘debris’ and the energy of the collapsed one are transformed into pressure pulses. It is noteworthy that the formation of the ‘debris’ further facilitates the development of cavitation. It is assumed that acoustic cavitations in liquids develop according to a chain reaction. Therefore, individual cavities on real nuclei are developing so rapidly that within a few microseconds an active cavitations region is created close to the source of the ultrasound probe. The development of cavitations processes in the ultrasonically processed melt creates favorable conditions for the intensification of various physic-chemical processes. Acoustic cavitations accelerate heat and mass transfer processes such as diffusion, wetting, dissolution, dispersion, and emulsification.

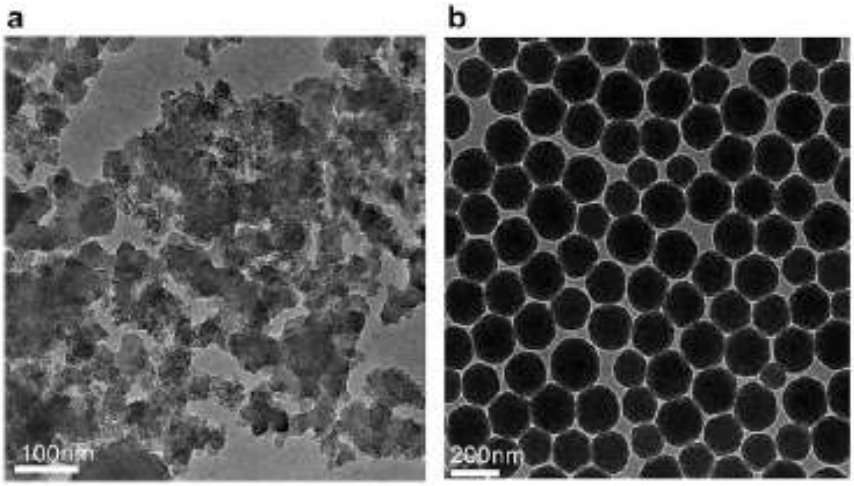

Fig.1.19. TEM micrograph for (a) silica nanoparticles and (b) colloidal silica solution.

Based on such experiences, the objective of the present research in this field (see below Sect.1.3.2) is to synthesize a shear thickening fluid in a single step reaction through high power ultrasound technique, fabricate STF/fabric composite and characterize it for ballistic resistance applications. The shear thickening fluid adopted is a combination of silica nanoparticles suspended in a PEG-made liquid polymer . This mixture of flowable and hard components at a particular composition, results in a material with remarkable properties. The shear thickening fluid is prepared by ultrasound irradiation of silica nanoparticles dispersed in liquid polyethylene glycol polymer. The as-prepared STFs are then tested for their rheological and thermal properties. Kevlar fabrics are soaked in STF/ethanol solution to make STF/fabric composite and ballistic tests are performed on the neat fabrics and STF/fabric composite targets. The results will show that STF impregnated fabrics have better penetration resistance as compared to neat fabrics without affecting the fabric flexibility. This indicates that the addition of STF to the fabric enhance the fabric performance and can be used in ballistic applications.

1.3 Experimental: Nanocomposites manufacturing

In the following sections the experimental activity related to the nanocomposites production for the ballistic test (object of the third chapter) is presented. The manufacturing procedures for both CNT-filled Epoxy-based and STF-reinforced Kevlar-based composite materials are reported and widely discussed, as well as the physical/chemical methods for the characterization of the nanofillers themselves and, in a row, of the resulting nanocomposite materials.

Of course this kind of experimental activity (sample realization and ballistic characterization) was not just sequential, but required a concurrent approach: the specimens manufacturing was tuned on the experimental set-up availability, and, vice versa, the experimental results (in particular the preliminary tests) have often suggested several modification/improvements to be provided during the materials processing. For such reason, the manufacturing procedure description is somewhere referred to in general terms, while elsewhere, it refers to experimental features discussed in more details in the third chapter.

One critical aspect in the practical use of micro and nanoparticles in composites consists in achieving a random dispersion inside the matrix, in order to obtain an homogeneous material. The widely used compounding technique to prepare conventionally filled polymers is still the most convenient and practical way when nano-sized fillers are considered to replace micron-sized fillers for high-performance polymers. But the dispersion of nano-fillers in polymer matrix is more difficult than that of micro-fillers due to the strong tendency to agglomerate for the nano-fillers. In particular for what concerns the CNT-filled composites, the full potential of employing CNTs as reinforcements has been severely limited because of the difficulties associated with dispersion of entangled CNT during processing and poor interfacial interaction between CNTs and polymer matrix. The nature of dispersion problem for CNTs is rather different from other conventional fillers, such as spherical particles and carbon fibers, because CNTs are characteristic of small diameter in nanometer scale with high aspect ratio (>1000) and thus extremely large surface area. In addition, the commercialized CNTs are supplied in the form of heavily entangled bundles, resulting in inherent difficulties in dispersion.

As a consequence, an accurate dispersing process is required, able to homogeneously mix the powders within the matrixes, as well as to avoid air bubbles formation inside the mixtures. With such an aim, manual and mechanical mixing conventional techniques have to be assisted by advanced ultrasonication methods (see Fig.1.20). For polymeric nanocomposites, the high power dispersion methods, such as ultrasound and high speed shearing, are the simplest and most convenient to improve the dispersion of nanoparticles in a polymer matrix. Ultrasonication is the act of applying ultrasound energy to agitate particles in a solution for various purposes. In the laboratory, it is

usually achieved using an ultrasonic bath or an ultrasonic probe/horn, also known as a sonicator. It is the most frequently used method for nanoparticle dispersion. The principle of this technique is that when ultrasound propagates via a series of compression, attenuated waves are induced in the molecules of the medium through which it passes. The production of these shock waves promotes the 'peeling off' of individual nanoparticles located at the outer part of the nanoparticle bundles, or agglomerates, and thus results in the separation of individualized nanoparticles from the bundles. Ultrasonication is an effective method to disperse nanoparticles in liquids having a low viscosity, such as water, acetone and ethanol. However, most polymers are either in a solid or viscous liquid state, which requires the polymer to be dissolved or diluted using a solvent to reduce the viscosity before dispersion of nanoparticles. Standard laboratory sonicators (in a water bath) run at 20-23 kHz with a power less than 100 W. Commercial probe sonicators have an adjustable amplitude ranging from 20% to 70% and a power of 100-1500 W. The probe is usually made of an inert metal such as titanium. Most probes are attached with a base unit and then tapered down to a tip with a diameter from 1.6 to 12.7 mm. This means that the energy from the wide base is focused on the tip, thus giving the probe high intensity. The consequence of this configuration is that sonication can generate substantial heat rapidly. Therefore, for nanoparticles dispersed in volatile solvents, such as ethanol and acetone, the samples should be kept cold (e.g. using an ice bath) and the sonication must be done in short intervals. If the sonication treatment is too aggressive and/or too long, the nanoparticles can be easily and seriously damaged, especially when a probe sonicator is employed. Thus a trade-off between an effective nanoparticles disentanglement and a not too hard treatment must be reached. Such an issue has been tackled by means of ultrasonic liquid processor (*Sonics and Materials* VCX 750, Fig.1.20), allowing to blend at the same time nanopowder, polymeric matrixes and solvent with high homogeneity, few inner voids, optimum degree of reproducibility, and in turn, to define a not invasive procedure.

Morphological characterization of both the nanofillers and the realized nanocomposites have been performed by means of scanning electron microscopy analysis (*TESCAN-Vega LSH,* Large Stage High Vacuum SEM, Fig.1.20), able to value the nanoparticle dispersion and the homogeneity degree of the nanocomposite samples before the ballistic test, as well as the damage characteristics after this latter. As far as the carbon nanotubes-reinforced composites are concerned, a functionalization treatment has been carried out in order to improve the CNT chemical blending with the polymeric matrix: FE-SEM characterization, Raman and FT-IR spectroscopic analysis have been performed to assess the effectiveness of the adopted procedure. Further, differential scanning calorimetry (DSC) was used to analyze the polymerization process for the nano-reinforced thermosetting polymer systems. Regarding the shear tickening nanofluid, a rheological characterization (viscosity v.s. shear rate) has been carried out by means of parallel plate rheometer measurements. All these latter experimental activities were performed by means of external collaborations.

Fig.1.20. *SASLab* facilities for nanocomposite realization and characterization: on the top, BS Laboratory *(VELP Scientifica)* Magnetic Stirrer BS Type 0÷2000rpm; on the centre, *Sonics & Materials* VC 750 Ultrasonic Liquid Processor; on the bottom, *TESCAN-Vega* LSH Scanning Electron Microscope.

1.3.1 CNT-composites production

The mechanical properties of a nanostructured composite material are strongly affected by the dispersion of the nano-fillers within the polymer matrix, which depends on the interface bonding with the polymeric chains. Based on this consideration, an important role in the energy absorption mechanism of a composite material is played by the functionalization treatments of the filling nanoparticles. Such treatments provide for a chemical modification of the nanoparticles surface, making them compatible with the polymer matrix.

In the following, the CNT functionalization process by thermal and chemical treatments is described. Scanning electron microscopy (SEM) analysis, as well as Raman and FT-IR spectroscopies were used to verify the surface modifications of the CNTs by the added radical groups. Then, the manufacturing of the CNT-reinforced epoxy composite is schematically presented. Differential scanning calorimetry (DSC) was used to analyze the polymerization process for the nano-reinforced thermosetting polymer systems.

In order to assess the influence of the nanoparticles content as well as the effectiveness of the nano-filler itself and after chemical treatments, samples with different percentages of functionalized MWCNTs embedded in two different epoxy resins were tested and compared with samples reinforced by pristine MWCNTs and micrometric graphite powder.

Medium viscosity epoxy resin EPON 828 (*Hexion Speciality Chemical Inc.*) and low viscosity epoxy resin PRIME 20LV (*Gurit Holding AG*) were used as base polymeric matrixes, together with their own specific hardener in fixed weight ratio. Two carbon materials have been adopted as reinforcements: graphite micro-powder (*Sigma Aldrich* Graphite, granulometry 20μm) and multi-walled carbon nanotubes (*Carbolex* MWCNT, diameter 20-30nm, length 10-30μm, purity > 95%, specific surface area > 110m^2/g). Conventional solvents and chemical products necessary for the MWCNT functionalization procedure were purchased from *Sigma Aldrich*.

A procedure for high quality dispersion and low time processing was developed, in order to set an ongoing scaling-up procedure for CNT-filled nanocomposite production. Such an issue has been tackled by means of ultrasonic liquid processor allowing to blend at the same time powder, resin and hardener with both high homogeneity and few inner voids. Also air gaps between the realized (solid) sample and the holder must be avoided as much as possible. Such a required accuracy has been obtained by pouring the composite mixture (i.e. still in the liquid status) directly into the sample holder acting as mould. The subsequent polymerization grants a perfect join between metallic holder and composite samples, with no air gaps. All these attentions are required in order to present a material as homogeneous as possible, thus improving the measurement's accuracy.

1.3.1.1 *CNT functionalization*

It is well known that oxidation or chemical functionalization of CNTs and covalent attachment of polymer chains to the CNTs make the dispersion better and strength of the interfacial bonding between the CNTs and the polymer matrix stronger. However, the functionalization may weaken the interfacial bonding between graphene sheets of the CNTs and reduce the transfer efficiency of applied load. For such areason, in order to study tailored nanostructured composites, a chemical functionalization of MWCNTs was tuned to improve the bonding at the polymer-filler interface.

The method to modify chemically the MWCNT surface broadly followed a widely employed procedure based on the CNT chemical oxidation in acidic environment [245-250]. The technique is a case of covalent functionalization where C-C bonds are broken and carbon atoms passivated with hydroxyl and carboxylic groups. Schematically (see Fig.1.21), the procedure consisted of the four following steps: thermal oxidation (~2h in air at 350°C) needed for a first material purification (i.e. removal of amorphous carbon or other impurities); acidic oxidation (in a 3:1 mixture of H_2SO_4 and HNO_3 at ~120°C for ~80min) to exfoliate the CNT bundles and introduce organic groups at breaking and defective points; vacuum-assisted filtration of the solution (washed in bi-distilled water) using PTFE-0.45μm and GV-0.22μm porous membranes; recovery of the oxidized MWCNTs from the membranes by dipping in isopropyl alcohol. Pictures taken at different steps of the procedure are reported in Figs.1.22-1.23. A first macroscopic evidence of the treatment effectiveness was the high homogeneity degree of the CNT suspension in the alcoholic solution, due to the interaction between the radical groups attached to the CNT walls and the polar molecules of the solvent. On the contrary, in analogous mixtures prepared by sonication of the as-received material, the pristine hydrophobic CNTs readily flocculated (see Fig.1.24). After chemical oxidation, acyl chlorination was performed by stirring the MWCNT in thionyl chloride at 70°C for 24h and, subsequently, a reaction with the desired amines (DETA - DGEBA) produced the amino-functionalized MWCNTs.

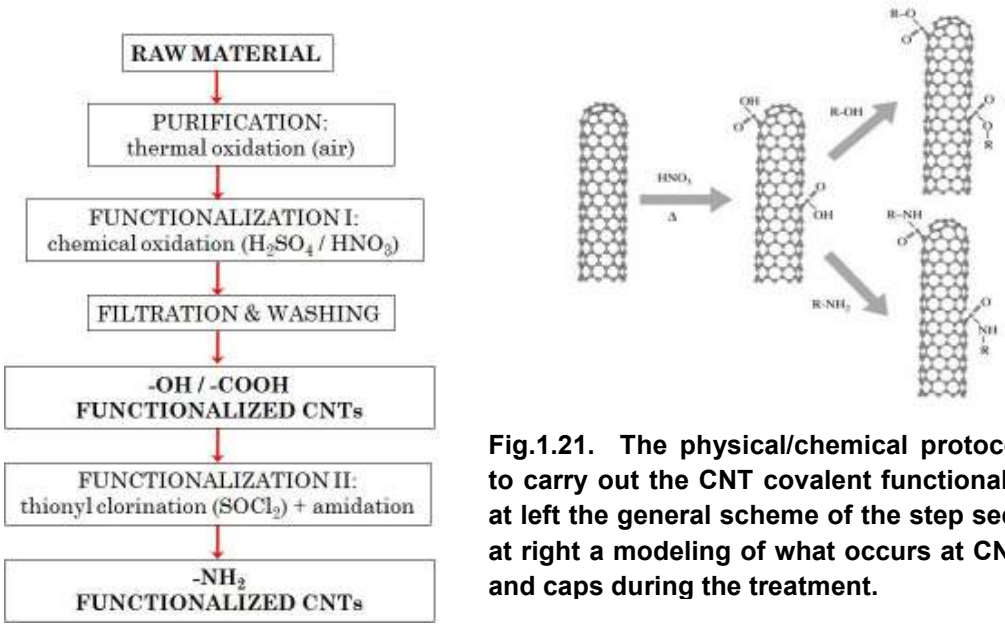

Fig.1.21. The physical/chemical protocol used to carry out the CNT covalent functionalization: at left the general scheme of the step sequency, at right a modeling of what occurs at CNT walls and caps during the treatment.

Fig.1.22. CNT functionalization procedure: in air oxidation step. A CVD oven (right) was utilized to remove impurities and amorphous carbon material from the as-received CNTs at ~350°C for ~2h. Ceramic holders (left) have been used in order to avoid any type of contamination during such treatment.

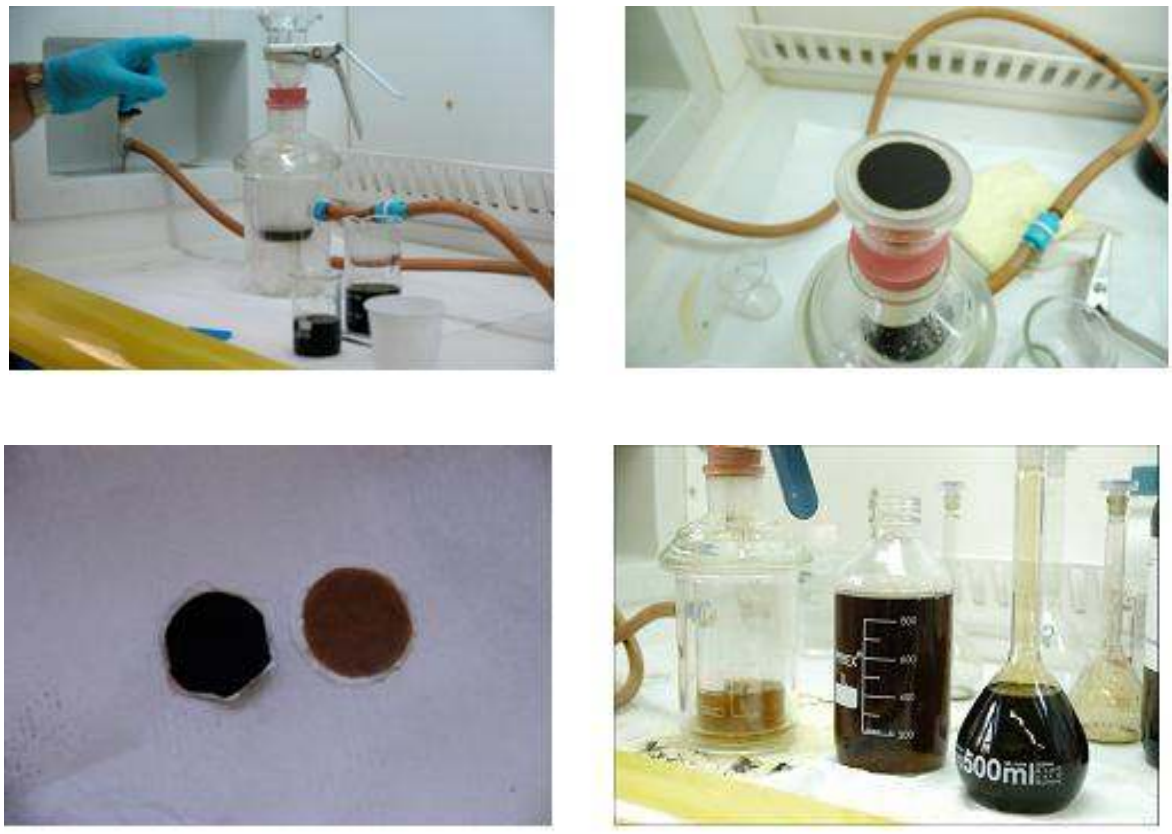

Fig.1.23. CNT functionalization procedure: vacuum-assisted filtration step. PTFE-0.45μm and GV-0.22μm porous membranes were employed to recovery the treated CNTs after the oxidation in acidic environment. The different colouring of both the solutions and the membranes stress the further purification/homogenization of the CNT material after the different stages of the filtration procedure.

Fig.1.24. CNT functionalization procedure: recovery of the chemically oxidized MWCNTs from the membranes by dipping in isopropyl alcohol. The visible evidence of the treatment effectiveness isthe high homogeneity degree of the treated CNTs in the alcoholic solution (bottom), due to the interaction between the radical groups attached to the CNT walls and the polar molecules of the solvent. On the contrary, analogous mixtures prepared by sonication of the as-received material result in very bad dispersing suspensions, owing to the hydrophobic behavior of the pristine CNTs.

Scanning electron microscopy (SEM) analysis was performed to compare the MWCNT morphology before, during and after the functionalization treatment. The micrographs reported in Fig.1.25 highlight the differences between the raw unclean and agglomerated material, the superficial clean 3D clusters after the thermal oxidation , and the disentangled 2D network morphology of the chemically treated CNTs. Also Fig.1.26 suggest the effectiveness of the process, in particular for what concerns the disentanglement of the highly packaged ropes of the pristine multi-walled carbon nanotubes that prevent a correct dispersion in the matrix. Bundles exfoliation seems thus to be a 'must', if one want to establish some kind of technical standard for the scale-up processing of such materials.

Raman spectroscopy was used to evaluate the efficiency of the chemical oxidation in terms of MWCNT structural and morphological modifications. The measurements were performed by means of a Micro-Raman confocal spectrometer (632.8nm He-Ne laser source, grating 1800g/cm, charge-coupled detector, spot size ~2μm, spectral resolution ~3cm^{-1}). In Fig.1.27 the Raman spectra of the as-received material, after the thermal oxidization, and after the treatment in acidic environment are shown. A common spectral characteristic of the treated materials compared to the raw one is the expected reduction of the breathing mode (RBM) due to the breaking of the radial symmetry [250-252]. A peak broad displacement to higher frequencies as a mark of a less agglomerated structures [253,254] can be noticed as well. The substantial difference

between the treated materials response is the significative softening of the G band in the spectrum of COOH-CNT: that is a clear trace of the strong acidic action, since the G resonances are typically connected to the CNT graphitic walls integrity, thus suggesting the conversion from sp^2- to sp^3-carbons on the surface and the existence of grafted chemical groups [249,250,255,256]. The spectrum of functionalized CNTs shows the so called cut-CNT behavior, with a sharp length distribution peaked around low values (~200 nm) [257].

FT-IR spectroscopic analysis was conducted in order to qualitatively characterize the effect of the treatments performed on the pristine MWCNTs. FT-IR spectra were recorded with Biorad FTS-575C spectrometer with spectral resolution of $2cm^{-1}$. Samples were dispersed in KBr and compressed in pellets. Fig.1.28 shows the FT-IR spectra in the range of $1000\text{-}2000cm^{-1}$ of MWCNTs as received and after functionalization with the amine groups. A band at about $1562cm^{-1}$ can be observed in both spectra, and is representative of the nanotube C=C vibrational modes. After functionalization with the amines, a strong band at $1654cm^{-1}$ appears, corresponding to amide carbonyl stretching mode. The band at 1269 and $1384cm^{-1}$ are consistent with C-N and N-CH_3 stretching vibrations. The band at $1457cm^{-1}$ might be due to CH_4 absorption on the nanotubes during production [258].

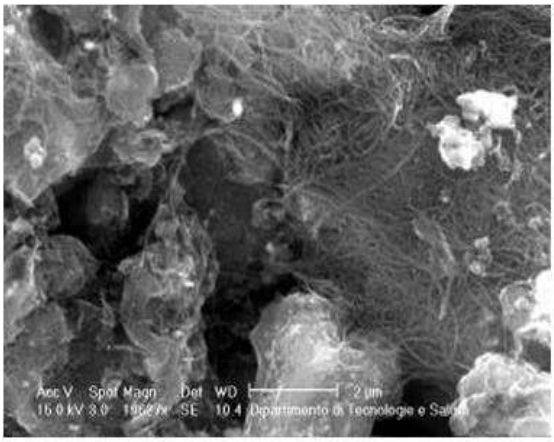

Fig.1.25. SEM characterization of the CNTs at different steps of the covalent functionalization treatment. On the left, the raw pristine CNTs, with a lot of impurities and highly entangled. On the bottom, the material after in-air oxidation (left) and after chemical oxidation (right), showing further morphological improvements, in terms of purity and disentanglement.

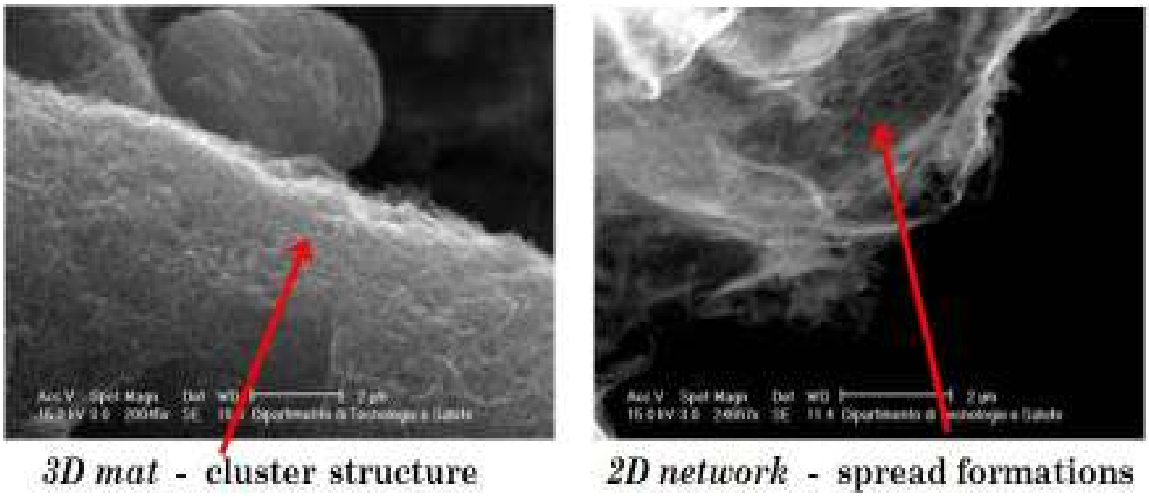

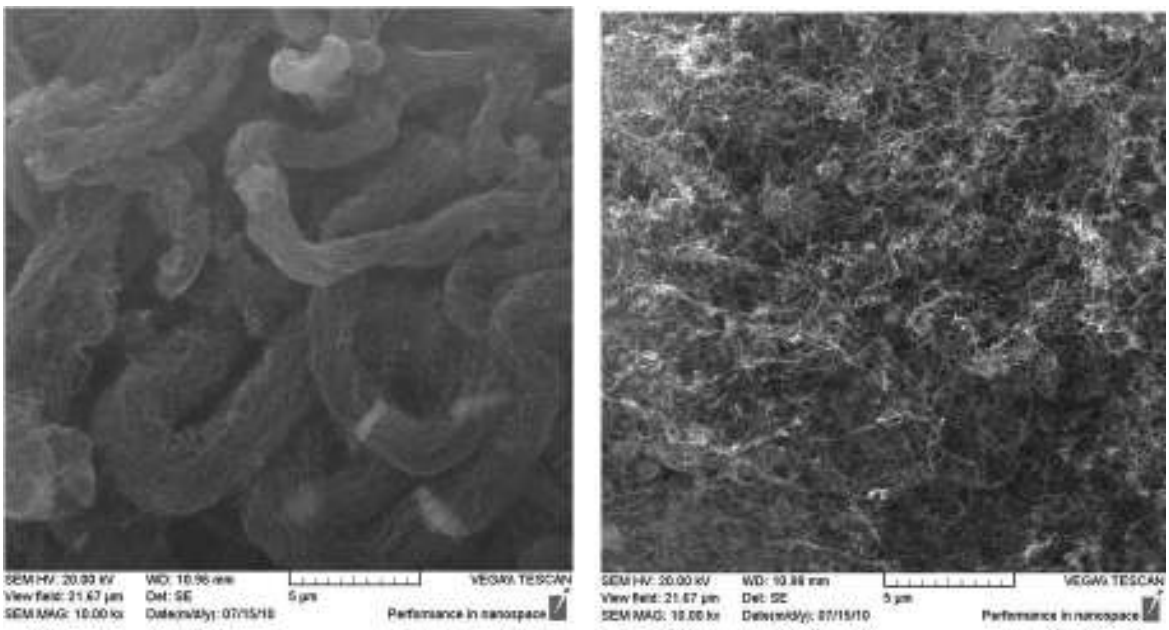

Fig.1.26. SEM images of the CNTs before (left) and after (right) the chemical treatment, highlighting the impressive morphological changes due to the functionalization.

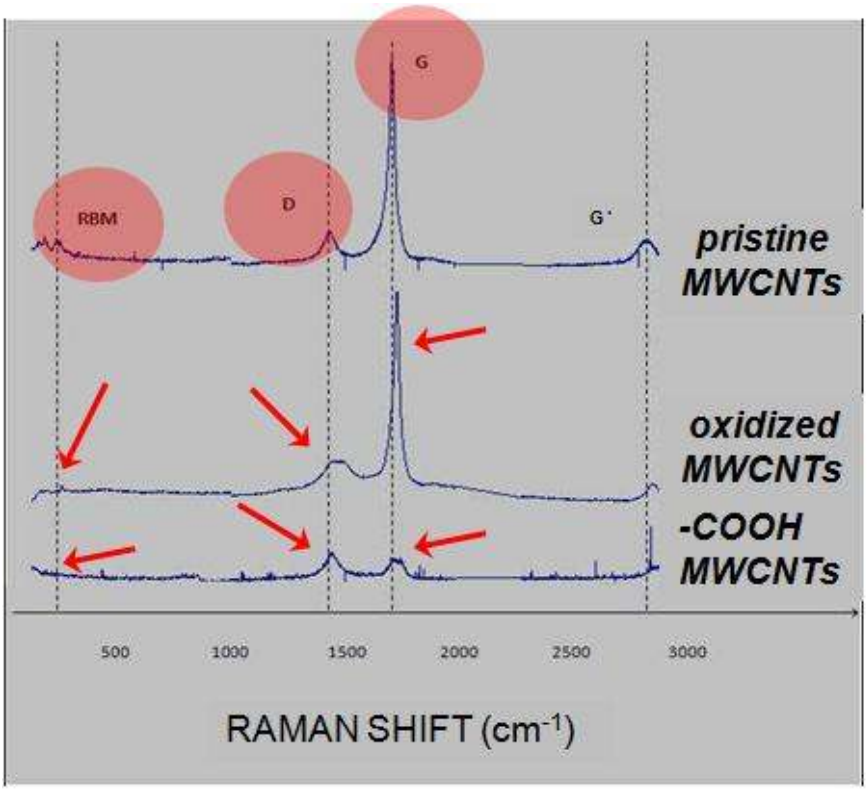

Fig.1.27. Raman spectra of the MWCNT powder during different steps of the chemical treatment (arbitrary units on the vertical axis): in comparison to the typical CNT spectrum, peaks displacements and softening due to the physical/chemical treatments are highlighted.

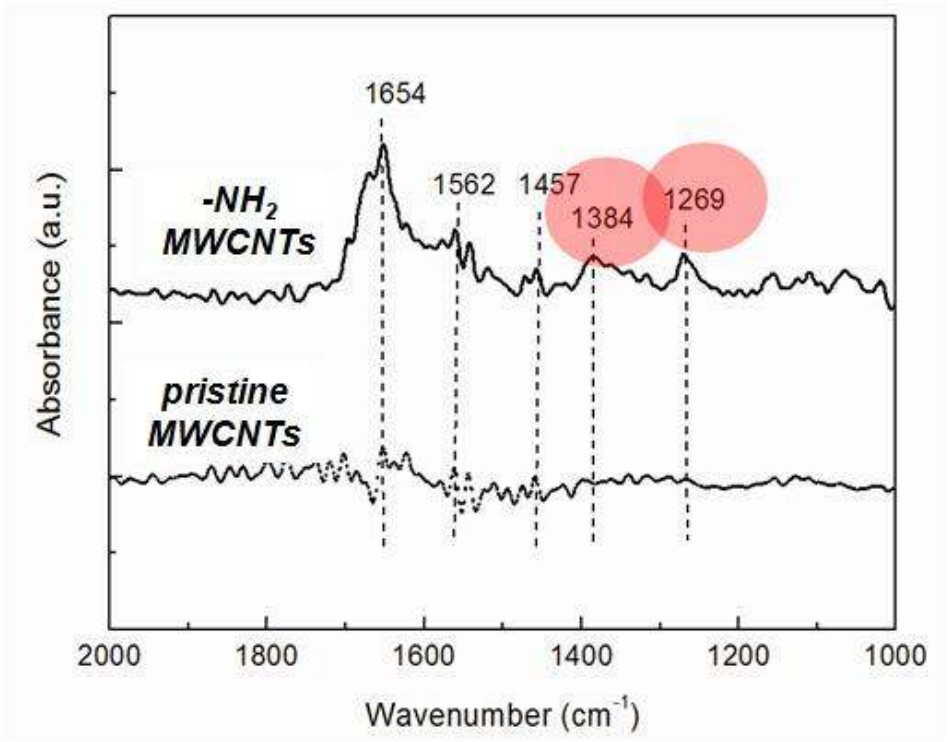

Fig.1.28. FT-IR absorbance spectra in KBr of pristine MWCNTs and functionalized MWCNTs: the occurrence of the amino-related bands are highlighted in the upper spectrum.

1.3.1.2 *CNT-Epoxy processing*

This section describes the procedures to prepare samples and panels for the different impact tests. A preliminary thermo-analysis was performed, in order to evaluate if the presence of nanoparticles could alter the process parameters related to the matrix. In particular, characteristic temperature and curing time of the neat resin may vary upon adding the MWCNTs. The polymerization phase of the resin is an important step during the manufacturing of the samples, which influences the mechanical performance of the resulted material.

Dynamic DSC analyses were performed on a DSC822e/400 Mettler Toledo instrument in inert atmosphere of nitrogen flux, in the temperature range between -50°C and 250ºC with a rate of 10ºC/min. Results showed that as the MWCNT weight percentage is increased, the exothermic peak due to the curing reaction occurs at lower temperatures for both the epoxy systems. For the sake of argument, Fig.1.29 reports the DSC analysis performed on the neat PRIME 20LV (top curves) compared to 0.5wt% functionalized MWCNT-reinforced matrix (bottom curves). The phenomena can be explained considering that MWCNTs are functionalized with amino radicals: at a given state of

dispersion, these groups interact with the polymer chains varying their degrees of freedom, which depend on the surface chemistry of the filling particles. The isothermal DSC analysis, performed at the recommended temperature for the polymerization phase, proved that the MWCNTs were effective in retarding the cure of the epoxy resin. Fig.1.29 also shows the trend of PRIME 20LV reinforced with different weight percentages of functionalized MWCNTs. It is possible to observe that as the MWCNT amount increases the kinetic reaction slows down. These results are particularly important from both the manufacturing and the mechanical performance point of view, because the assurance of reaching an high grade of polymerization guaranties the expected mechanical properties. Taking in consideration these results, the cure time was extended of 60 minutes above the recommended one.

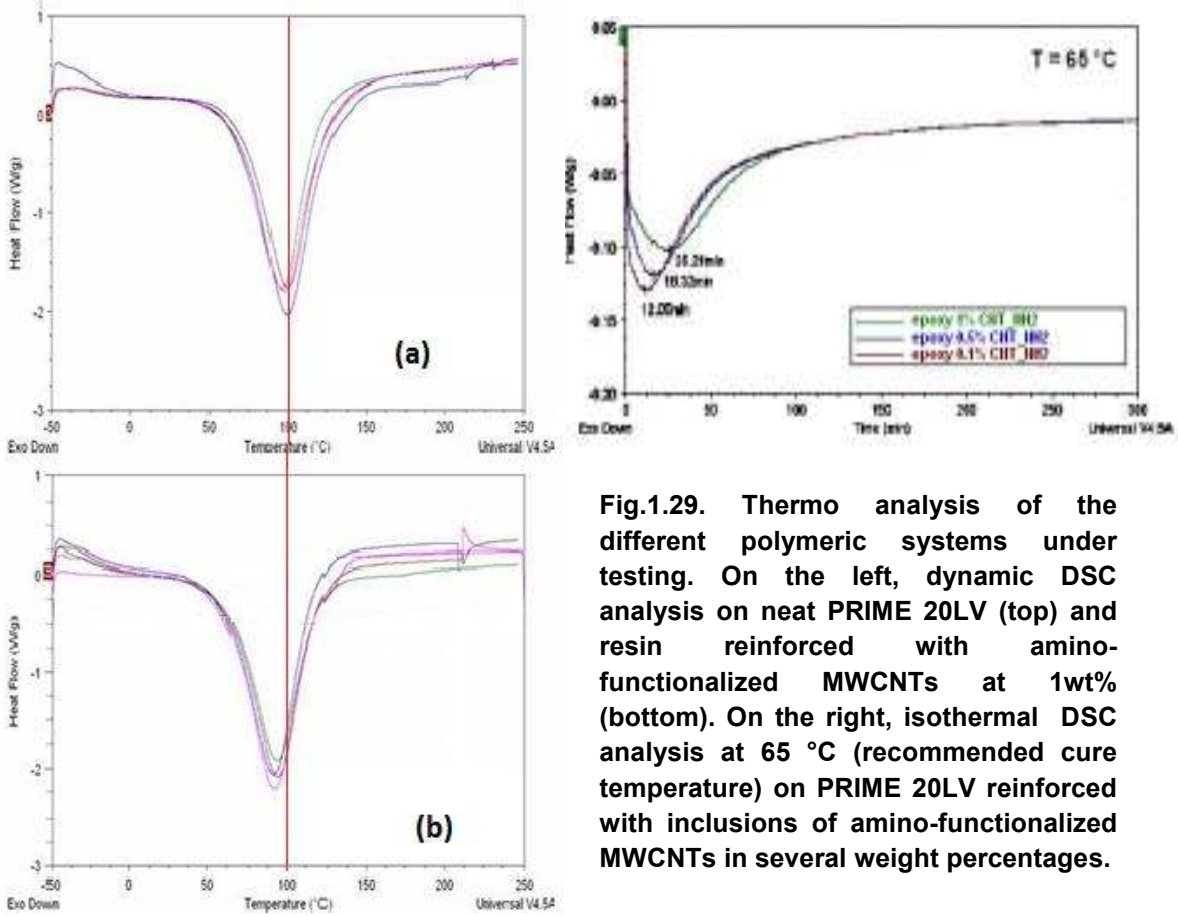

Fig.1.29. Thermo analysis of the different polymeric systems under testing. On the left, dynamic DSC analysis on neat PRIME 20LV (top) and resin reinforced with amino-functionalized MWCNTs at 1wt% (bottom). On the right, isothermal DSC analysis at 65 °C (recommended cure temperature) on PRIME 20LV reinforced with inclusions of amino-functionalized MWCNTs in several weight percentages.

Schematically, the manufacturing procedure adopted to realize two samples for the test described in the third chapter provides for: mixing of carbon nanoparticle powder (in a given wt% versus resin) with about 10g of resin and 2.6g of hardener by means of ultrasonication (power 750W, frequency 20kHz, amplitude 30%) for 90s, pouring of the liquid mixture into the mold (see Fig.1.30), and final polymerization at 65°C for 8h. Filler dispersion quality and material porosity are key features for the knowledge of the

mechanical properties: the surfaces of sample fracture have been examined by SEM in order to determine the quality of the structure, and to validate the manufacturing process. One critical aspect in the practical use of micro and nanoparticles in composite materials consists in achieving a random dispersion inside the matrix and so obtain an homogeneous material. As a consequence, an accurate dispersing process is required to uniformly mix the carbon powders within the resin and to avoid air bubbles formation inside the mixture as well (see Fig.1.31). Such an issue has been tackled using an ultrasonic liquid processor, allowing to blend powder, resin and hardener with high homogeneity and few inner voids formation. The results obtained (see Fig.1.32) have confirmed us about the goodness of the sample manufacturing process.

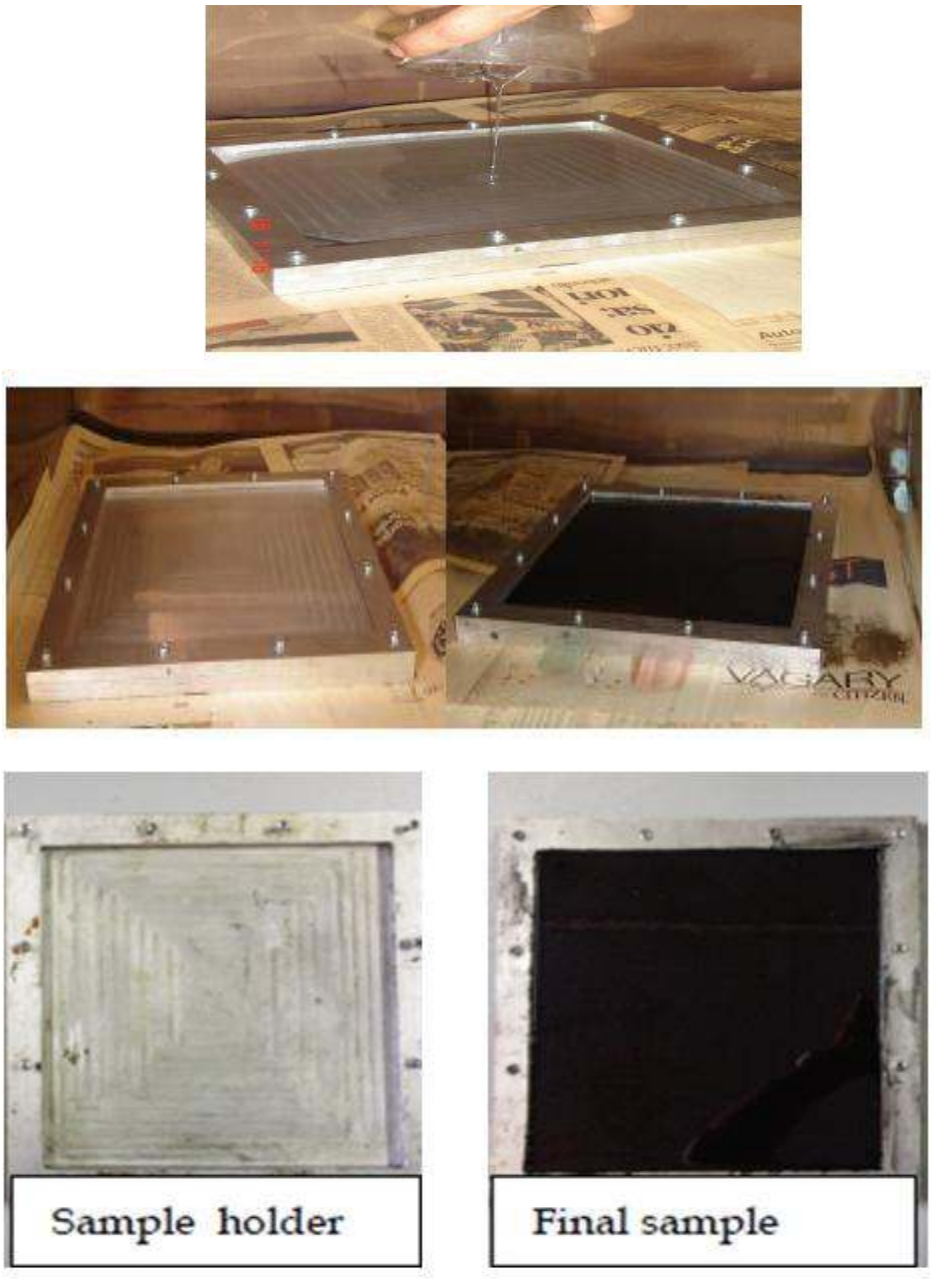

Fig.1.30. CNT-reiforced Epoxy-based composite sample preparation: pure and CNT-filled Epoxy pouring into the Aluminum molds .

Fig.1.31. CNT-reiforced Epoxy-based composite sample preparation: viscosity lowering and air voids removal by means of ultrasonication methods.

Dispersion quality is a key feature for the knowledge of the desired properties, as well as porosity and roughness are essential for the measurement of the mechanical properties. The nanocomposite samples were examined by SEM in order to determine the quality of the structure. Typical FE-SEM images of pristine and amino functionalized MWCNT-based composites are shown below. To evaluate both composites porosity and dispersion state of the nanoparticles in the epoxy matrix, Fig.1.32a-d show the SEM images of fractured cross section of the composites. They show high level of dispersion in the functionalized-MWCNT filled composites versus the pristine MWCNT filled ones, although occasional small aggregates were observed in the higher viscosity samples of 1wt%: this aggregation should affect the mechanical properties as described above. The comparison between the medium and low viscosity epoxy composites showed that the dispersion of low viscosity epoxy composites was better than the high viscosity epoxy composites due to the different polymer viscosity. In fact, the medium viscosity Epoxy-based materials were very viscous and the homogenization process was difficult. A good dispersion of nanoparticles with an enough large aspect ratio seems to be control parameters, suggesting to use pretreatments on the nanofillers before they are added into the matrix. Fig.1.32e-f show SEM images of voids on the fracture surfaces of nanocomposites. Occasional voids are particularly observed in the epoxy matrix when the fillers content is made by treated-MWCNTs, whereas larger inhomogenities can be revealed in the case of raw CNT-based filler. As expected, the void contents and voids size increases with increasing MWCNT loading. This may be attributed to the existence of voids in the interface between the nanoparticles and the polymeric matrix due to poor wettability. This indicates that the infiltration of liquidized epoxy becomes more difficult with increasing MWCNT loading. The removal of voids in the composites becomes difficult with increased filler content, because the viscosity of epoxy resin before curing is increased with nanofiller content and is difficult to expel the bubbles. By previous experience it was estimated that the dispersion of nanoparticles was not good using the manual mixing process because of the high viscosity of the epoxy polymer: therefore, some means to inhibit the formation of void is necessary. Our research indicate that the

ultrasonication process adopted gives good results in terms of high reproducibility and dispersion, and low porosity; of course the manufacturing procedure can be improved by optimizing the sonication parameters (amplitude, time, mixture amount) as well as performing suitable chemical pretreatments of the nanofillers.

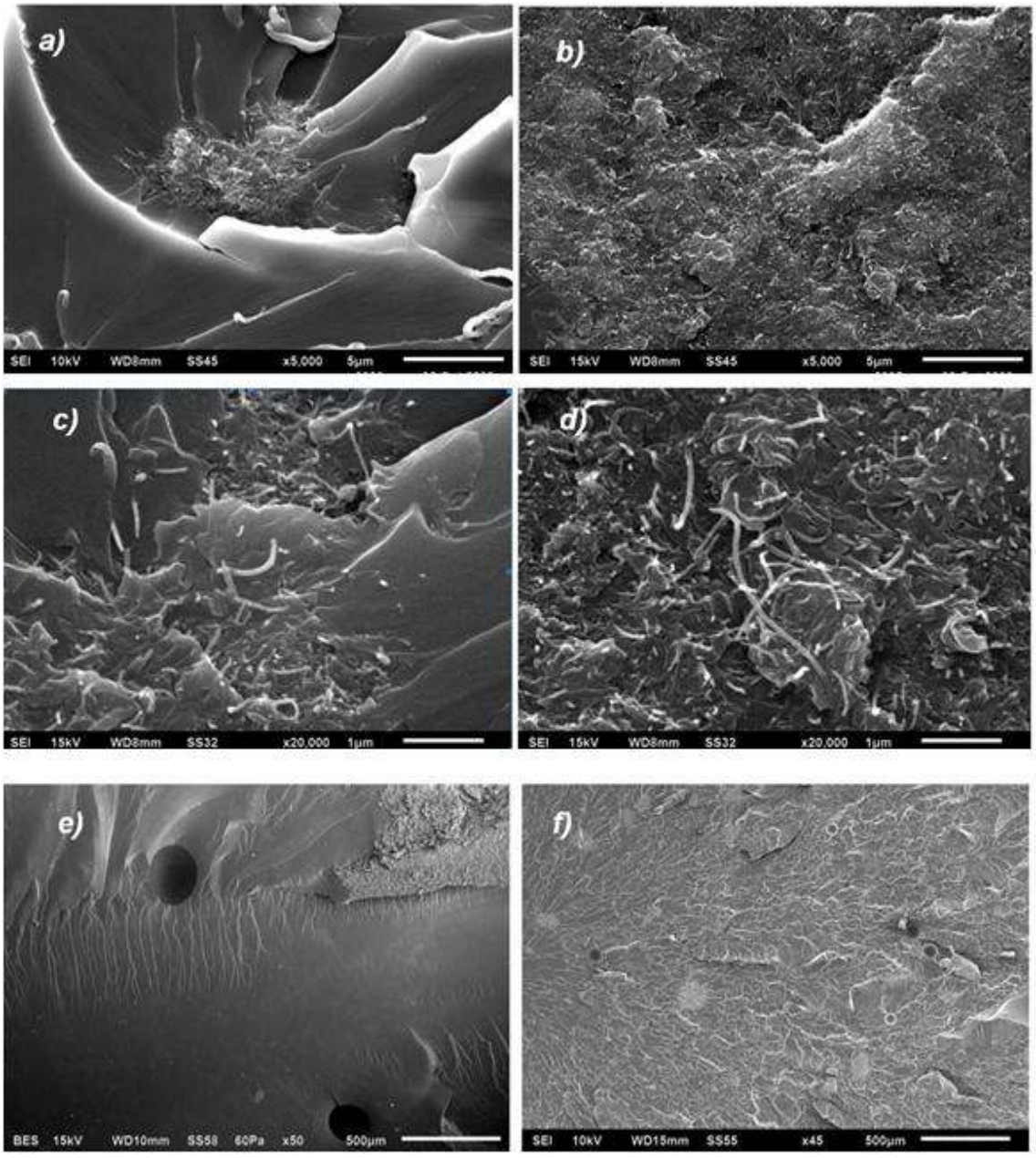

Fig.1.32. SEM characterization of 1wt% MWCNT-reinforced Epoxy-based composite materials (images taken by means of *Jeol* FE-Scanning Electron Microscope). Medium (a-b) and high (c-d) magnification of samples fracture surface highlight the poor degree of dispersion of pristine (left) MWCNTs inside the matrix, when compared to the highly homogeneous morphology of the amino-MWCNT reinforced composites. Low magnification micrographs on the bottom show the porosity level of the realized samples, with the larger voids in the case of not-treated filler (e) than the occasional lacks of homogeneity discovered in the functionalized-MWCNT reinforced materials.

1.3.2 Nanofluid-reinforced fabric production

In this section the procedures adopted for the shear thickening nanofluids realization and the Kevlar-reinforced fabrics manufacturing are basically described, providing rheological and morphological characterization of the materials under testing too. Silica nanoparticles (n-SiO_2, *Sigma Aldrich* Fumed Silica powder 0.007μm) and Polyethylene glycol (PEG, *Sigma Aldrich* Poly(ethylene glycol) average mol wt 200) have been chosen as nanofiller and carrier fluid respectively, to follow the tracks of the most remarkable results in STF applications for absorbing impact energy [259-261]. Ethanol (*Sigma Aldrich* Ethanol puriss. p.a., ACS reagent) was used as solvent for nanopowder disentanglement and dispersion within the polymeric matrix. SEM images of the as-received silica nanoparticles are shown in Fig.1.33 below.

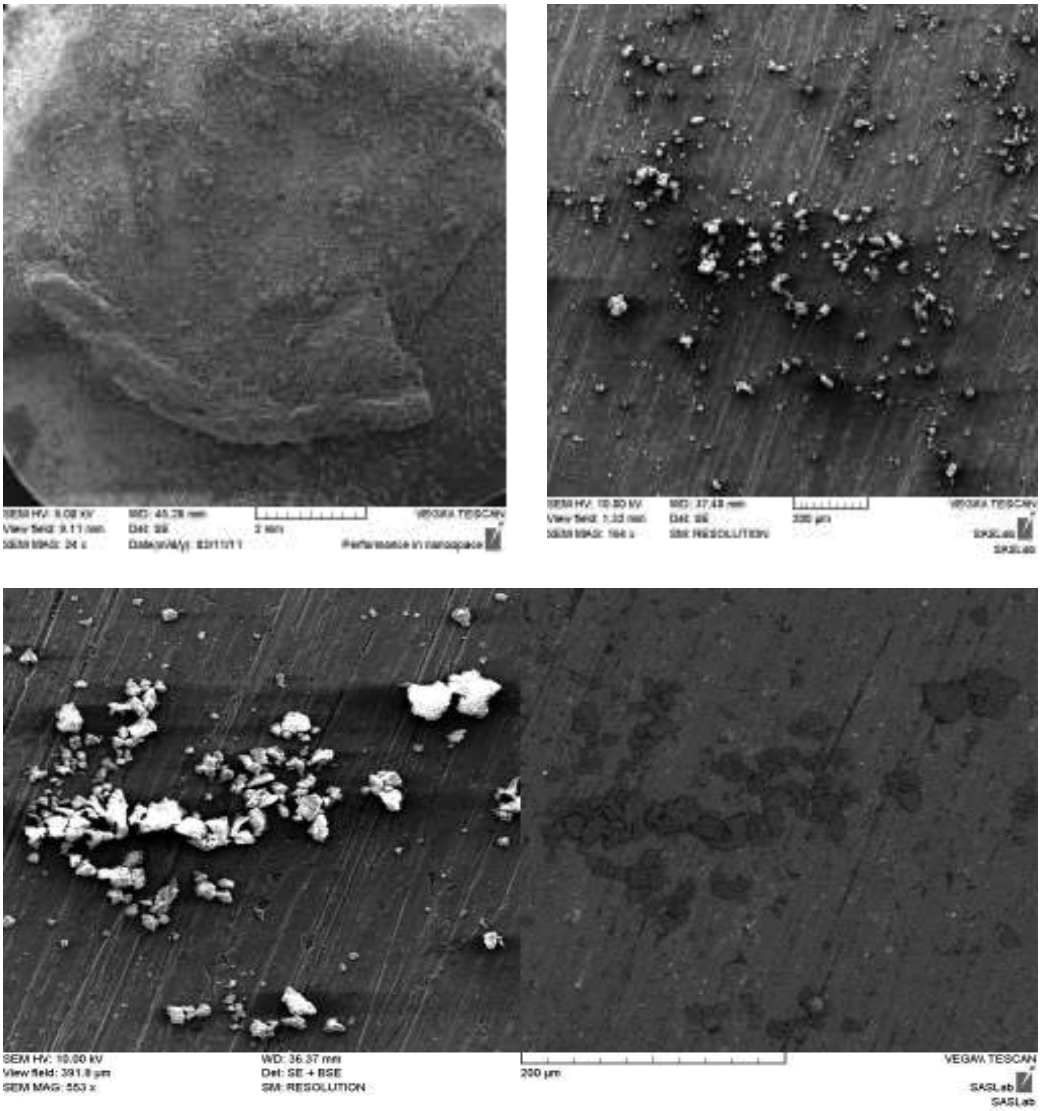

Fig.1.33. Low (top-left), medium (top-right), and high (bottom) magnification SEM photos of the silica nanoparticles adopted; the BSE image enhances the high degree of the as-received material homogeneity.

1.3.2.1 *STF preparation*

Several are the parameters of the procedure for the solution preparation and, moreover, their combination greatly affects the efficacy of the later fabrics impregnation (i.e. the effective nanofluid amount intercalated between the fibers) as well as the ballistic behavior of the final manufactured test article. Mixing tools are fundamental to achieve a correct preparation of the nanostructured solution, since a suitable nanoparticles dispersion inside the liquid matrix and the subsequent mixture homogenization are absolutely not trivial tasks, in particular in case (as the present) of substantial filler weight percentages.

Nanopowders very high "surface area" (surface/weight ratio, in the case of the adopted nanoparticles the value 390 m^2/g is reported in the data sheet) give rise to so huge volumetric gaps between the host fluid and the filler (dry nanopowder volume may be one order of magnitude greater than the matrix volume). Beside the dilution in organic solvent (which must be used in controlled excess to avoid the whole mixture degradation) a first mechanical mixing to gradually introduce the nanoparticles in solution has been needed. Then, 20kHz ultrasonication technique was adopted to exfoliate the micrometric agglomerates in which the nanoparticles are typically entangled, in order to increase the mixture homogeneity as well as to reduce the presence of internal air voids. During this step an increase by several tens degrees of the solution temperature may occur, due to the relatively high energy quantities exchanged: as each case requires (i.e. depending on parameters as solvent amount, evaporation rate, compound thermal stability, etc.) the sonication can be carried out in thermostatic environment or not. Of course, the timing procedure strictly depends on the material quantities utilized, which in turn are linked to the characteristics (surface dimensions and absorption rate) of the specific fabric typology treated.

Schematically, the method for the preparation of by about 120g of nanofluid loaded at 20wt%, an amount estimated to perform the full treatment of eleven 16×16cm layers of reference batavia Kevlar fabric (see later) consists of the following steps: 60g of PEG mechanical 500rpm mixing in 200÷300ml of solvent for about 10 minutes, gradual addition of 12g of silica nanoparticles, high energy ultrasonication (50% of mixer maximum power) for about 30 minutes, low energy ultrasonication (25% of mixer maximum power) for about 4 hours in low temperature (0÷5°C) environment, and low energy ultrasonication for about 2 hours in warming temperature (up to 50°C). The result of such procedure is an homogeneous solution of volume reduced to 80÷120ml, mainly due to the evaporation of a certain amount of solvent as well as to the nanoparticles/polymeric macromolecules coupling inside the solution (testified by an evident chromatic transition from opaque to quasi-transparent solution).

Whereas the next step for the fabric-reinforced manufacture should be the fabric impregnation in the solution (followed by the total evaporation of the solvent in excess), in order to obtain directly a fluid with non-newtonian (bulk) properties the complete solvent evaporation is required (6÷8 hours at 70÷80°C are typically enough). In

Figs.1.34-1.35 the morphological and rheological characterizations of several nanosilica wt% filled PEG solutions are respectively reported: in the SEM images the n-SiO_2/PEG chemical interaction is highlighted, while the viscosity/shear measurements (performed by parallel-plate rheometer) give evidence of the STF fashion as from 10wt% of nanosilica inclusion (showing the typical knee [5,9,10] at shear of about 10Hz) and a quasi-solid behavior for 15wt% and over loading.

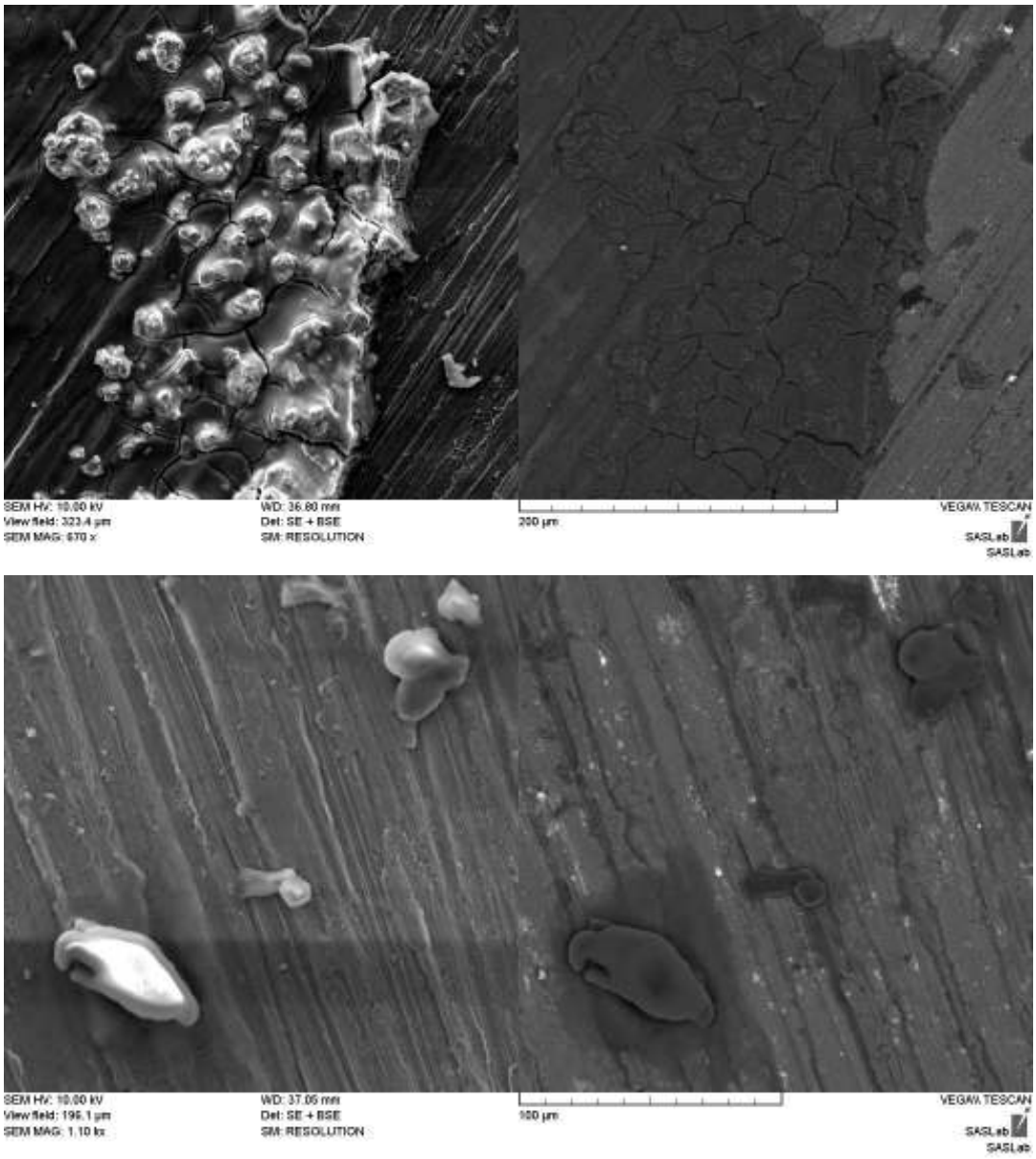

Fig.1.34. Low (up) and medium (down) SEM photos of a drop-sample from a solution realized with n-SiO_2 at 20wt% inside PEG matrix after the ethanol evaporation. The SE images (left) shows the coupled morphology of the two chemical species, the correspondent BSE ones (right) enhances the excellent mixture uniformity degree and the very low amounts of inner voids.

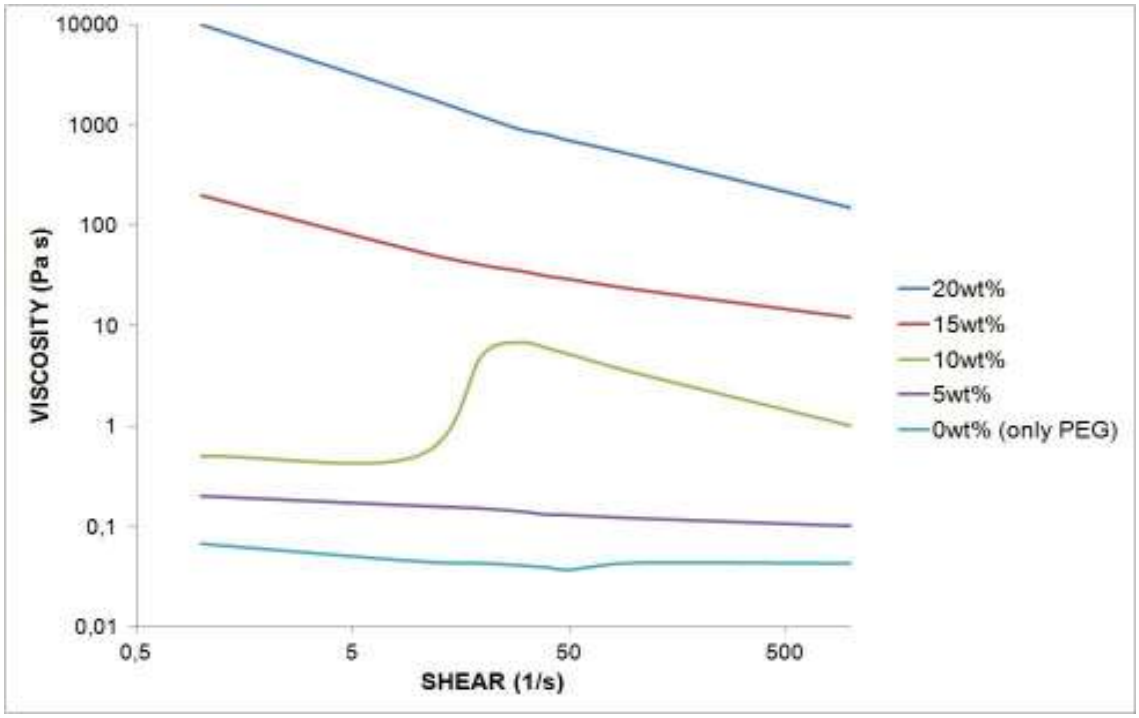

Fig.1.35. Viscosity/shear behavior of mixtures loaded with different weight percentages of nanosilica (measurements performed by parallel plate rheometer, shear 1 1/s to 1000 1/s, T 25°C): an evident phase transition (non newtonian behavior) is detectable around shear values of 10 Hz for the solution loaded at

1.3.2.2 *STF-Kevlar processing*

Three textile materials have been treated with the different wt% loaded solutions realized. In Tab.1.4 below their main characteristics are listed. XP Kevlar is highlighted to pick out its reference as starting best material in terms of density and claimed ballistic properties: this advanced *DuPont* material is produced by not trivial polymeric/fiber intercalation treatment, resulting in high compact thin lightweight paper-like flexible structure. B Kevlar is a conventional typology of aramidic fiber woven, while hybrid KN material results from an experimental try to couple spongy waste Kevlar to commercial Nylon fabric.

material	symbol	areal density (kg/m^2)
DuPont^{TM} Kevlar XP	**XP**	0.51
Saatilar batavia 4/4	**B**	0.62
hybrid Kevlar-Nylon	**KN**	0.65

Tab.1.4. Main characteristics of the three Kevlar-based fabric tested.

The fabric impregnation with n-SiO_2/PEG mixtures diluted in solvent has to take place in relatively prompt way, in order to avoid unevenness treatment of the several layers due to potential physical/chemical changes of the post-sonicated solution (further solvent evaporation, filler sedimentation, cluster formation, etc.).

For each kind of fabric and of mixture concentration the suitable fluid amount needed to achieve the maximum absorption is preliminary estimated. That is necessary because the highly diluted solutions saturate the fabrics with an effective n-SiO_2/PEG absorption lesser than how potentially possible, as clear from halfway imbibitions and weight control operations. Such evaluation is performed by wetting drop by drop a layer of fixed dimensions until the first saturation, waiting for solvent evaporation in oven at 70÷80°C (considered run out when the weight reduction is less than 1% for measurements taken one hour apart), impregnating again and so on, until the dry layer weight has stabilized. For each kind of material the absorption properties (i.e. the weight increase) must be strictly linked to the results of the ballistic test, thus are reported in details in the experimental section. From a qualitative point of view, the following general considerations can be pointed out by visual inspection as well as SEM morphology investigations (Figs.1.36,1.37).

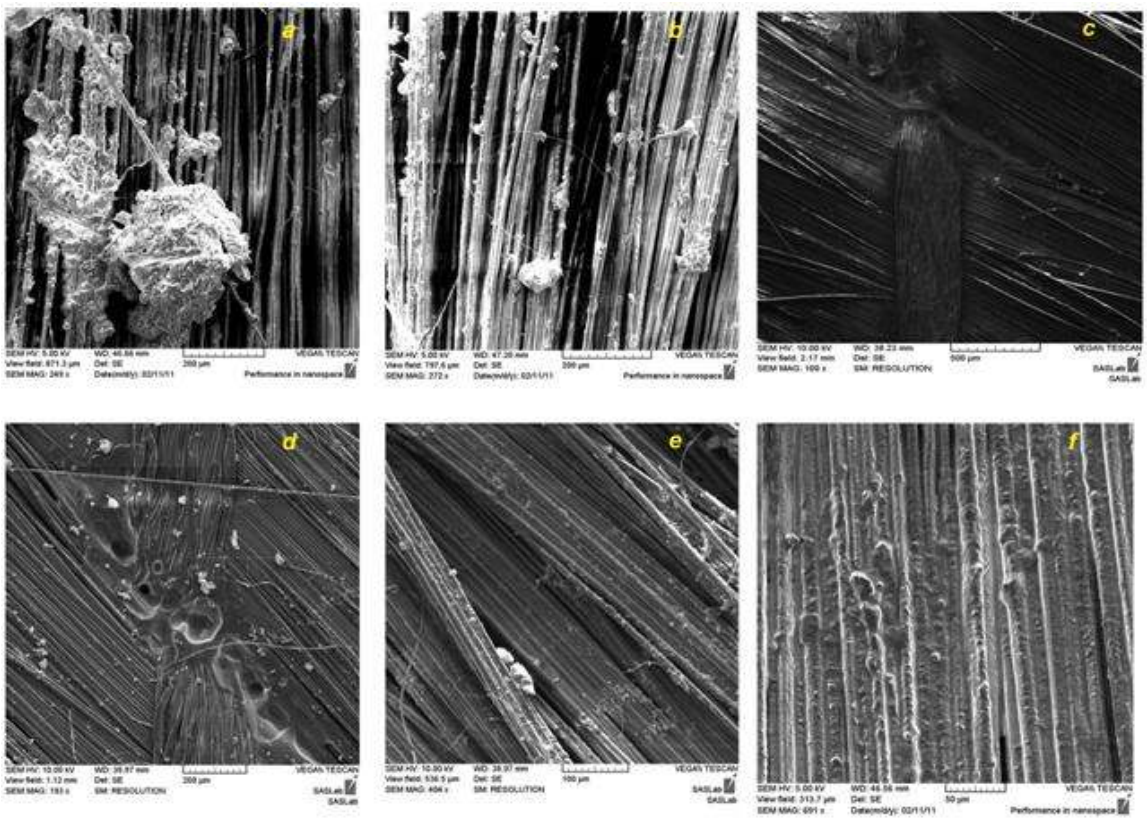

Fig.1.36. SEM images of neat/STF-reinforced fabrics: a)-b) B fabric treated with 50wt% STF solution; c) XP fabric neat morphology; d) XP fabric treated with 10wt% STF solution; e)-f) B fabric treated with 10wt% STF solution.

Very high concentration (>20wt%) mixtures reinforced fabric show a so poor manufacturing degree (Figs.1.36a-b), with the presence of a clotty gloss weakly attached to the layer surfaces; XP fabric is basically refractory to the treatment due to its above mentioned chemical composition, as clear from so low absorption rates and structure degradation phenomena (cfr. Figs.1.36c-d); B fabric shows the best behavior in terms of fibers-nanofluid interaction, resulting in highly uniform woven bulk structure (Figs.1.33e-f); KN fabric is treated only on the Kevlar side, which presents a tridimensional woven mat (Fig.1.37a) that assists the absorption mechanism (Figs.1.37c-d), while the hydrophobic Nylon backside surface (Fig.1.37b) doesn't show any kind of interaction with the fluid.

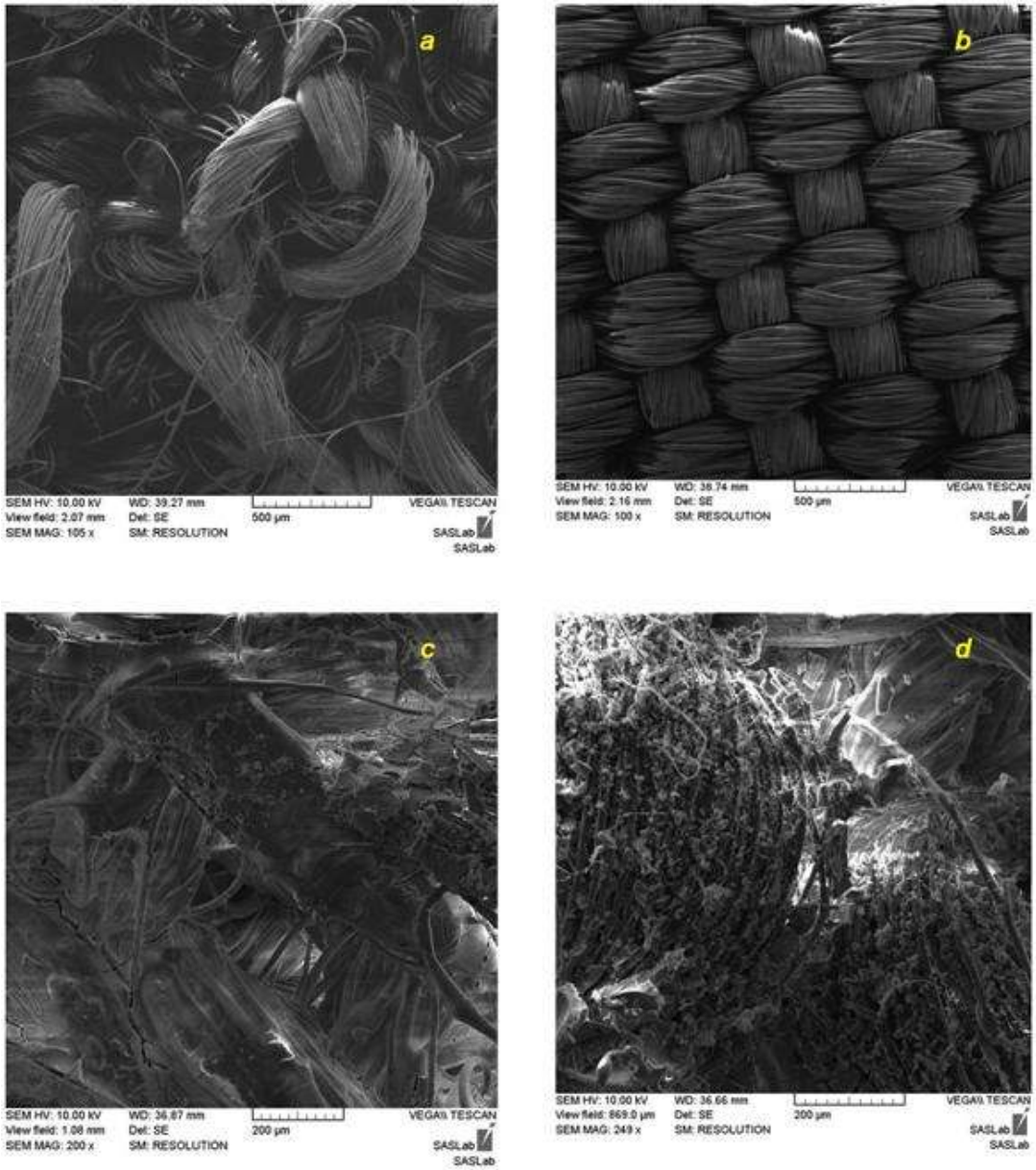

Fig.1.37. SEM images of neat/STF-reinforced fabrics: a) KN fabric neat morphology, Kevlar side; b) KN fabric neat morphology, Nylon side; c) KN fabric treated on Kevlar surface with 10wt% STF solution; d) KN fabric treated on Kevlar surface with 20wt% STF solution.

The procedure of fabric impregnation consists in the simply dipping within a bowl filled with the suitable solution amount, then the layers are squeezed (Fig.1.38a) and put inside the oven for the solvent evaporation (typically 6÷8h at 70÷80°C, see Fig1.38b). Finally, the treated layers are enveloped with polyethylene sheets (Fig.1.38c-d) in order to minimize the loss of material not perfectly stuck on the surfaces and to avoid unwanted interaction at the interfaces between neat/treated surfaces (lubrication or degradation of fluid incompatible fabrics). Fabric-reinforced flexibility has been discovered essentially unchanged comparing with neat material, even in the case of treatments with high concentration nanofluid mixtures.

Fig.1.38. Different steps of Kevlar-reinforced based antiballistic panels manufacturing: a) fluid application onto layers surface, b) solvent evaporation in oven, c) enveloping procedure, d) the panels ready for the ballistic test.

2 BALLISTIC EQUIPMENT

The ballistic characterization of the above described manufactured materials has been performed by means of an in-house built device called Coil Gun, that is a typology of the more general electromagnetic accelerators equipment class. The idea to use intense electromagnetic pulses to exploit the intriguing matter/field interaction for propulsion applications is not so new, the first scientific researches in this area being carried out since many decades ago. Several important results have been achieved in terms of ballistic performances, at the present time, anyway, the technological challenge is to reduce the system devices cost, weight and dimensions in order to compete with the conventional ballistic facilities. After a brief remarks on the topic of the electromagnetic accelerator, in this chapter the realization and characterization of the in-house built Coil Gun is presented and discussed.

INDEX

2.1 Electromagnetic Accelerators

Electromagnetic (EM) launch has the potential to revolutionize a wide range of defense applications including tank gun, artillery, and aircraft launch [262]. The EM launch concept has been demonstrated as the Army and other services have recently fabricated and tested several prototype gun systems. Advanced materials and manufacturing techniques played a major role in this achievement [263]. The engineering development necessary for a fieldable system is considerably more difficult than the laboratory systems. The design of the current laboratory system is not fully optimized from a mechanical and materials performance aspect. Application of advanced materials with innovative design concept in various critical components of the system is in progress under the current program at the US Army Research Laboratory (ARL) and Armament Research and Development Center (ARDEC).

The first recorded mention of cannon launch to space is in the novel *From the Earth to the Moon*, written by Jules Verne in 1865. Research on the subject has an equally long history, and includes both explosively and electrically powered cannons. However, throughout this history, none of the concepts have been studied to an extent that could be considered exhaustive, compared to, for example, the amount of research and development that led to successful commercial aircraft. Because of contemporary improvements in materials and electronics, promising ideas from the past can be further advanced through experiments performed on a modest budget [264, 265].

The first large effort to develop EM launch was undertaken by Kristian Birkeland [266]. Birkeland's background was in electromagnetic waves, especially their role in energy transfer. He performed pioneering research on the aurora borealis, Saturn's rings, cosmology, and comets. Birkeland also conducted research on hydroelectric power stations. It was during the course of one of these experiments that he observed pieces of iron being pulled through coils, turning the iron into a projectile. Within a year, Birkeland had obtained funding to build his first electromagnetic gun, the patent for which was filed September 16, 1901 (see Fig.2.1). In this gun, a magnetized iron projectile is pulled by a series of solenoids. As the projectile passes each solenoid, an attached wedge pushes apart contacts, opening the circuit of each solenoid in succession. A few months after the first patent application was filed, Birkeland filed a second application, for the use of a coil instead of solid iron as the projectile. In April 1902, Birkeland filed his last patent related to electromagnetic gun research. It contained several improvements, the most significant of which was the switching method. The inductances of the projectile and drive coils would be matched so that the back EMF due to the drive coil would equal the voltage applied to the projectile coil as the projectile passed; the switches would then open at zero current. This idea was rediscovered in 1993 by Ingram. The highest speed achieved was 100 m/s, with a mass of 10 kg, fired from a 4 m cannon. Birkeland also appreciated the main obstacle to higher speeds, "the problem of finding an energy source that could deliver enough

power within a fraction of a second." The experimental guns were powered by dynamos. A rotating wheel power supply, most likely a Faraday disc, appeared in the first patent application. This power supply would be important in electromagnetic launch research beginning in the 1970s. Birkeland's cannon design seemed poised for success. A well-funded public company, Birkeland Firearms, had been organized. In order to raise enough capital for other research, an electromagnetic gun demonstration was held in 1903. During this demonstration, before which Birkeland had promoted the gun as operating silently, a very high current short occurred, which was not at all silent, and the value of the company's stock decreased to zero.

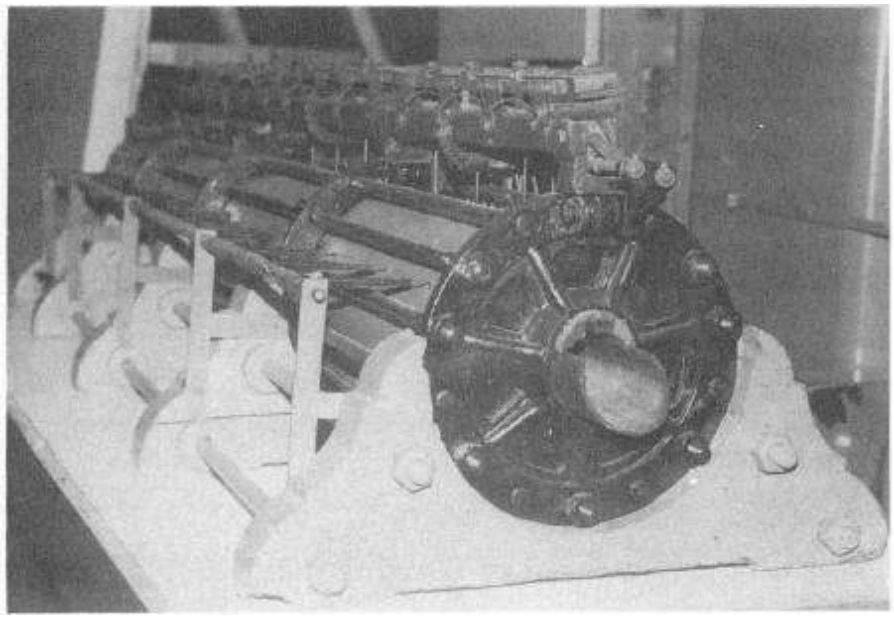

Fig.2.1. 1901 Birkeland gun.

The so-called "Paris Guns" were built by the Krupp company during WWI for delivery of explosives to Paris from positions near the German front lines, a distance of about 130 km. The project was supervised by Fritz Rausenberger and Max Bauer, and was technically successful, although it had little strategic effect. The muzzle speed of the 106 kg shells was over 1500 m/s (see Fig.2.2). All of the guns were destroyed at the end of the war to prevent capture [267].

The next notable electromagnetic launch effort occurred during the 1930s, and was led by Edwin Northrup. Northrup was a professor at Princeton University, and founded a profitable induction furnace company. Unlike the Birkeland guns, which were intended for use by the military, Northrup advocated the use of EM launch for reaching orbit, as presented in his novel *Zero to Eighty* [268]. The Northrup design, several of which were constructed, used a three-phase AC power supply. The gun barrel was divided into

sections, with each section consisting of six coils, connected so that each was 60 degrees out of phase with the next (Fig.2.3). The traveling wave of the drive coils induced a current in the projectile coil. A scheme was also presented for using a sliding contact attached to the projectile to energize one section of drive coils at a time. The coils were wound from copper tubing so that cooling water could be provided. Speeds were not published.

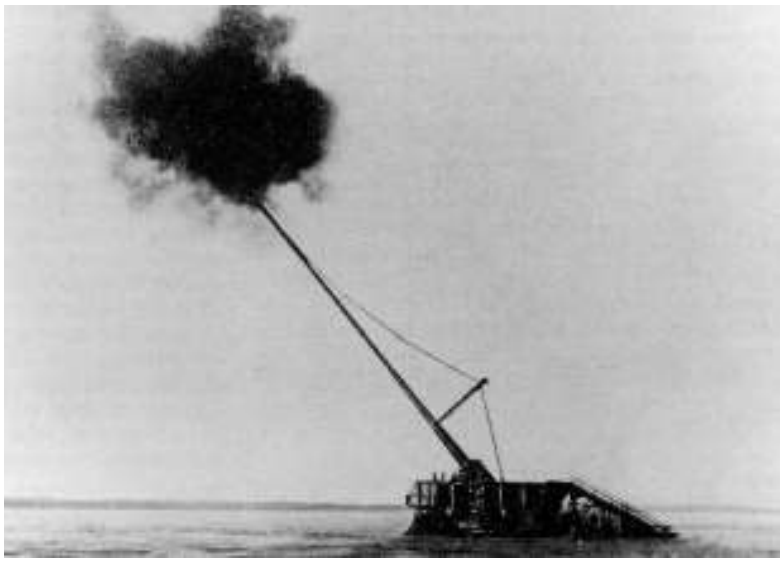

Fig.2.2. 1918: the Paris Kanonen.

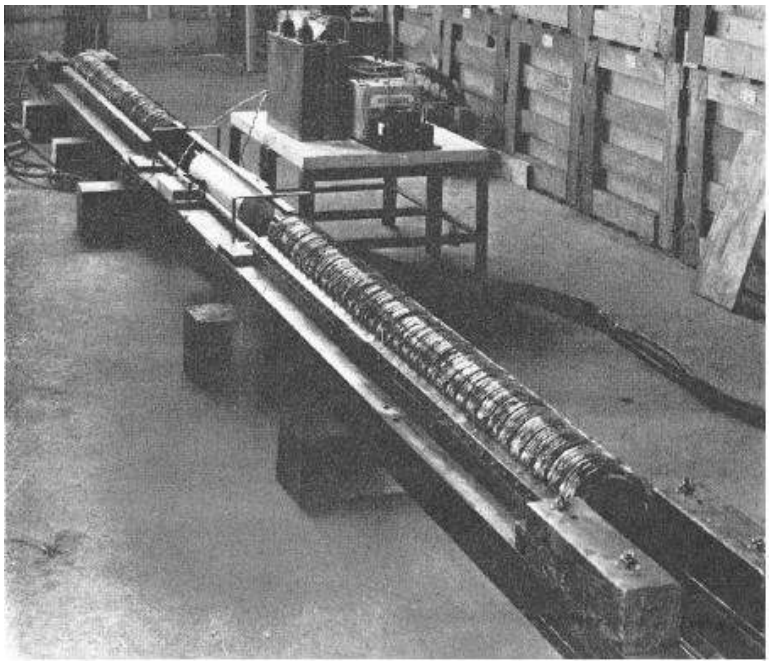

Fig.2.3. 1936 Northrup coil gun.

The traveling magnetic field in the Thom and Norwood [269] accelerators was created by sliding contacts that moved with the projectile coil (see Fig.2.4). They tried three configurations. In the first, four sliding contacts carried current from the power supply into the coils. One contact carried current from the supply rail into the driven coil. From the driven coil, another contact supplied the drive coil. A third contact picked up current from the drive coil, and a fourth contact carried current back to the return rail. In this way, only a section of the drive coil that moves with the driven coil is energized. The second and third configurations used two sliding contacts, one to pick up current from the supply rail, and one to make a connection between the driven coil and the drive coil. The current returned to the supply through the drive coil. The length of the energized section of the drive coil therefore changes during the shot. In configuration two, the winding sense of the coils is such that the driven coil is pushed ahead of the energized drive coil. The energized section lengthens behind the driven coil. The third configuration is similar, but the driven coil is pulled, and the energized length decreases. These methods of brush commutation were investigated by Kolm et al. [270] at the Bitter magnet lab at MIT in the 1980s and are now being studied at the U.S. Naval Research Laboratory. The sliding-coil accelerators were powered by a 2000 V, 5000 J capacitor bank. A capacitor bank of this size costs only about a thousand dollars today. Thom and Norwood also derived a minimum mass for accelerators in which the projectile is a conductor in a magnetic field that is generated by another part of the circuit. The projectile is heated by ohmic losses. For a given speed, there is a minimum mass projectile that can absorb the losses without melting. Winterberg in 1966 [271] sought to circumvent this limit by using a superconducting solenoid with a persistent current as the projectile.

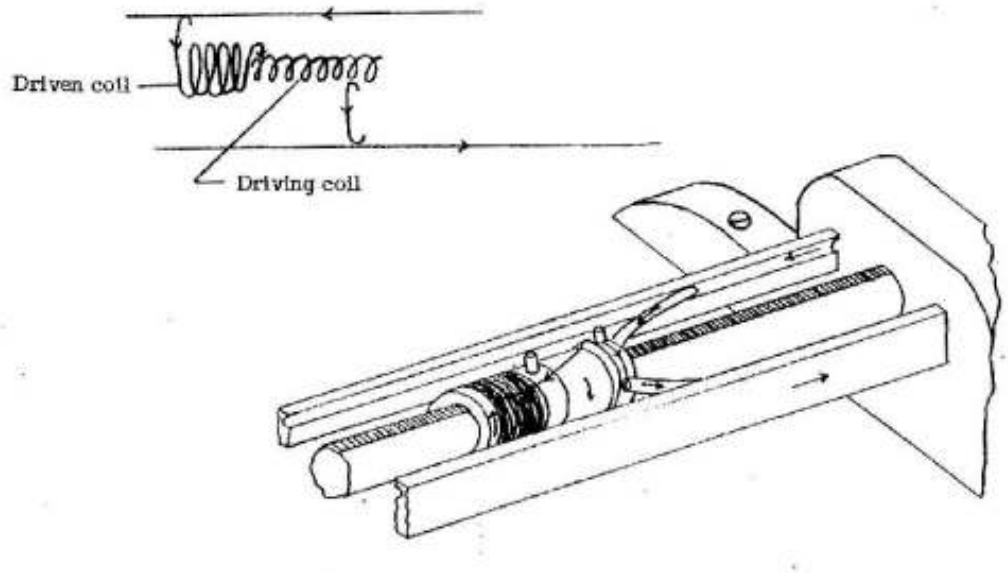

Fig.2.4. 1961 Thom and Norwood coil gun with sliding contacts.

The High Altitude Research Program (HARP) was funded by McGill University, under the direction of Gerald Bull, and the U.S. Army Ballistic Research Laboratory, under the direction of Charles Murphy [272]. The goal of the program was to develop a low-cost method of conducting atmospheric and space research (Fig.2.5). HARP produced cannon launch altitude records that have yet to be broken. The highest apogee, achieved not just once, but 15 times during a four-day period in 1966, was 180 km. The mass of the rocket-shaped projectiles launched to this altitude was 100 kg, and the muzzle speed was 2100 m/s. This altitude is well above the conventional definition of the threshold of space, 100 km, and in fact above the altitude that is necessary for a satellite to orbit without excessive atmospheric drag, 150 km. The barrels of the HARP cannons had smooth bores, so fin stabilization was necessary, and sabots were used to transmit the pressure of the combustion gases to the projectiles. Later projectile designs included fins that popped out of the projectile body after launch. Guidance and sensor electronics were developed that withstood the large initial accelerations.

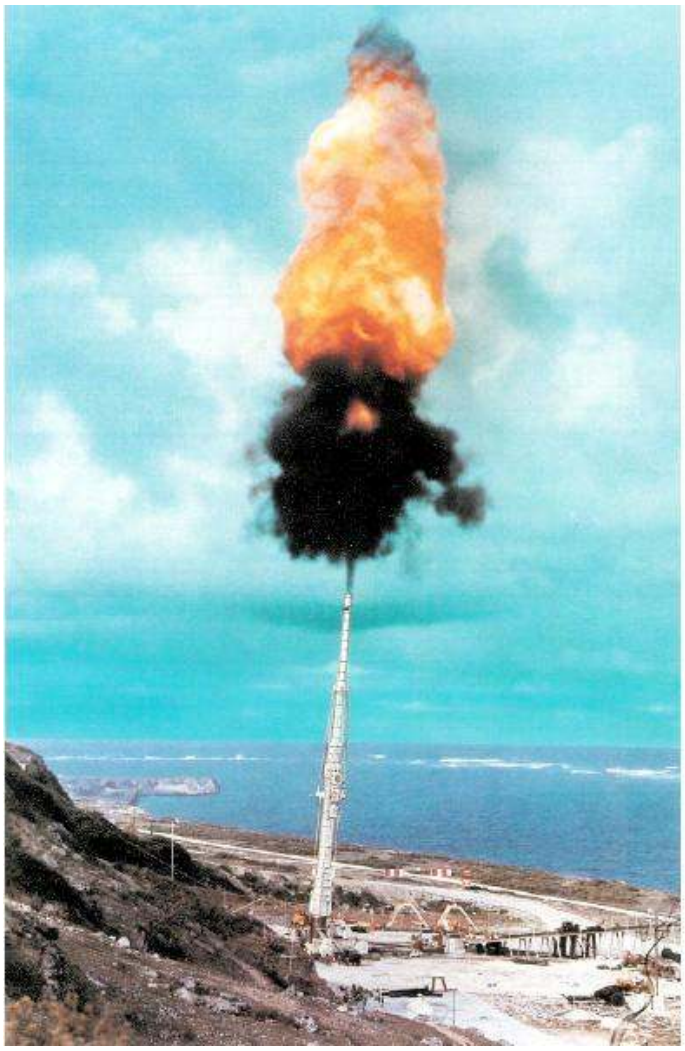

Fig.2.5. 1960s High Altitude Research Program (HARP).

The driving coils in the Winterberg design are powered by capacitors, one capacitor per drive coil. For properly selected component values, the capacitors and coils act as a transmission line (Fig.2.6). Synchronization of the projectile with barrel is not necessary; othe than the single initial switch, operation is passive. Unfortunately, no device based on this idea has been built. However, the term “collapsing field” which was to reappear at the University of Texas in 1993, was used by Winterberg.

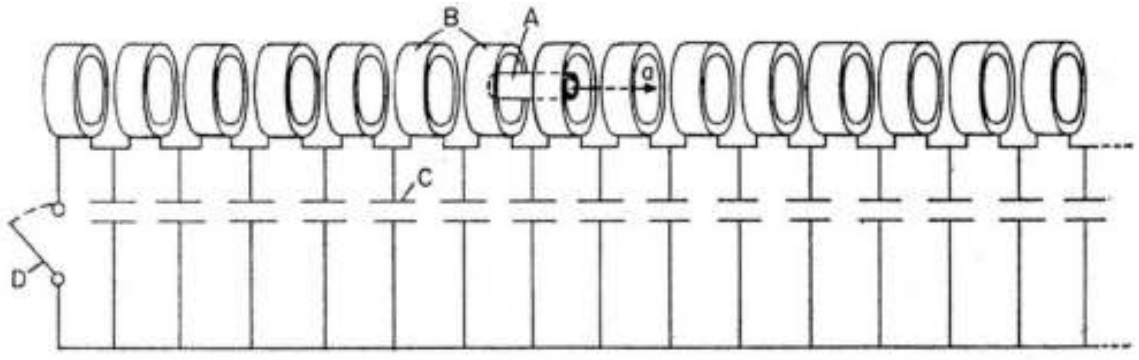

Fig.2.6. 1966 Winterberg transmission line coil gun.

The great interest in electromagnetic launch for military applications began in Canberra, Australia, in the early 1970s. Richard Marshall and others, including John Barber, attached a homopolar generator to a rail gun [273-275]. Rail guns consist of two conducting rails with a sliding conductor between them (Fig.2.7). When current is applied to the rails, the magnetic field generated by the rails interacts with the current flowing through the sliding conductor, producing acceleration. The Canberra generator, which was surplus from high-energy physics research, was two stories tall and stored 500 MJ. The system accelerated 3 g polycarbonate cubes to 6 km/s in 5 m. The current between the rails was carried by a metal vapor arc behind the polycarbonate cube. The impressive speed generated by the Canberra group led to investigations by other groups. Although work continues on rail guns, and has increased projectile masses to the order of kilograms, rail guns have several disadvantages compared to other types of launchers. The plasma armature causes damage to the rails, which shortens their life. This problem can be overcome. However, a more serious drawback is the rail gun inherent inefficiency. Rail guns operate at very high currents and relatively low voltages, so resistive losses are high. A large magnetic field is also left stored in the barrel at the end of acceleration. These problems can be mitigated by staging the gun, but doing this makes a railgun as complicated as a coil gun, negating out its main advantage, simplicity.

Gerard O’Neill gained a large amount of publicity for EM launch as part of his space colonization proposal during the 1970s. ONeill rebuilt the synchrotron at Cornell University during work on his Ph.D., and his experience was directly applicable to EM launcher construction. The first of O’Neill's accelerators was constructed using surplus

particle accelerator magnets. This accelerator was referred to as a mass driver. O'Neill was also involved in the construction of two more mass drivers. The mass drivers used superconducting driven coils. The goal of the research was achieving high accelerations as opposed to high speeds, so only short test sections were built.

Mongeau and Kolm [270,276] proposed storing energy in the barrel of a superconducting accelerator in 1991. They referred to the accelerator as a quench gun, and planned to use a magnetic attachment leading the projectile to induce a quench. Although the accelerator was never constructed, this is the first appearance of the idea of combining long-term energy storage with the structure of the accelerator. Independently, Samuel Ingram noted in a paper on a collapsing field accelerator using copper coils that, if the coils were superconducting, a very small power supply could be used to energize them before launch. Ingram also published the condition necessary for inductive commutation.

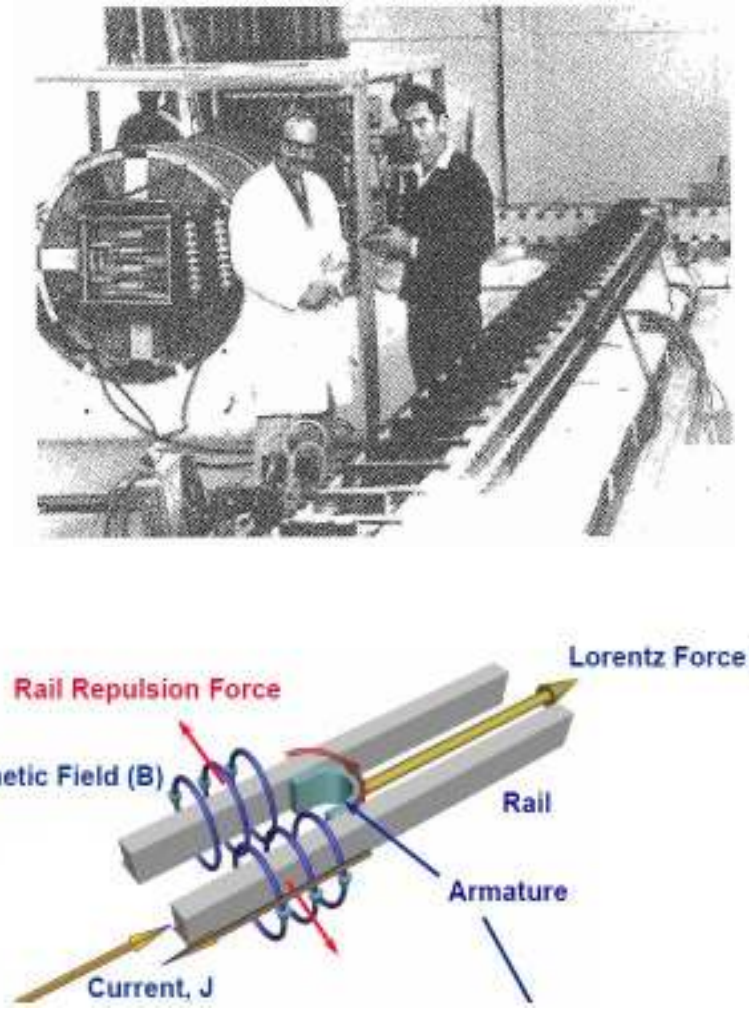

Fig.2.7. 1972 Marshall rail gun.

At Sandia National Labs, under the direction of Bill Cowan, several launchers were constructed. The first launchers had an unusual design that uses the main field of solenoidal coils rather than the fringing field. The projectile is a flat plate, which fits between two similarly-sensed drive coils. As the plate reaches the drive coils, current is switched on in them. Currents are induced in the plate that oppose the increase in magnetic field. The Lorentz force propels the plate. This can be visualized as magnetic lines of force being stretched behind the plate, and straightening as the plate passes (Fig.2.8). The launcher was therefore called the "reconnection gun" [278-280]. The reconnection idea was later applied to more conventional coaxial geometries. In these launchers, the projectile is tubular, and fits inside solenoidal magnets. The best performing guns were one flat-plate type, which achieved a speed of 1 km/s with a 150 g projectile, and two cylindrical guns, which both achieved speeds of 335 m/s (Mach 1), one with a 10 g projectile, and the other with a 5 kg projectile. A similar device, reaching a speed of 100 m/s with a kg projectile, has been constructed by a group in Chengdu, China.

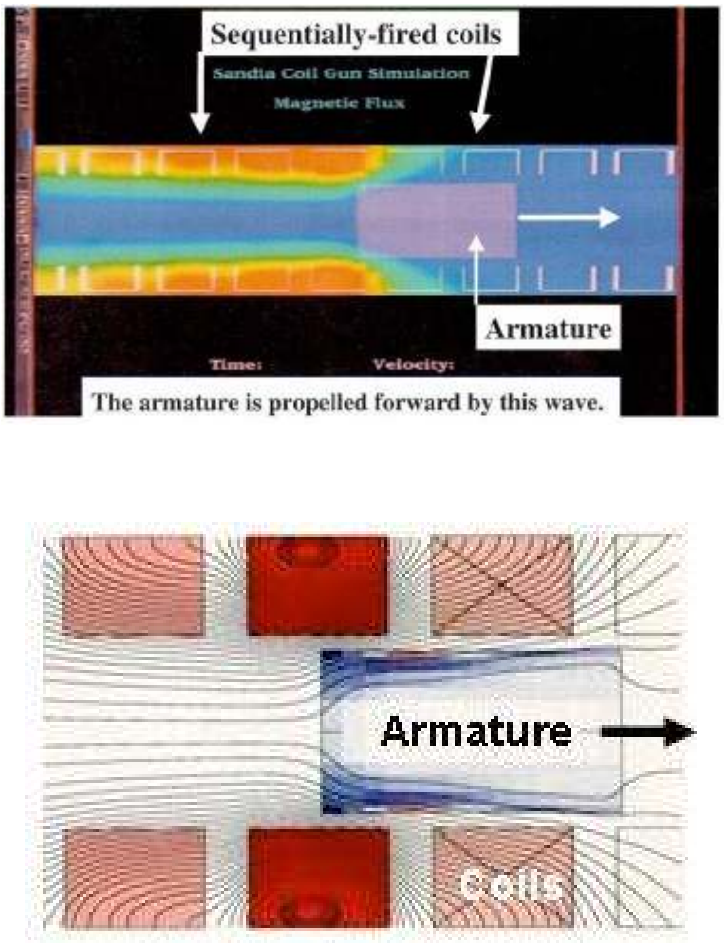

Fig.2.8. 1990s Sandia coil gun.

A project at Lawrence Livermore uses a special array of permanent magnets, called a Halbach array, to provide levitation for a projectile that can be accelerated by a linear electric motor [281-287]. In a Halbach array, magnets are tiled with orientations such that their magnetic fields reinforce to create a sinusoidally varying field on one side, and cancel on the other. As the array travels above a conductor, the sinusoidal field induces currents in the conductor, resulting in a repulsive force. The force is large enough that permanent magnets can be used for magnetically levitated trains or rocket assist. Because the force is dynamic, the system can be stable without feedback. A demonstration track has been constructed that uses capacitors (and, according to the LLNL web site, a bungie cord) to reach 10 m/s. The power source in a full-scale version would probably be existing power lines. Marshall Space Flight Center had two test tracks, one of them using the Halbach technology from LLNL. The first track was built by PRT Advanced Maglev Systems (Park Forest, IL). Originally developed at the University of Sussex, a linear induction motor provides both thrust and lift. A 14 kg mass can be accelerated to 25 m/s. The second track was constructed by Foster-Miller Inc. (Wortham, MA). It is 14 m long, with 7 m of acceleration and 7 m of passive braking. Acceleration is provided by a linear synchronous motor, while levitation is by means of a Halbach array. A sled and payload with a combined mass of 5 kg reaches 25 m/s. According to press releases, there were plans to build larger test tracks at Kennedy Space Center, but these appear to have been cancelled (Fig.2.9).

Fig.2.9. 2000 NASA Maglev tracks.

2.2 Experimental: *SASLab* Coil Gun

The goal of the present study is to perform a ballistic characterization of the nanocomposites by means of an in-house built electromagnetic Coil Gun (CG), able to explore a relatively large range of bullet velocity (up to 90m/s) with excellent precision and high degree of test reproducibility. The realization of such experimental apparatus, and mostly the optimization with a view to space debris testing planes, is quite complex since the fundamental machine parameters have high non-linearity theoretical behavior [288]. Hereafter experimental preliminary results of a prototypal device are presented and discussed. The idea to use intense electromagnetic pulses to exploit the intriguing matter/field interaction for propulsion applications is not so new, the first scientific researches in this area being carried out since many decades ago [288-290]. Several important results have been achieved in terms of ballistic performances, at the present time [291,292], anyway, the technological challenge is to reduce the system devices cost, weight and dimensions in order to compete with the conventional ballistic facilities.

2.2.1 Basic backgrounds

The CG basic background is the well known phenomenon of attraction suffered by a ferromagnetic body toward the middle of an hollow coil when a fixed current flows through this latter. As schematically depicted in Fig.2.10, the current flow produces an axial magnetic field (B_{max}) inside the coil with maximum value proportional to current intensity (I) and coil turns number (n)

$$B_{\max} = \mu_0 n\, I \tag{4}$$

around the coil central zone; the magnetic field decreases of about one half nearby the two coil's ends and goes rapidly to zero outside. A ferromagnetic object located not so far from one end of the coil suffers a strong magnetization (usually several order of magnitude greater than the magnetic induction, due to the high magnetic permeability of ferromagnetic materials), thus resulting in an axial force depending in intensity and sign from the first derivative of the magnetic field [293]:

$$\begin{array}{l} M >> B/\mu_0 \\ (\mu_r \sim 10^3 \div 10^4) \end{array} \qquad F_x = M\,\frac{\partial B_x}{\partial x} \tag{5}$$

In the case of a continuous steady current, the object's equilibrium position is clearly the center of the coil (i.e. where the body's center of mass fits to that of the coil), that is reached by friction after some (very fast) oscillations back and forth around the equilibrium center.

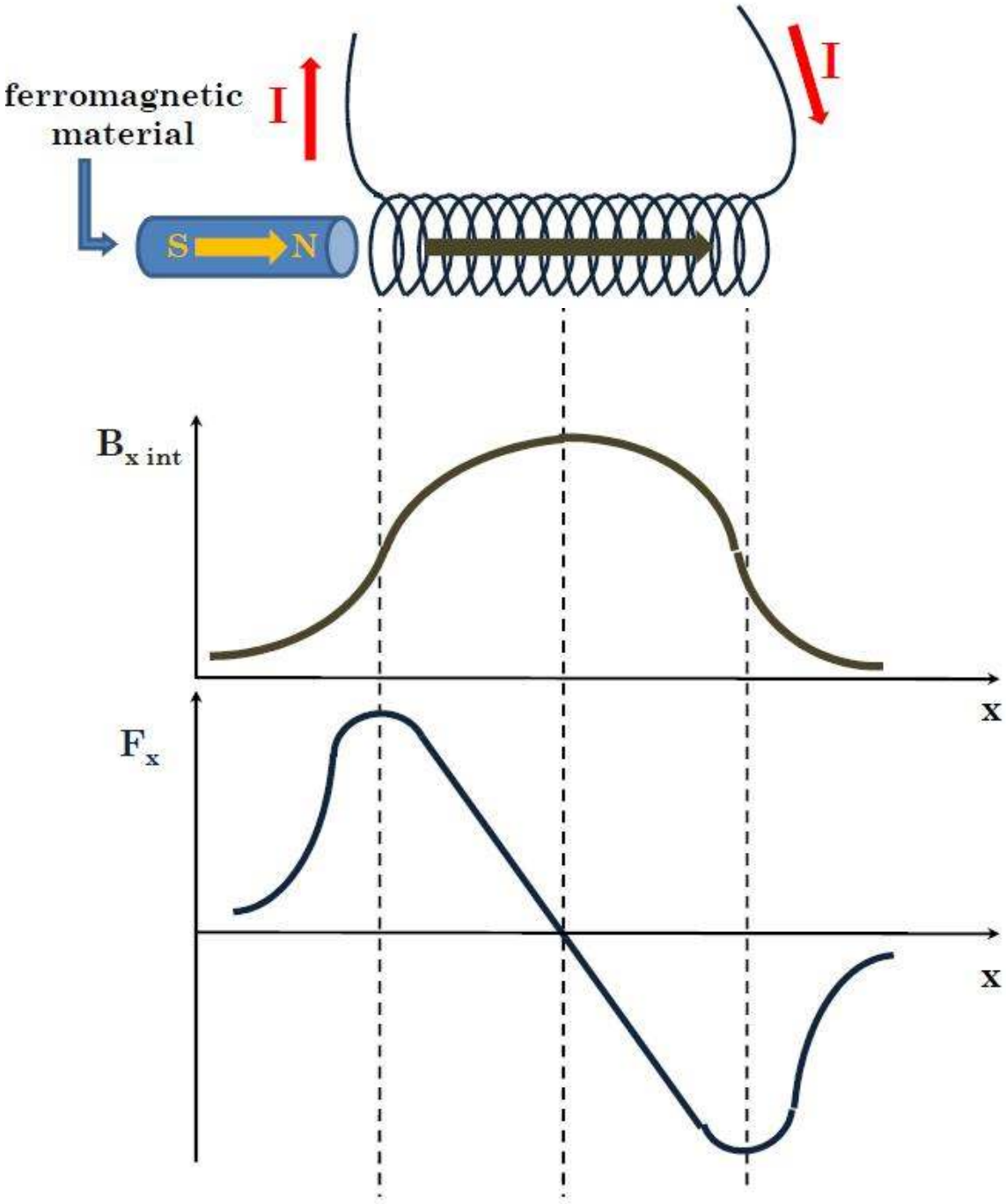

Fig.2.10. Coil Gun basic background: schematic representations of the magnetic field inside the coil due to the current flow and of the force acting on an inducing-magnetized ferromagnetic body placed in the neighborhood of one of the coil's end.

If, on the contrary, an high current pulse is provided in such a way (i.e. with a characteristic time-constant) that the intensity falls to zero when the object is just coming to the coil's middle zone, then the backward recalling force is cut off and the object may move fast forward (and outside the coil) without kinetic energy loss. One simple way to obtain a pulse of current is to produce a capacitor discharge: a CG system thus works by exploiting a capacitor discharge across an inductance, that is via an RLC circuit discharge (Fig.2.11). In other words, the aim of the CG is to shoot a ferromagnetic bullet by converting the electrostatic energy stored in a capacitance into projectile's kinetic energy, thanks to the switch to magnetic energy inside an inductance coiled round the projectile's barrel.

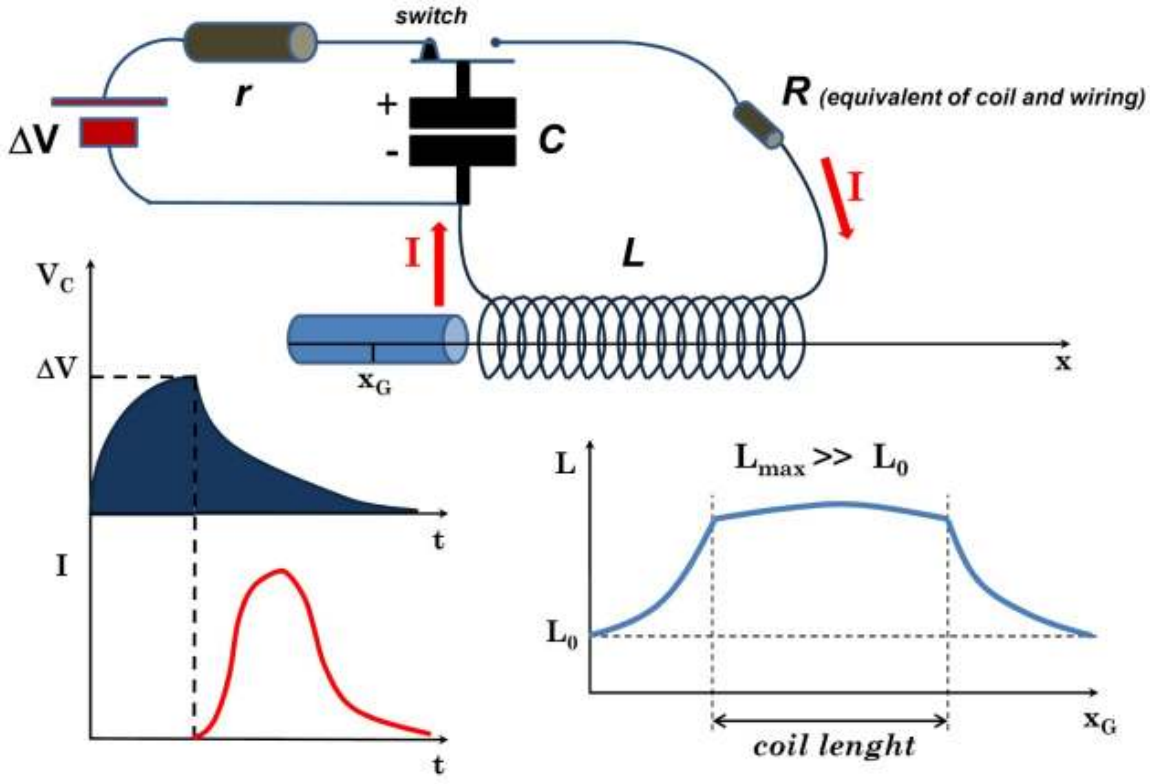

Fig.2.11. Coil Gun working: schematic representation of the RLC circuit (the charging phase concerns the r-C circuit, r being the capacitor loading resistance) with temporal behavior of capacitor voltage and intensity of current inside the coil. The qualitative variation of the circuit inductance, highly dependent on the projectile's position during the discharge, is also highlighted.

The coil inductor increases the acceleration of the projectile during its passage across itself. Its dimensions and turns number are crucial parameters; in fact, since the greater is the inductor turns number the higher is the inductance, then the electric discharge impulse rises, and above all decay time could result too much higher compared to the velocity of the projectile within the inductor. In such a case the efficiency of the CG could be compromised. The greatest efficiency is obtained when the impulse is shorter than the time took by the projectile to cross the half coil inductors length. If this

condition is not satisfied then the inductors will apply an attractive force on the projectile. This force will act in the opposite direction with respect to the projectile motion, thus decreasing the projectile acceleration. The dimensioning of the inductor and the capacitors must be computed in order to obtain the maximum efficiency. This means that the coil inductor should have the lowest time charge constant while the capacitors the fast discharge time constant. This is the fundamental condition required in order to avoid the forward-back projectile magnetic strength effect. In fact, once the projectile has overcome the half coil length, the back magnetic action strength starts to act on the projectile decreasing the initial forward acceleration imparted to the projectile. Since the capacitance discharge acts across the coil inductors, the best compromise can be found taking into account contemporary both the capacitance discharge constant time and the inductor charge one. Such a compromise can be obtained by reducing the coil inductor turns' number, as well as the capacitors' capacitance.

2.2.2 Ballistic set up

The in-house built CG is shown in Fig.2.12: the main parts of the CG are the coil inductor, the projectile's barrel (that acts as support for the coil wrapping), the capacitors bank, the switch system, and the rectifier diodes. The diodes connected to the coil in the opposite polarity with respect to the capacitors are necessary to dump the negative voltage semi-wave oscillation caused by the capacitors discharge and inductors charge process. Preliminary numerical simulations [294,295] have indicated that by a suitable arrangement of high capacitance ($4\times10^3\mu F$) capacitors as discharge trigger for a typical bullet/barrel system (mass projectile ~10g, gun length ~40cm), it's possible to reach values of 1÷2km/s for the bullet's speed, thanks to an effective coil propulsion force of by about 10^3kN. By now the highest measured speed was near below 90m/s with capacitors of $12\times10^3\mu F$; next implementation will surely give the opportunity to come nearer the computed values. In such a case the device will be really appropriate for ballistic aerospace testing, by providing faithful results about the interaction between materials and space debris (~8km/s). It has to be pointed out, on the other hand, that any numerical approach toward the system optimization deals with a so complex analytical problem. In fact, the system of second order differential equations (Eq.6) for the two time laws I(t) and x(t), at first sight of relatively simple resolution (starting from the trivial expression of I(t) for RLC discharge), actually hides a tremendous non linear coupling due to the really appreciable variation of L during the discharge. The inductance of an hollow coil, as well known, can raise by several order of magnitude if a magnetic material is located inside the coil's core: since the body is magnetized (with M not constant too, since it depends on the magnetic field, i.e. on the current intensity) the circuit inductance is thus highly unsettled during the projectile's motion (see also inset of Fig.2.11, with obvious consequences on the system time evolution.

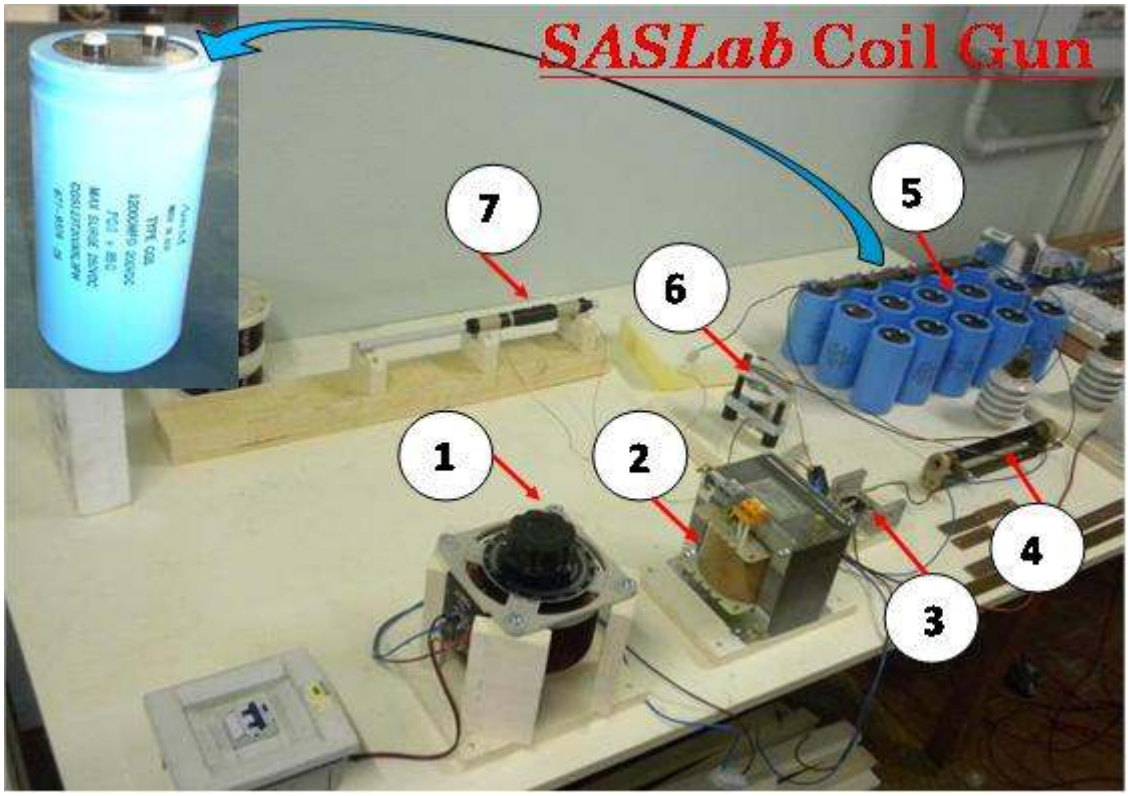

Fig.2.12. Picture of the Coil Gun system in-house realized (*SASLab-DIAEE* of *Sapienza* University):

1. Resistive Variac (V_{input} 220 V, V_{output} 0-250 V CA);
2. Transformer (V_{input} 250 V, V_{output} 1200 V CA, 1A);
3. Rectifier Diodes to convert AC in DC supply;
4. Resistor (1kΩ, 50W);
5. Capacitors (12000 μF, 200 V DC);
6. High power SCR (3000V_{max}, 300A);
7. CG inductor (copper coil winded on aluminum barrel).

$$
\begin{aligned}
& L\frac{d^2 I(t)}{dt^2} + R\frac{dI(t)}{dt} + \frac{1}{C} I(t) = 0 \\
& m\ddot{x}_G = F_x = M\frac{\partial B_x}{\partial x} \quad \left[B_x = B_x[x; I(t)]\right] \\
& I(0) = 0\,, \quad V_C(0) = \Delta V\,, \\
& x_G(0) = x_0\,, \quad \dot{x}_G(0) = 0
\end{aligned}
\tag{6}
$$

The modeling has thus to take into account for the physical changes of the fundamental parameters

$$M = M\left[I(t)\right]$$
$$L = L[x(t); M(I(t))] \tag{7}$$

so that the system (6) should be solved with an heuristic recursive approach, starting from the experimental measurements of velocity hereafter reported (Tab.2.1). These latters are obtained by varying the charging applied voltage (at one's pleasure) and the CG macroscopic parameters (within the technical limits), that are: the iron bullets (S - length 8cm, diameter 6.3mm, mass 17.2g; L - length 16cm, diameter 6.3mm, mass 36.6g; see Fig.2.13a), the coils (A - wire diameter 2.1mm, length 15cm, 58 coils, 8 turns, L_0=1.54mH; B - wire diameter 3.2mm, length 14cm, 40 coils, 7 turns, L_0=0.55mH; see Fig.2.13b-c), and the bank capacitors (C=12000μF) configuration (C1 - 5 C series, C_{eq} = 2400μF; C2 - 2 C1 parallel, C_{eq} = 4800μF; C3 - 3 C1 parallel, C_{eq} = 7200μF). The gun barrel is kept fixed (aluminum tube: length 31.6cm, outer diameter 10mm, inner diameter 7.6mm), the speed measurements are recorded by means of a ballistic chronograph (*ProChrono* chronograph, minimum speed 17m/s, precision 0.5m/s; see Fig.2.13d), the results are averaged over five shots for each arrangement.

BULLET SPEED (m/s)								
d.d.p. (Volts)	***COIL A***						***COIL B***	
	C1		**C2**		**C3**		**C3**	
	S	**L**	**S**	**L**	**S**	**L**	**S**	**L**
350	-	-	<17	-	22.2±0.7	<17	33.1±1.1	27.1±1.1
400	-	-	19.5±0.7	-	23.5±0.6	17.1±1.1	37.1±1.1	32.1±1.1
460	-	-	23.3±0.6	-	24.5±0.6	17.6±0.6	40.0±1.5	35.2±1.0
500	-	-	25.2±0.8	-	25.1±0.4	19.1±0.8	43.5±1.3	38.4±1.0
550	<17	-	27.7±0.6	-	25.0±0.6	22,7±1.0	45.9±1.2	42.8±1.3
600	<17	-	28.5±0.6	<17	24.2±0.5	25.0±0.6	49.2±1.2	48.5±1.2
660	<17	-	30.0±0.6	<17	23.6±0.6	28.1±0.7	53.1±1.2	55.6±1.1
700	18.1±1.8	-	31.3±0.7	<17	23.0±1.0	29.5±0.9	55.3±1.5	61.6±1.2
750	19.5±1.3	-	31.5±0.8	19.3±1.3	22.3±1.1	31.5±0.8	57.2±1.5	68.3±1.1
800	21.7±1.2	<17	32.1±0.6	27.1±1.2	20.5±1.2	32.6±0.6	58.8±1.4	74.9±1.0
850	24.6±0.9	<17	32.4±0.5	29.4±1.1	19.1±1.7	33.3±0.5	59.5±1.3	80.3±0.7
900	26.5±0.8	<17	32.2±0.8	32.7±1.1	<17	34.2±0.5	59.2±1.3	84.1±0.5
950	29.9±1.0	25.4±1.3	31.5±1.0	35.3±0.9	<17	34.5±0.3	58.1±1.0	86.0±0.4
1005	31.5±0.8	31.5±1.0	31.2±1.0	37.1±0.7	<17	34.0±0.5	55.4±1.1	85.7±0.6
1050	33.1±0.7	35.2±0.5	30.5±1.1	37.5±0.5	-	33.3±0.6	50.3±1.5	82.5±0.8
1095	34.2±1.0	38.9±0.7	29.3±1.1	37.3±0.6	-	31.5±0.7	42.2±1.4	78.5±0.8

Tab.2.1. Speed measurements at different input voltages for the several CG arrangements tested.

Fig.2.13. CG set-up pictures: a) short (S) and long (L) iron bullets; b) different copper coils tested; C) inductance static measurements by *Agilent* LCR Meters; d) ballistic *ProChrono* chronograph for bullet's speed measurements.

The several trends of the bullet's speed depending on the input voltage for the different arrangements highlight the intriguing, complex and highly non linear behavior of the system with respect to its physical main parameters. A first preliminary analysis of the experimental results listed in Tab.2.1 and outlined in Fig.2.14 stresses in fact the not obvious dependence between the several variables involved, mainly between the time charge/discharge circuit response and the mass of the bullet. The bell-shaped curves demonstrate that the energetic system balance, defined by

$$\eta = \frac{K}{E_C} \qquad \left(E_C = \frac{CV^2}{2} \quad , \quad K = \frac{mv^2}{2} \right) \tag{8}$$

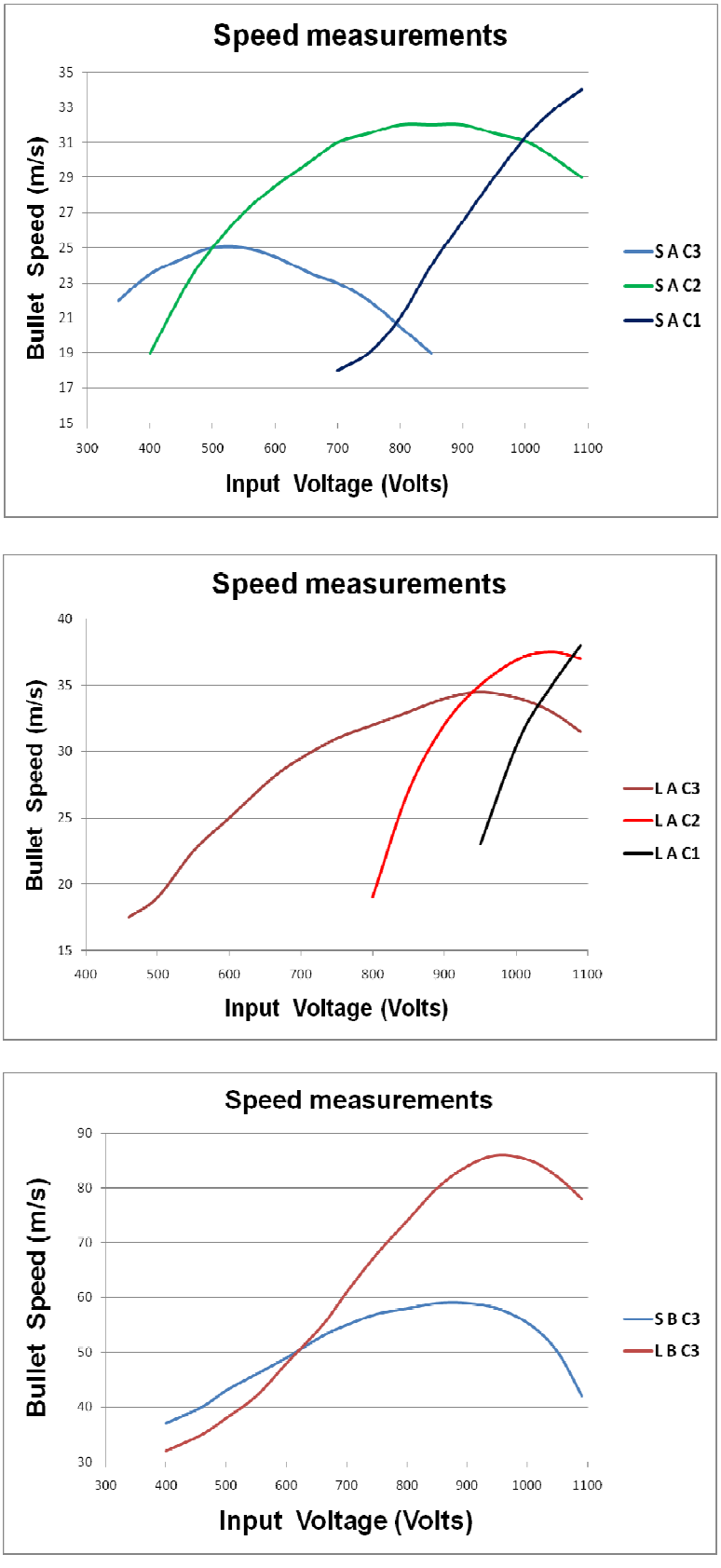

Fig.2.14. Graphic representations of the speed measurements reported in Tab.2.1.

with obvious physical meaning of the symbols, doesn't follow a trivial trend (speed increasing for higher voltages). It's clear, for example, that for coil A, with the bullets adopted and around the maximum voltage that can be applied to not more than five capacitor in series (each one can be charged up to 250V), the system efficiency raise up by decreasing the total capacitance, thus supplying less energy to the system (E_c): from Eq.8 one can find a best efficiency $\eta \sim 2\%$ for LAC1 configuration at the maximum voltage. For coil B in C3 configuration, on the other hand, the heavier L bullets results faster than the lighter S over almost the whole voltage range, with maximum efficiency $\eta \sim 4.5\%$ around 850V. Such results, of course, are connected to the time employed by the bullets to reach the coil center, over which they are recalled back, as explained above. To get higher speed and efficiency all the parameters have to be accurately matched: the results obtained for coil B and bullet L suggest that a suitable arrangement of capacitors bank may let one able to raise the bullet's speed up to 100m/s only with the present Coil Gun stage. Anyway, to perform an as precise as possible material ballistic characterization, a good test reproducibility rather than higher bullets kinetic energies has been addressed by now.

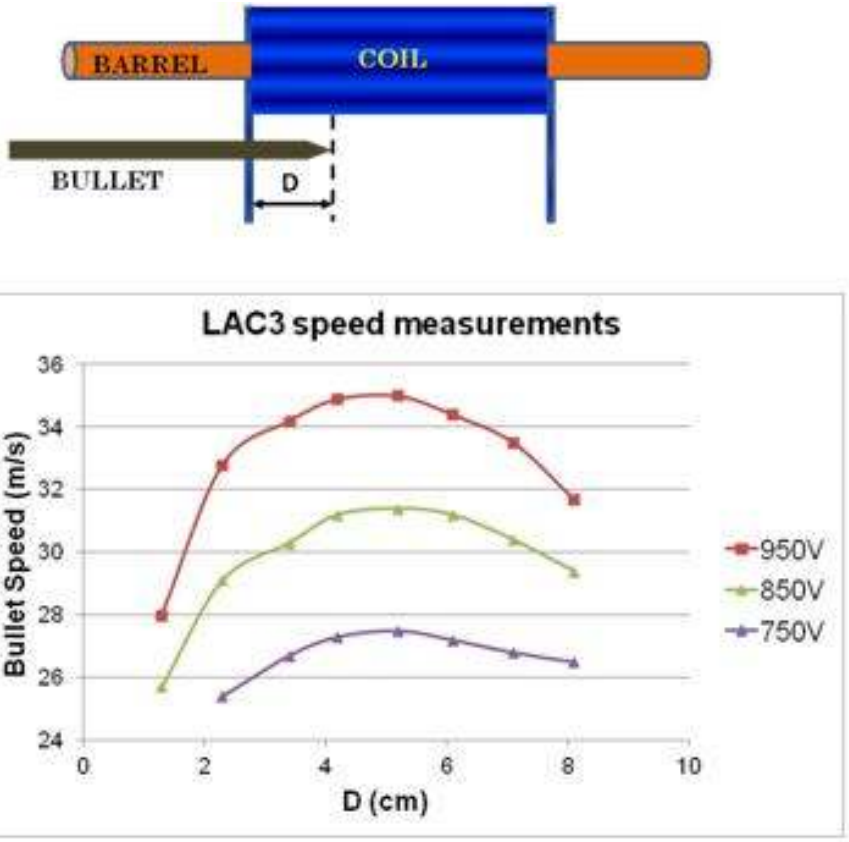

Fig.2.15. Bullet velocity versus initial position: the measurements performed in the same arrangement (LAC3) for three different input voltages showed that the CG efficiency may considerably change by few millimeters shift of bullet initial positioning.

With such aim, two fixed configurations with the lowest statistical dispersions in terms of bullets velocities were chosen: LAC3 and LBC3 both at 950V, in what follow related to the low energy (~22J) and high energy (~135J) test respectively. By watching at the experimental error values in Tab.2.1, in fact, it's clear that it's worth operating around maximum points of the curves of Fig.2.14 in order to avoid ballistic characterization mismatches as much as possible. Furthermore, the use of the longer bullet ensures more stable conditions about the relevant error source due to the bullet initial position: in fact, the coil inductance increases appreciably even with a not magnetized (metallic) body inside its core (changes up to 6÷8 times were found by inductance static measurements performed by inserting both bullets, partially and totally, inside the coil; cfr. Fig.2.13c), thus resulting in speed changes for same coil/bullet/capacitance arrangements at same input voltages (Fig.2.15) that cannot be neglected.

3 IMPACT CHARACTERIZATION

In this chapter the impact characterization by means of the ballistic equipment described in the second chapter of the nanostructured composite materials presented in the first chapter is reported and analyzed. As far as the CNT-filled Epoxy-based materials are concerned, some results of preliminary measurements of energy absorbing (Charpy and dropped weight test) are also reported, in order to give hints about the choice of the parameters (matrix typology and wt% of filling nanoparticles) adopted for the Coil Gun characterization. The results obtained have indicated that, by means of the functionalized CNT inclusion in low viscosity resin as well as of the STF addition to conventional ballistic fabrics, an intriguing enhancement of the materials impact resistance can be achieved, thus suggesting further investigations in order to make such nanoreinforced materials effective for ballistic applications.

INDEX

3.1 CNT-Epoxy Composites ballistic test

In this section, the nanostructured composite materials reinforced with multi-walled carbon nanotubes are investigated in terms of their capability of absorbing energy during an impact. An experimental study was set to determine the effect of the MWCNT reinforcement on polymeric composite materials under different levels of impact energy by varying the strike velocity. In order to study tailored nanostructured composites, a chemical functionalization of MWCNTs was tuned to improve the bonding at the polymer-filler interface. Charpy and dropped weight tests were conducted at different weight percentages of functionalized MWCNT inclusion within commercial epoxy resins. Results of the Charpy test showed that the presence of MWCNTs enhances the toughness of the epoxy polymer up to an inclusion threshold of 0.5wt %. Experimental results of dropped weight test showed an intriguing response by the chemical treated MWCNT-based materials. Low/high energy impact tests with projectile velocity ranging from ~34 to ~86 m/s were performed on Epoxy tiles and their equivalent reinforced by MWCNTs. The panels reinforced with MWCNTs showed improved ballistic behavior in comparison with the reference ones.

3.1.1 Preliminary test

The response of the manufactured MWCNT-reinforced Epoxy-based composite materials to several levels of impact energy has been preliminary investigated. Charpy impact and weight drop tests were performed to obtain a preliminary ballistic characterization of the powder-reinforced epoxy composite in the low energy impact range. In order to assess the influence of the nanoparticles content as well as the effectiveness of the nano-filler itself and after chemical treatments, samples with different percentages of functionalized MWCNTs embedded in two different epoxy resins were tested and compared with samples reinforced by pristine MWCNTs and micrometric graphite powder. The effects of the MWCNTs on the penetration failure and the impact absorbing mechanism has shown an interesting and effective fashion.

Medium viscosity epoxy resin EPON 828 (*Hexion* Speciality Chemical Inc.) and low viscosity epoxy resin PRIME 20LV (*Gurit* Holding AG) were used as base polymeric matrixes, together with their own specific hardener in fixed weight ratio. Two carbon materials have been adopted as reinforcements: graphite micro-powder (*Sigma Aldrich* Graphite, granulometry 20μm) and multi-walled carbon nanotubes (*Carbolex* MWCNT, diameter 20-30nm, length 10-30μm, purity > 95%, specific surface area > 110m^2/g). Conventional solvents and chemical products necessary for the MWCNT functionalization procedure, widely described in the first chapter, were purchased from *Sigma Aldrich*.

Charpy impact tests were performed in order to compare the tenacity of the two resin systems by filling them with different weight percentages of amino-functionalized MWCNTs. Tests were realized with the pendulum PSW 750 (*Zwick GmbH & Co.KG*) in according with ASTM 256-04 standard (Fig.3.1). From the results summarized in Tab3.1, a great improvement of the impact strength can be noticed for both matrixes with the MWCNT addition (see also Fig.3.2). In the case of EPON 828, the tenacity increases of 27% for MWCNTs at 0.1wt% and 40% for MWCNTs at 0.5wt%. In the case of PRIME 20LV, the tenacity increases of 44% for MWCNTs at 0.1wt% and 56% for MWCNTs at 0.5wt%. On equal terms, the difference between the two resins in percentage increment can be assigned not only to the better initial properties of the PRIME 20LV, but also to the more homogeneous filler dispersion that can be achieved. In fact, the PRIME 20LV presents a very low viscosity (50cps at room temperature) that facilitates the homogeneity of the mixture. At 1wt%, a slight reduction of the tenacity of the EPON 828 can be observed with respect to the neat resin, whereas the PRIME 20LV shows no significant improvements. Both systems show a worsening of the tenacity at 1wt% with respect to the case of 0.5wt%. Such results induces to believe that, in the adopted manufacturing set-up, an inclusion threshold occurs at filler concentrations between 0.5wt% and 1wt%. Around such concentration, further inclusions of nanoparticles make the composite mechanical properties worse, due to agglomeration and entanglement problems that may cause defects in the bulk material and degrade the interface bonding. Based on these results, the PRIME 20LV was selected as epoxy matrix, and the 0.5% filler concentration was set as reinforcement weight percentage for the subsequent tests.

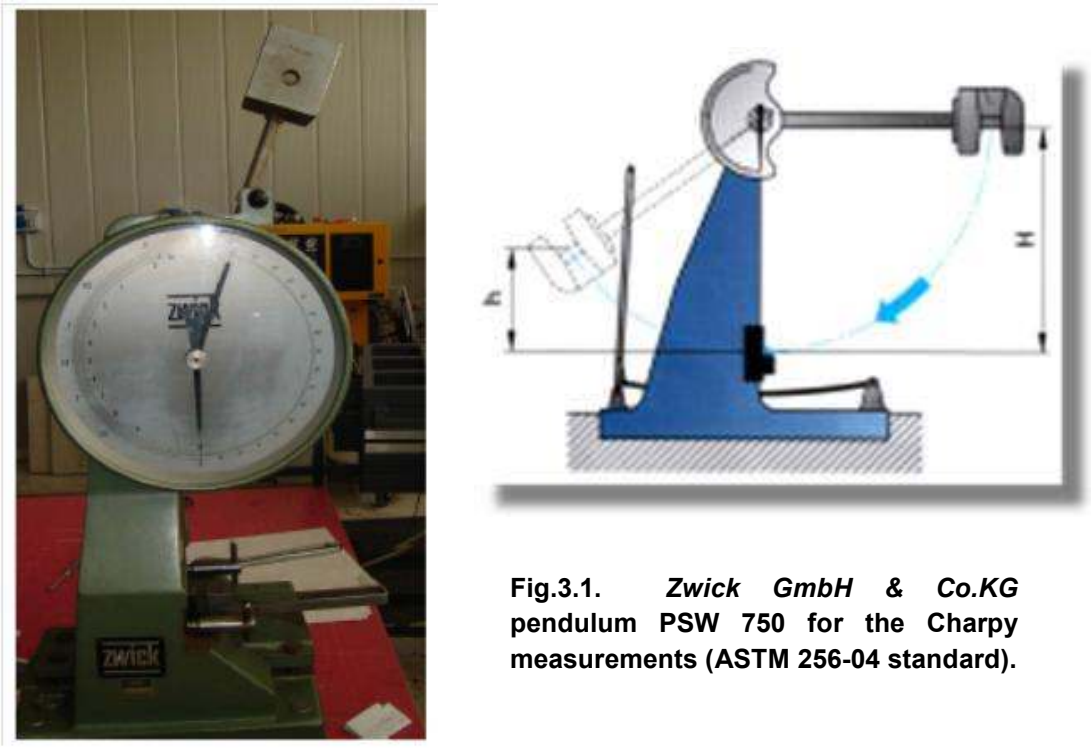

Fig.3.1. *Zwick GmbH & Co.KG* pendulum PSW 750 for the Charpy measurements (ASTM 256-04 standard).

MWCNT content (wt% v.s. resin)	PRIME 20LV (kJ/m^2)	EPON 828 (kJ/m^2)
0	2.5±0.4	1.5±0.3
0.1	3.6±0.5	1.9±0.2
0.5	3.9±0.6	2.1±0.2
1	2.6±0.4	1.4±0.5

Tab.3.1. Results of Charpy test.

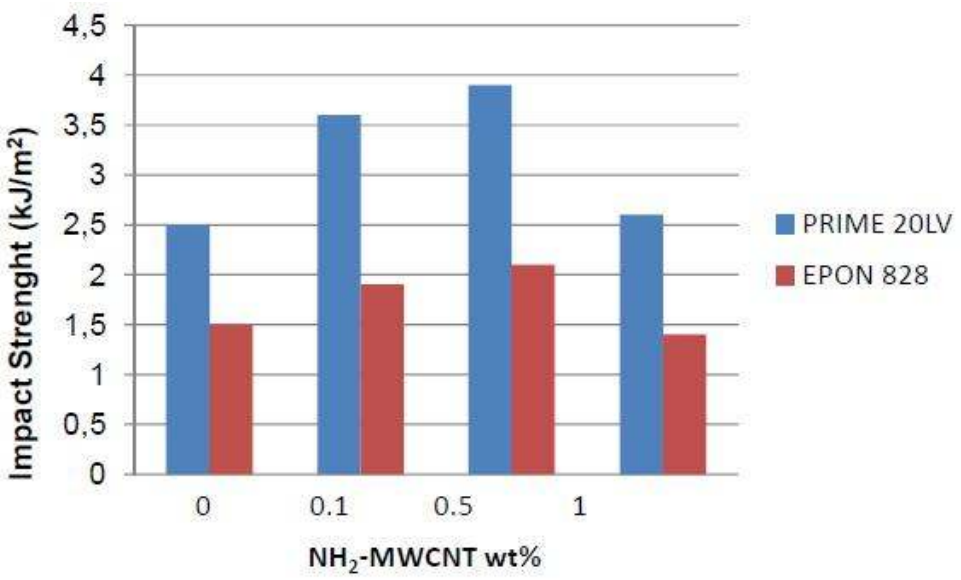

Fig.3.2. Graphic representation of the results listed in Tab.3.1: the improvement of the material strength as a function of the MWCNT wt% of inclusion is clarified, as well as the difference in terms of effectiveness between the two polymeric matrixes employed.

Further investigations in the low impact range were conducted on carbon filler-reinforced epoxy materials by means of a dropped weight test, in order to assess on a whole the impact resistance properties of such materials. The experimental set-up consists of an in-house built drop tower system, where low velocity impact conditions can be simulated. The performances evaluation is firstly linked to the observation of the samples behavior during the test, followed by the visual inspection of the fragments and the SEM analysis of the fracture surfaces. Such a ballistic characterization is not exhaustive, mainly regarding a quantitative point of view. However, thanks to an high degree of test reproducibility, the adopted set-up allowed to achieve a direct validation of both the research line and the samples manufacturing process. This latter follows the

technique reported in Sect.1.3.1.2, with molds and material quantities suitably evaluated in order to realize square tile samples of 25cm side with thickness in the range of 3 to 5 mm. With the aim to check the effect of MWCNT purification and functionalization treatments on the composite mechanical properties, three kinds of filler were employed at 0.5wt% of inclusion within the selected polymeric matrix (PRIME 20LV): pristine MWCNT, amino-functionalized MWCNT, and micrometric graphite powder. After the curing step, the composite samples were pulled out from the molds by carefully handling to avoid residual stresses that could alter the ballistic test.

The drop tower system for low impact ballistic tests is an aluminum-made structure in which a 190cm-high hollow pipe can be hooked in adjustable way to a shorter column fixed on the apparatus platform (Fig.3.3,3.4). On the top of the pipe a 0.5kg sharpened weight is inserted into the hollow (diameter ~42mm), so that it may impact by gravity free-fall on the tile square sample clamped at the bottom. The diameter of the weight is only a split mm lower than the inner pipe diameter. This latter acts thus as a guide to the vertical motion of the weight, whereas advisable greasing operations of both the weight and the pipe inner wall are necessary to minimize the friction effects as much as possible. The pipe is positioned on such a level that there is no longer contact with the weight during the impact, in order to not affect the bullet-target interaction dynamics. In such conditions, the impact kinetic energy $E_c = mg\Delta h$ may be evaluated around 9.8J and the corresponding velocity $v=(2g\Delta h)^{1/2}$ around 6.2m/s.

Fig.3.3. Picture of the in-house built dropped weigh tower system for the low energy ballistic characterization. On the left, the whole apparatus; on the right, the 0.5kg weight adopted (above), and the sample positioning (below).

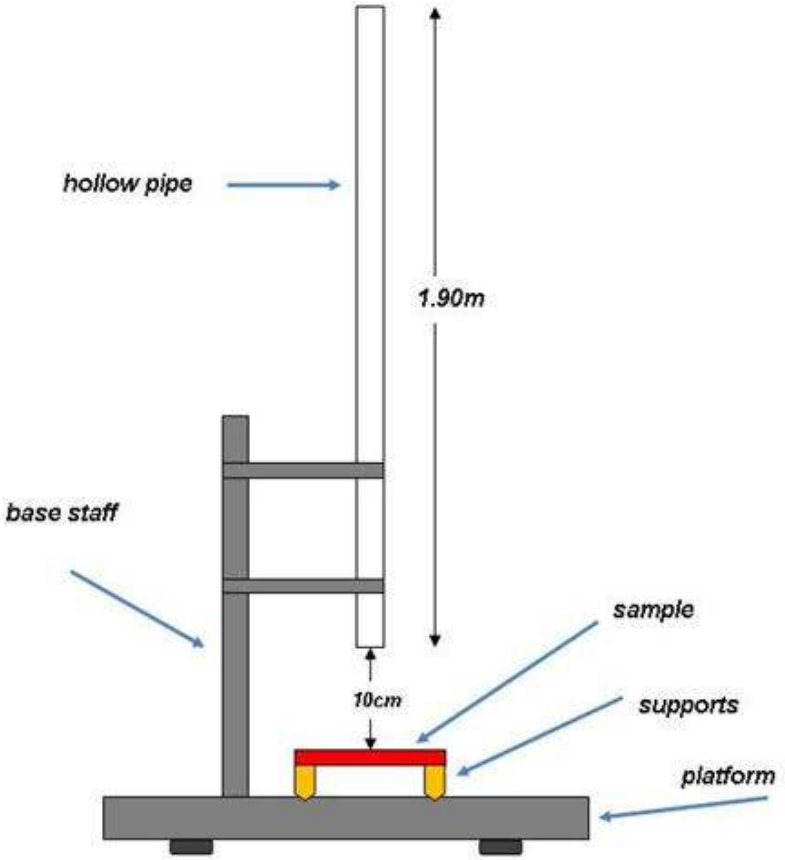

Fig.3.4. Drop tower system: schematic diagram of the experimental set up.

Four typologies of tile samples have been tested: neat resin (thickness 4.5±0.9 mm) as not-reinforced reference samples, 0.5wt% micro graphite-reinforced (3.9±0.6 mm), 0.5wt% pristine MWCNT-reinforced (3.7±0.5 mm), and 0.5wt% amino-functionalized MWCNT-reinforced (3.9±0.6 mm). In Fig.3.5 the responses of the different materials under testing are illustrated. All the samples did not withstand the impact and have broken in several fragments; however the breaking route has taken different fashions in the several cases. In particular, the reinforced materials broke in a number of pieces noticeably less than what occurred for the neat resin samples (instead disintegrated by the knock), thus highlighting an effective improvement by the powder fillers in terms of energy absorption capability. The most striking result was discovered in the tiles made of functionalized MWCNT-reinforced composite, which have split in only two parts due to fractures originating quite far from the impact point where, in addition, no macroscopic trace of the hit was discovered. Such an intriguing response gives evidence of a real efficient ballistic behavior of a composite filled by chemically modified carbon nanoparticles, since the energy absorption capability is widely increased by the matrix-filler load transfer optimization. This feature is even more clear by the short videos recorded during the several tests: unlike the other cases, the heavy bullet does not perforate the 'optimized' tile but bounces on it, thus inducing visible flexure vibrations to the slab till the breaking (probably due to a not perfect sample homogeneity). Such

mechanical behavior is in agreement with the well-known MWCNT elastic properties, capable to withstand tensional, torsional, buckling and compression stresses that are unsustainable by common materials. On the other hand, the need of a suitable chemical treatment of the MWCNTs before their employment inside the polymeric matrix has to be underlined, since pristine MWCNT-reinforced materials have shown a behavior not so better than what was obtained with micro graphite-reinforced ones. This behavior is clearly due to the pure MWCNT strong entanglement leaning that gives rise to big agglomerates (even of micrometric dimensions) thus preventing a correct dispersion of the filler inside the host matrix. The SEM analysis of the fracture surfaces gives further confirmations of that, by emphasizing the poor degree of dispersion inside the untreated MWCNT-reinforced material compared to the more homogeneous morphology of the optimized one (see Fig.1.32).

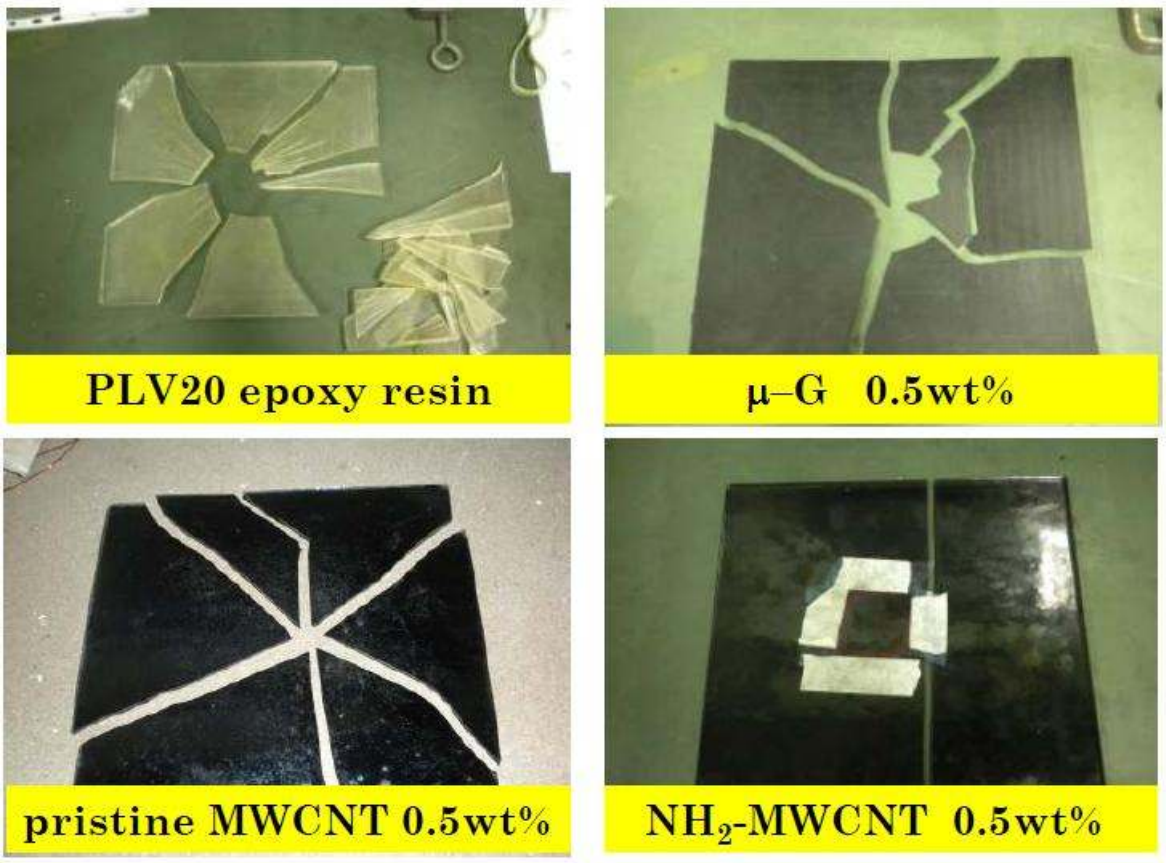

Fig.3.5. Response of the different materials tested with the low-energy impact dropped weight facility. All the samples don't withstand the impact and broke in several fragments, but with different fashions in the several cases: the reinforced materials broke in a number of pieces noticeably less than what occurred for the neat resin samples, actually disintegrated by the knock). The tiles made of functionalized MWCNT-reinforced composite split in only two parts, due to fractures originating quite far from the impact point where, in addition, no macroscopic hit's trace is discovered.

3.1.2 Coil Gun test

In this section the most significant results of the ballistic characterization of the CNT-filled Epoxy-based composite materials by means of the CG device are reported and discussed. The choice of the test panel composition (Fig.3.6) has been suggested by the preliminary results, beside the experimental set up best solutions. Preliminary characterization test of the experimental apparatus have indicated the most suitable ensemble of physical parameters (bullet typology, shot energies, gun-target distance, etc.) in order to achieve the best compromise between test efficacy and reproducibility. In particular, the combined constraints of gun and projectile's direction stability during the shot to obtain a 90° central impact on the targets have suggested to keep the sample surface dimensions inside 20×20cm (such value was further lowered cause the big quantity of materials required to carry out a significant number of experimental test). In Fig.3.7 the experimental set up adopted is schematically depicted: the samples are fixed by elastic clamps to the wood support, where a plasticine witness is centrally positioned to estimate the different panel performances in terms of absorbed energy.

Fig.3.6. The four typologies of tile samples before the characterization by the Coil Gun facility: neat resin as not-reinforced reference samples, 0.5wt% micro graphite-reinforced, 0.5wt% pristine MWCNT-reinforced, and 0.5wt% amino-functionalized MWCNT-reinforced. Two reference thickness were defined for each kind of material typology: ~3mm and ~6.5mm.

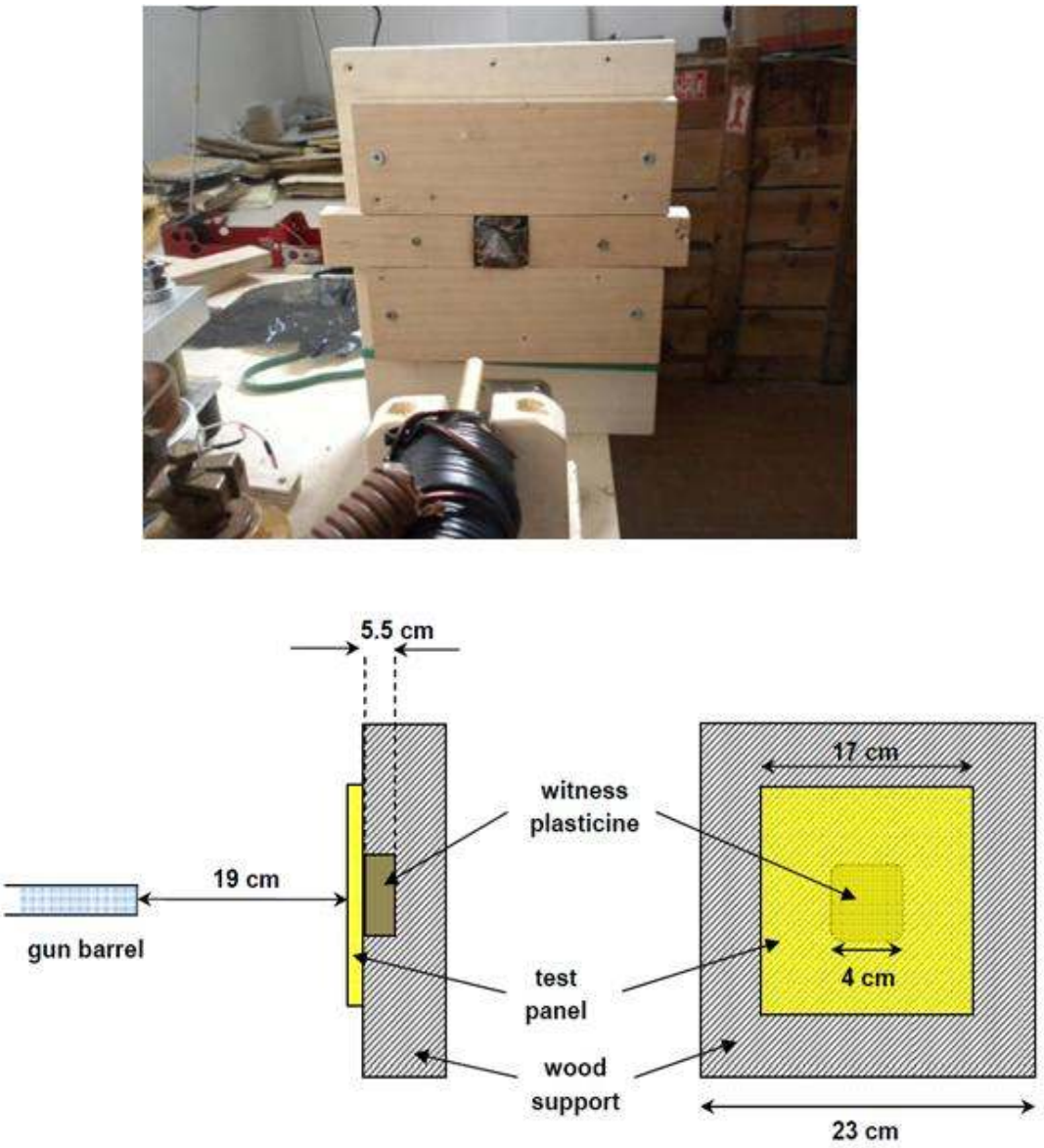

Fig.3.7. Ballistic characterization test by CG: on the top, picture of the plasticine witness located in the square hole of the sample's support in front of the CG barrel; on the bottom, lateral (left) and frontal (right) schematic views of the adopted set-up.

In the following Tab.3.2 the results of the CG ballistic characterization are presented. For the two energy range established (see Sect.2.2.2) and for each typology of sample material (composition and thickness) the plasticine witness depth and the relative absorbed energy are listed. This latter is estimated by the simple relationship $(L_0\text{-}L)/L_0$ with L and L_0 penetration depths within the witness with and without the sample respectively (low energy test: L_0=9.2mm; high energy test: L_0=50.8mm). The obtained values, as well as the graphic representation of Fig.3.8, outline the better performances of the materials filled with the amino functionalized MWCNTs.

sample			LOW energy		HIGH energy	
material		slab thickness (mm)	witness depht (mm)	relative energy absorbed	witness depht (mm)	relative energy absorbed
blank	PLV 20	3.1 ± 0.4	8.4 ± 0.2	**8.7%**	47.3 ± 0.4	**6.9%**
		6.5 ± 0.4	8.1 ± 0.2	**12.0%**	45.8 ± 0.2	**9.8%**
0.5wt% reinforcement	micro-graphite	3.0 ± 0.3	7.7 ± 0.3	**16.3%**	43.1 ± 0.4	**15.1%**
		6.7 ± 0.6	7.0 ± 0.3	**24.0%**	39.5 ± 0.5	**22.2%**
	pristine MWCNT	3.0 ± 0.6	7.9 ± 0.2	**14.1%**	43.7 ± 0.5	**14.0%**
		7.1 ± 0.5	7.2 ± 0.1	**21.7%**	41.2 ± 0.3	**18.9%**
	NH_2-MWCNT	3.3 ± 0.4	7.1 ± 0.1	**22.8%**	35.8 ± 0.2	**29.5%**
		6.5 ± 0.4	5.6 ± 0.2	**39.1%**	28.9 ± 0.4	**43.1%**

Tab.3.2. Numerical results of the CG ballistic characterization test performed on four typology of composite materials. The relative absorbed energy is evaluated by the relation $(L_0-L)/L_0$ with L and L_0 penetration depths within the witness with and without the sample respectively (low energy test: L_0=9.2mm; high energy test: L_0=50.8mm).

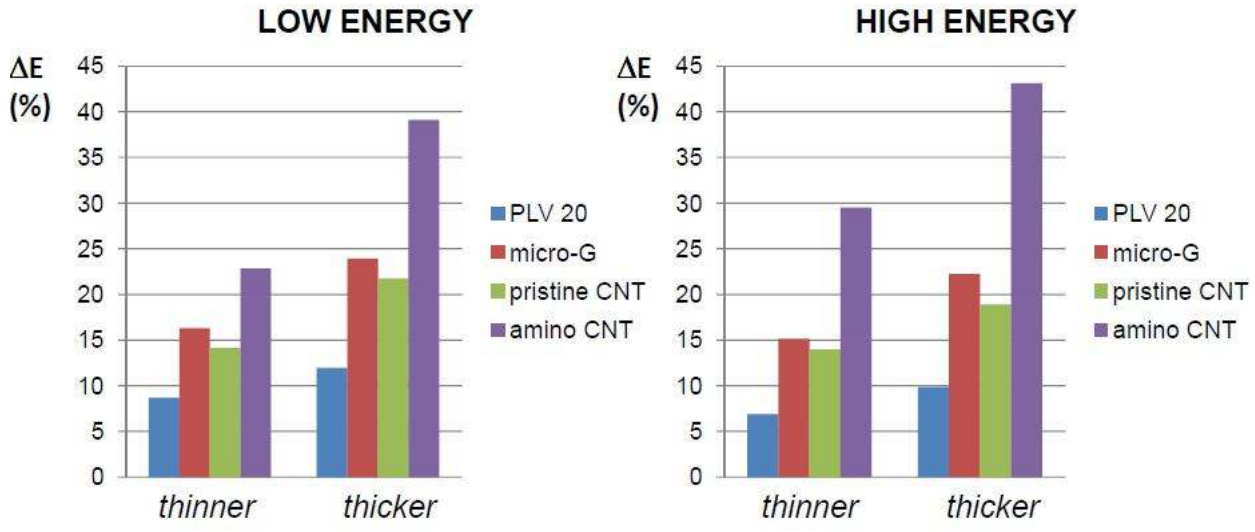

Fig.3.8. Graphic representation of the results of Tab.3.2. The improvement of the reinforced-composite capability of absorbing energy versus the neat epoxy compared is stressed, as well as the best performances of the functionalized-MWCNT filled composite materials. The dependence of the resistance on both the sample thickness and the impact energy is also outlined.

In particular, the most striking results from a qualitative point of view are the trend of the absorbed energy as a function of the thickness and of the impact energy. A functional increase of ΔE with thickness and an uncommon increase of ΔE with impact energy for NH_2-MWCNT reinforced material v.s. other cases can be noticed. The first issue gives confirmation of the high benefit that the inclusion of suitably treated carbon nanoparticles can give to a polymeric matrix in terms of ductility: the higher the thickness, the greater is the physical work necessary to the material penetration, without any brittle fracture, as underlined by the visual inspection of the fragments (see Fig.3.9). The second characteristic discovered is more complex to explain, because suggests an intriguing 'active' interaction between the nanoparticles when subjected to an external stress: due to their incredible pliability, the MWCNTs could provide a greater (relative) resistance to higher compressive loads. Second-order effects in the electron-phonon structure can also be referred to in order to explain such non-linearity of the lattice deformation. Further investigations (i.e., more experimental data) are needed in this field to achieve a better comprehension of such intriguing mechanical behavior.

Fig.3.9. Ductile behavior of the NH2-MWCNT reinforced composite materials during the high energy ballistic CG test (up: font side; down: back side).

3.2 Nanofluid-Kevlar Fabrics ballistic test

In this section the most significant results of the ballistic characterization of the nanofluid-reinforced Kevlar-based fabric by means of the CG device are reported and discussed. The choice of the test panel configurations (layers type and number, target surface, alternation and coupling between neat and treated layers, assembling modality, etc.) has been first suggested by the experimental set up best solutions, beyond the purpose to obtain performances similar or even better than the best reference samples in terms of weight/resistance ratio. Preliminary characterization test of the experimental apparatus have indicated the most suitable ensemble of physical parameters (bullet typology, shot energies, gun-target distance, etc.) in order to achieve the best compromise between test efficacy and reproducibility. In particular, the combined constraints of gun and projectile's direction stability during the shot to obtain a 90° central impact on the targets have suggested to keep the sample surface dimensions inside 20×20cm (such value was further lowered cause the big quantity of fluid required to carry out a significant number of experimental test). The experimental set up adopted is analogous to what reported in the previous setion.

About the layers number, the investigation has been oriented by the reference fabric (neat XP) performances: the number of layers was set to eleven, such to obtain a precise quantitative evaluation of its ballistic properties with the operating experimental conditions. As a consequence, the prototype panel configurations have been established by taking into account most of all the panel total weight requirements, in order to carry out a reliable comparison. For the same reason the results obtained with high (>20wt%) STF concentration have not been taken into consideration, since the critical manufacturing issues due to overfilled solutions produce not homogeneous structures and thus a poor test reproducibility (beyond a not practically useful material). Direct measurements and evaluations for several panel configurations are summarized in Tab.3.3 below, the results being averaged over five shots for each ballistic test. For each panel typology are indicated symbol, layers sequence (following the nomenclature of Tab.1.4 for the fabric type, and subscribing the STF concentration for the treated materials), and total weight (P); for the two low/high energy test above defined the measured penetration depth in the plasticine witness (L), and the computed relative absorbed energy in percentage (ΔE) and efficiency (Q) are then reported. The penetration depth is measured by depth gauge (precision 0.05mm, see Fig.3.10), the relative absorbed energy and efficiency are simply defined as follow

$$\Delta E = \frac{L_0 - L}{L_0} \quad , \quad Q = \frac{\Delta E}{P} \tag{9}$$

where L_0 indicates the penetration depth into the plasticine witness without sample (low energy test: L_0 = 9.2 mm; high energy test: L_0 = 50.8 mm). The absorbed energy is an index of the intrinsic ballistic effectiveness of the tested material, while the efficiency factor represents, by weighting on the material density, a balanced evaluation of the global material properties in view of applications in which both lightness and resistance are contemporaneously required.

panel typology			low energy test (~22J)			high energy test (~135J)		
symbol	***configuration***	***P (g)***	***L (mm)***	***ΔE***	***Q***	***L (mm)***	***ΔE***	***Q***
XP	*11 XP*	175 ± 2	1.2 ± 0.2	87%	**0.50**	10.8 ± 0.5	79%	**0.45**
b_0	*1 XP / 9 B / 1 XP*	284 ± 5	5.8 ± 0.3	37%	**0.13**	36.0 ± 1.1	29%	**0.10**
b_0*	*1 XP / 9* B_{15} */ 1 XP*	319 ± 8	5.1 ± 0.3	45%	**0.14**	29.3 ± 1.0	42%	**0.13**
B	*5 XP / 3 B / 1 XP*	180 ± 4	5.5 ± 0.4	40%	**0.22**	34.1 ± 0.4	33%	**0.18**
B_{10}	*5 XP / 3* B_{10} */ 1 XP*	192 ± 6	5.3 ± 0.3	42%	**0.22**	31.5 ± 0.5	38%	**0.20**
B_{15}	*5 XP / 3* B_{15} */ 1 XP*	196 ± 4	4.8 ± 0.3	48%	**0.24**	27.6 ± 0.6	46%	**0.23**
B_{20}	*5 XP / 3* B_{20} */ 1 XP*	199 ± 5	4.1 ± 0.2	55%	**0.28**	22.8 ± 1.1	55%	**0.28**
KN	*5 XP / 4 KN / 1 XP*	184 ± 3	5.2 ± 0.3	43%	**0.24**	33.1 ± 0.7	35%	**0.19**
KN_{10}	*5 XP / 4* KN_{10} */ 1 XP*	199 ± 6	4.3 ± 0.2	53%	**0.27**	26.0 ± 1.0	49%	**0.25**
KN_{15}	*5 XP / 4* KN_{15} */ 1 XP*	203 ± 4	3.2 ± 0.3	65%	**0.32**	18.2 ± 0.5	64%	**0.32**
KN_{20}	*5 XP / 4* KN_{20} */ 1 XP*	205 ± 4	1.9 ± 0.2	79%	**0.39**	10.5 ± 0.6	79%	**0.39**

Tab.3.3. Ballistic characterization results (the horizontal blocks enclose the results for single groups of blank/treated materials).

Fig.3.10. Pictures of a panel sample just after the ballistic test.

By analyzing the numerical results of Tab.3.3 the effectiveness of the fabric reinforcement treatment by the STF solutions realized is evident at first sight: the performances of every blank typology (b_0, B and KN) are improved by the corresponding STF-reinforced configurations in terms of absorbed energy. Moreover, the higher is the nanosilica concentrations within the STF solutions, the greater is the percentage of absorbed energy, as shown in Fig.3.11, thus enhancing the direct role of reinforcing element played by the n-SiO_2 based nanofluids when coupled to B and KN type fabrics. That is supported by the observation of the zone perforated by the bullets: a more collective resistance work done by the fibers of the reinforced fabric comparing to the neat one is detectable in the panels backside images after the shot (Fig.3.12), as well as in the SEM photos of the impact point (Fig.3.13). Such improvements are confirmed by the Q-factor trend, even if in a less effective way: the more concentrated solution raise the fabric saturation level in terms of weight increasing, thus lowering the panel global efficacy. In particular the Q values founded for the b_0 type panels give evidence of the drawbacks due to an overall utilization of the STF treatment, because the structure heaviness may offset the gain in impact resistance capability. For this reason the mix configurations with the first 5 layers made of neat XP were designed: as best reference material, the XP Kevlar has confirmed the better weight/resistance trade-off in these experimental conditions. On the other hand, as mentioned in the first section, the poor coupling between STF and XP doesn't give any contribution to the fabric's resistance, rather degrading the fibers structure. As far as the impact energy is concerned, an interesting property of the STF-based samples can be noticed: the quasi-unchanged ΔE and Q values of the reinforced panels (mainly of those with higher nanofiller wt%) in the two different energy range test, with respect to the correspondent lowering discovered in the neat samples. That is highlighted by the crossing around 20wt% of the two curve pairs (B type and KN type) in the graphic of Figure 16, while in the starting points (0wt%, i.e. neat panels) the ΔE values are well spaced, even for the best configuration (horizontal reference lines). Such results suggest an intriguing fashion of the impact resistance mechanism by the STF-treated materials. In a very simplified scenario, a conventional structure puts up resistance by a constant friction, so that the L quantities in (9) only depend on the intrinsic material properties: by this way the absorbed energy may be written as

$$\Delta E = \frac{E_{INC} - E_F}{E_{INC}} \tag{10}$$

where E_{INC} and E_F are the incident bullet's energy and the friction physical work respectively: if this latter is approximately constant (i.e. not dependent on the impact energy), the relative absorbed energy is clearly reduced by increasing the bullet's kinetic energy. In the energy range investigated this latter description seems to be reasonable for what concerns the untreated samples. On the contrary, the experimental results obtained for the treated fabric-based panels indicate a more complex mechanism of interaction (cfr. Fig.3.14), able to raise the friction effect (i.e. the fabric response

upon impact) at higher incident energies. This feature may be so promising, mainly for the globally good performances of the treated KN-based type panels. In this case, in fact, the nanofluid/fabric suitable coupling (due to the particular fabric morphology) enhances the STF behavior: that makes this kind of structure (at the highest concentration wt%) competitive with the reference one, even matching it in the high energy range in terms of impact absorption. The next steps of the research has to be then addressed to the further upgrade of the treated KN-based structures, in particular for what concerns the manufacturing reliability of high percentage STF-filled materials.

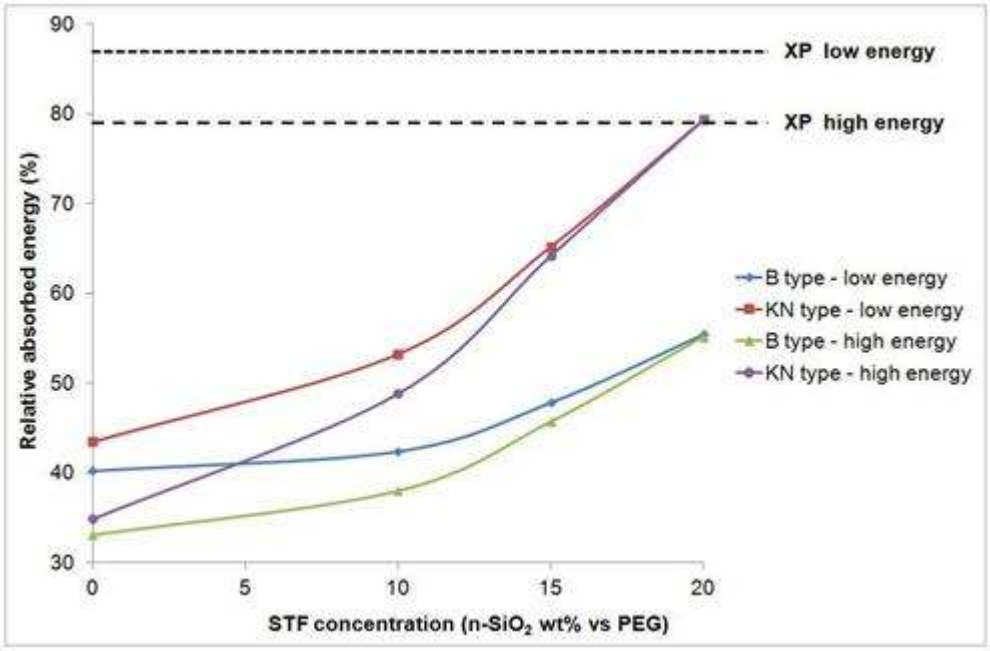

Fig.3.11. Absorbed energy dependence on nanoparticles wt% inside the several typologies of STF-reinforced fabric panels.

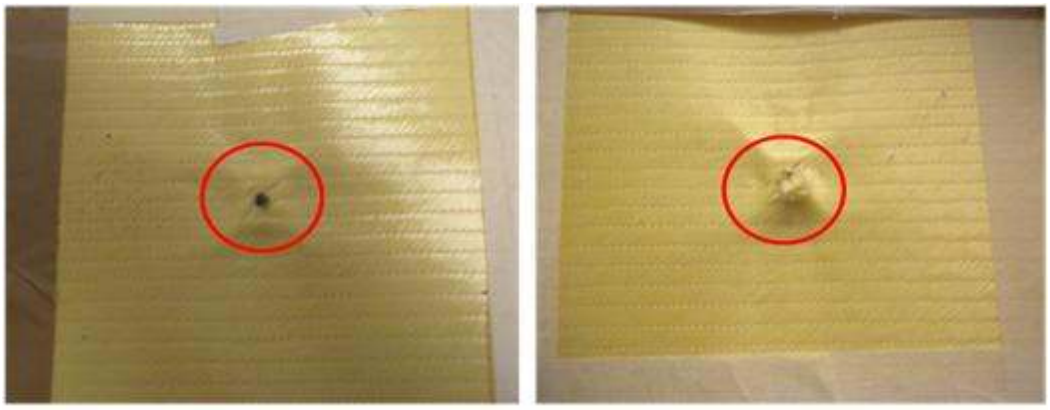

Fig.3.12. Backside (exit wound) pictures of a B (left) and a B_{20} (right) configuration panel samples after the low energy test.

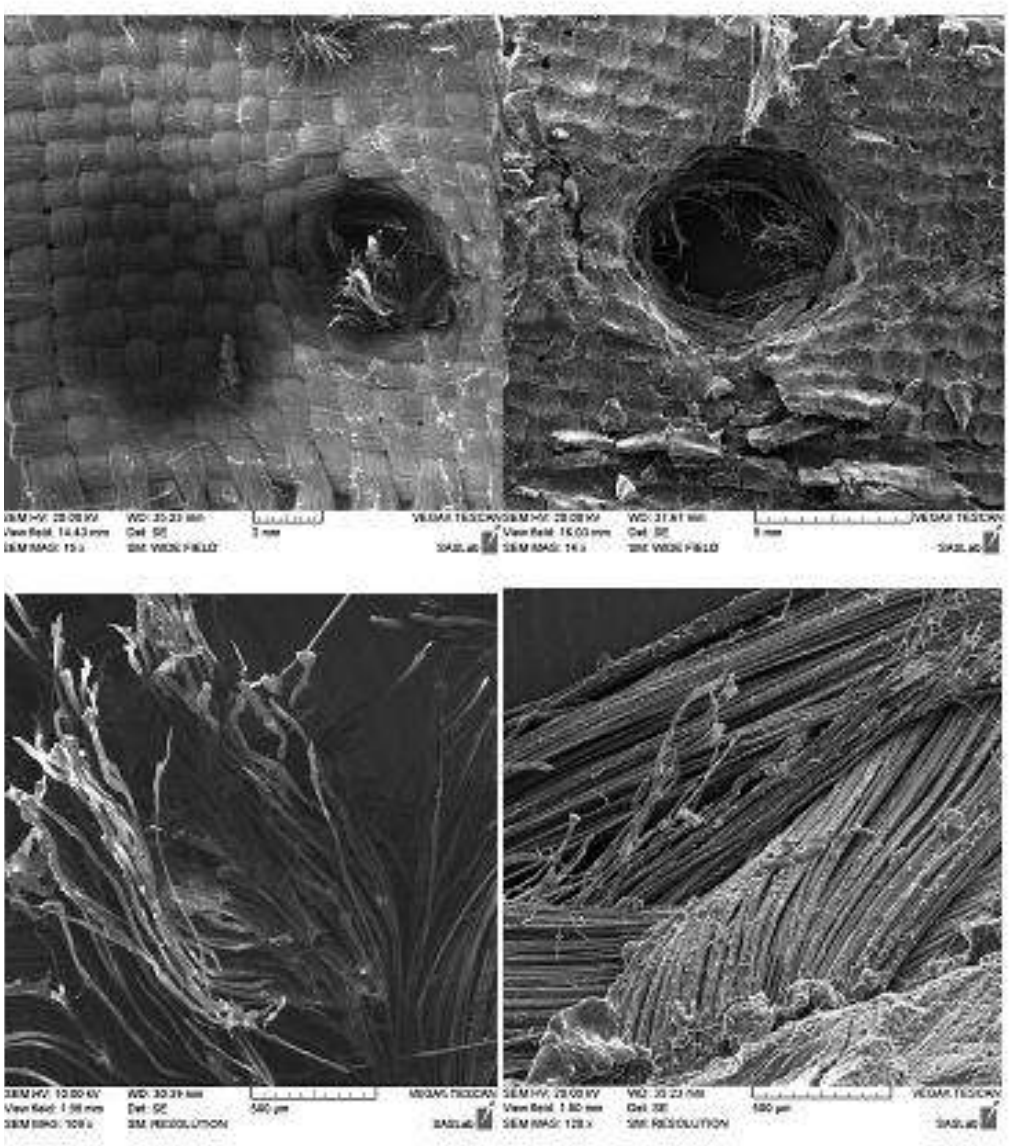

Fig.3.13. Low (up) and medium (down) magnification SEM photos of the impact zone in B (left) and B_{20} (right) configuration panel samples after the low energy ballistic test.

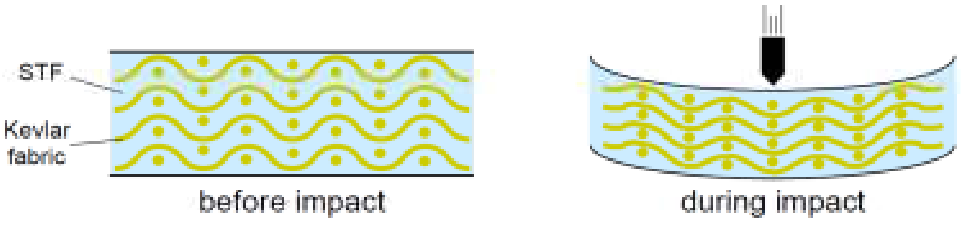

Fig.3.14. Schematic representation of elastic-like mechanical behavior of STF-reinforced Kevlar fabric upon a projectile impact.

CONCLUSIONS

In the present study the possibility to employ nanoparticles for improving the antiballistic properties of conventional materials has been investigated. The interest in developing advanced lightweight materials based on nanocomposites arise from the unconventional behavior of several nanomaterials in terms of impact energy dissipation. A rich and complex vibrational structure, in particular for acoustic phononic modes, gives to nanoparticles the possibility to withstand high external stresses without structural damages. Thanks to a suitable procedure of nanostructures intercalation within organic matrix, is thus possible to manufacture light composite materials with improved capabilities of ballistic protection, via energy spreading from local points over larger areas or by means of the so-called shear thickening effect.

The goal of the present work has been to perform a ballistic characterization of both CNT-based and STF-reinforced nanocomposites by means of an in-house built electromagnetic accelerator. Such device, called Coil Gun has been designed, realized and characterized to perform ballistic impact tests on several type of nanocomposite materials. The Coil Gun has been carefully set-up in terms of its main parameters (bullets velocity, energy efficiency, system stability, etc.): two particular configuration (low/high energy) have been established for the ballistic characterization, so that two different impact energy ranges have been investigated and, at the same time, the maximum test reproducibility has been achieved. This study fits in a more general research project followed at the *SASLab* of the DIAEE of the 'Sapienza' University of Rome, the aim of which is to realize, study and characterize several types of nanocomposite materials.

Nanostructured composite materials reinforced with multi-walled carbon nanotubes (MWCNT) were investigated in terms of their capability of absorbing energy during an impact. An experimental study was set to determine the effect of the MWCNT reinforcement on polymeric composite materials under different levels of impact energy by varying the strike velocity. In order to study tailored nanostructured composites, a chemical functionalization of MWCNTs was tuned to improve the bonding at the polymer-filler interface. Scanning electron microscopy as well as Raman and FT-IR spectroscopies were used to analyze the morphology and the chemical modifications induced on the MWCNT walls. Charpy and dropped weight tests were conducted at different weight percentages of functionalized MWCNT inclusion within commercial epoxy resins. Results of the Charpy test showed that the presence of MWCNTs enhances the toughness of the epoxy polymer up to an inclusion threshold of 0.5wt %. Experimental results of dropped weight test showed an intriguing response by the chemical treated MWCNT-based materials. High energy impact tests performed by means of the in-house Coil Gun device have shown that the panels reinforced with MWCNTs showed improved ballistic behavior in comparison with the reference ones. The explanation of the mechanical characteristics of the CNTs is really complex, and by

now debated in the scientific literature. The dramatic changes in mechanical properties observed in nanofillers challenge existing theories of mechanical reinforcement. In traditional composites, the modulus can be predicted, usually between upper and lower bounds, by modeling the effectiveness of load transfer from the matrix to the polymer. As the particles are, in large part, stiffer than the surrounding matrix, this load transfer results in a stiffer composite than the neat polymer. With the CNTs, however, the 'span' required for effective load transfer is extremely small and thus can contribute only a small portion of the dramatic gains in modulus seen in nanocomposites. In addition, because of their unique geometry, the theoretical modeling of the mechanical behavior of nanotube polymer composites is even more complex. The hollow shape of the nanotubes, the wallwall interactions in single MWCNTs, and the molecular level interactions between the nanotubes and the polymer matrix have to be considered in these models. Polymer nanocomposites incorporating carbon nanotubes or nanoparticles are a novel class of composite materials that are often multifunctional, adding the unique optical, electrical, or mechanical properties of the nanofillers while maintaining, if not enhancing, the neat polymer properties. These composites are often characterized by low volume fractions of filler, which may then affect the entire matrix, due to their large surface-area-to-volume ratio, through an interaction zone. The unique nature of these particles presents both challenges and unique opportunities to create a wide range of multifunctional polymer composites.

The possibility to employ nanoparticles-based shear thickening fluid for improving the antiballistic properties of Kevlar fabrics has also been investigated. Nanosilica particles have been used to realize the reinforcing solutions, made of polyethylene glycol. The fabric samples realization modality consisted essentially of two phases: the nanofluid preparation and the fabric impregnation treatment. The first one has to be accurately defined, in order to be confident of the basic effectiveness of the proposed reinforcing material: with such an aim, the combination of the main parameters (material amount percentages, mixing techniques, solvent influence, etc.) affecting the nanofluid preparation have been analyzed, and the several solutions characterized in terms of their rheological properties (viscosity/shear). The second one is strictly dependent on the physical/chemical coupling at the nanofluids/fabric interface: the macroscopic indications provided by the manufacturing procedure, as well as the morphological characterization analyses of the fabric surfaces, have suggested to employ two particular typologies of Kevlar fabric reinforced with nanofluid solutions with concentrations up to 20wt%. The results obtained have outlined a better resistance upon impact provided by the highest concentrations of nanofluid-reinforced materials against the corresponding unreinforced ones, thus suggesting further implementation of such nano-reinforced fabrics for antiballistic applications. In particular, a not conventional impact response mechanism seems to be dependent on the nanofluids employment, enhancing their effectiveness for energy increasing: such result can make the treated fabrics able to reach, and eventually overcome, the performances of the best commercial Kevlar-based material (here taken as reference). With such an objective, several technical improvements have to be supplied to the present state of art. Firstly, the manufacturing

technique has to be optimized in order to realize fabrics reinforced by higher concentrations of nanofluid solutions: the experimental results have shown, in fact, a clear influence of the nanosilica percentage of inclusion on the fabric absorbing energy capability. This goal, of course, has to be addressed without lack of material homogeneity and flexibility, in order to realize prototype materials of practical application.

Finally, a Coil Gun implementation in terms of efficiency is needed, in order to explore different (higher) energy ranges with the same degree of test reproducibility. Such step will be needful for achieving a deeper knowledge of the underlying impact response mechanism showed by the nanocomposite materials, thus giving the opportunity for their further optimization in terms of antiballistic performances.

References

[1] M.S.Dresselhaus, G.Dresselhaus, K.Sugihara, I.L.Spain, H.A.Goldberg, Graphite Fibers and Filaments, Springer Ser. Mater. Sci., Vol 5 (Springer, Berlin, Heidelberg 1988).
[2] M.Endo, Mecanisme de croissance en phase vapeur de fibres de carbone, PhD thesis, (University of Orleans, Orleans 1975).
[3] H.W.Kroto, J.R.Heath, S.C.O'Brien, R.F.Curl, R.E.Smalley, Nature (London) 318, 162 (1985).
[4] S.Iijima, Nature (London) 354, 56 (1991).
[5] S.S. Botha. Synthesis and characterization of nanofluids for cooling applications. South Sfrican Institute for advanced materials chemistry, Faculty of Natural Science, University of the Western Cape. October 2007.
[6] Keblinski, P.; Eastman, J. A.; Cahill, D. G. Mater. Today, June, 2005, 36.
[7] Eastman, J. A.; Choi, S. U. S.; Li, S.; Yu, W.; Thompson, L. J.; Appl. Phys. Lett., 78, 2001, 718.
[8] Samy J.-P., Gilles R., Cong T.-N. Heat transfer enhancement with the use of nanofluids in radial flow cooling systems considering temperature-dependent properties. Applied Thermal Engineering 26 (2006) 2209–2218.
[9] S.V. Garimella, B. Nenaydykh, Nozzle-geometry effects in liquid jet impingement heat transfer, Int. J. heat Mass transfer 39 (14) (1996) 2915–2923.
[10] S.V. Garimella, R.A. Rice, Confined and Submerged Liquid Jet Impingement Heat Transfer, J. Heat Transfer 117 (1995) 871–877.
[11] S.J. Downs, E.H. James, Jet Impingement Heat Transfer-A Literature Survey, ASME paper 87-HT-35 (1987) 1–11.
[12] H. Karabay, Wilson, J.M. Owen, Predictions of effect of swirl on flow and heat transfer in a rotating cavity, Int. J. Heat Fluid Flow 22 (2001) 143–155.
[13] M. Behnia, S. Parneix, Y. Shabany, P.A. Durbin, Numerical study of turbulent heat transfer in confined and unconfined impinging jets, Int. J. Heat Fluid Flow 20 (1999) 1–9.
[14] J.C. Maxwell, A Treatise on Electricity and Magnetism, 2nd ed., Oxford University Press, Cambridge, 1904, pp. 435–441.
[15] D.J. Jeffrey, Conduction through a random suspension of spheres, in: Proceedings of R. Soc. London, Ser. A, 335 (1973) 355–367.
[16] G.K. Batchelor, The effect of Brownian motion on the bulk stress in a suspension of spherical particles, J. Fluid Mech. 83 (1) (1977) 97–117.
[17] S.K. Gupte, S.G. Advani, P. Huq, Role of micro-convection due to non-affine motion of particles in a mono-disperse suspension, Int. J. Heat Mass Transfer 38 (16) (1995) 2945–2958.
[18] R.G. Boothroyd, H. Haque, Fully developed heat transfer to a gaseous suspension of particles flowing turbulently in duct of different size, J. Mech. Eng. Sci. 12 (3) (1970) 191–200.
[19] E.E. Michaelides, Heat transfer in particulate flows, Int. J. Heat Mass Transfer 29 (2) (1986) 265–273.
[20] Y. Kurosaki, T. Murasaki, Study on heat transfer mechanism of a gas-solid suspension impinging jet (effect of particle size and thermal properties), Proc. 8th Int. Heat Transfer Conf. 5 (1986) 2587–2592.
[21] D.B. Murray, Local enhancement of heat transfer in a particulate cross flow – I. Heat transfer mechanisms, Int. J. Multiphase Flow 20 (3) (1994) 493–504.
[22] R. Avila, J. Cervantes, Analysis of the heat transfer coefficient in a turbulent particle pipe flow, Int. J. Heat Mass Transfer, Vol. 38, No. 11, pp. 1923–1932.
[23] Y. Sato, E. Deutsch, O. Simonin, Direct numerical simulation of heat transfer by solid particles suspended in homogeneous isotropic turbulence, Int J. Heat Fluid Flow 19 (1998) 45–51.
[24] A.S. Ahuja, Thermal design of a heat exchanger employing laminar flow of particle suspensions, Int. J. Heat Mass Transfer 25 (5) (1982) 725–728.
[25] C.W. Sohn, M.M. Chen, Microconvective thermal conductivity in disperse two-phase mixtures as observed in a low velocity Couette flow experiment, J. Heat Transfer 103 (1981) 45–51.
[26] S.U.-S Choi, Enhancing thermal conductivity of fluids with nanoparticles, ASME Publications FED-Vol. 231/MD 66 (1995) 99–105.
[27] X. Wang, X. Xu, S.U.-S. Choi, Thermal conductivity of nanoparticles- fluid mixture, J. Thermophys. Heat Transfer 13 (4) (1999) 474–480.
[28] J.A. Eastman, S.U-S. Choi, S. Li, G. Soyez, L.J. Thompson, R.J. DiMelfi, Novel thermal properties of nanostructured materials, J. Metastable Nanocrystalline Mater. 2 (6) (1999) 629–634.

[29] Y. Xuan, W. Roetzel, Conceptions for heat transfer correlation of nanofluids, Int. J. Heat Mass Transfer 43 (2000) 3701–3707.
[30] H. Masuda, A. Ebata, K. Teramae, N. Hishinuma, Alteration of thermal conductivity and viscosity of liquid by dispersing ultra-fine particles (dispersion of c-Al_2O_3, SiO_2 and TiO_2 ultra-fine particles), Netsu Bussei 4 (4) (1993) 227–233 (in Japanese).
[31] J.A. Eastman, S.R. Phillpot, S.U.-S. Choi, P. Keblinski, Thermal Transport in Nanofluids, Annu. Rev. Mater. Res. 34 (2004) 219–246.
[32] P. Keblinski, J.A. Eastman, D.G. Cahill, Nanofluids for thermal transport, Materialstoday (2005) 36–44.
[33] J.A. Eastman, S.U.-S. Choi, S. Li, L.J. Thompson, S. Lee, Enhanced thermal conductivity through the development of nanofluids, Proc. Mat. Res. Soc. Symp. 457 (1997) 3–11.
[34] S. Lee, S.U.-S. Choi, S. Li, J.A. Eastman, Measuring thermal conductivity of fluids containing oxide nanoparticles, J. Heat Transfer 121 (1999) 280–289.
[35] Y. Xuan, Q. Li, Heat transfer enhancement of nanofluids, Int. J. Heat Fluid Flow 21 (2000) 58–64.
[36] J.A. Eastman, S.U.-S. Choi, S. Li, W. Yu, L.J. Thompson, Anomalously increased effective thermal conductivities of ethylene glycolbased nanofluids containing copper nanoparticles, Appl. Phys. Lett. 78 (6) (2001) 718–720.
[37] B.C. Pak, Y.I. Cho, Hydrodynamic and heat transfer study of dispersed fluids with submicron metallic oxide particles, Exp. Heat Transfer 11 (2) (1998) 151–170.
[38] S.K. Das, N. Putra, P. Thiesen, W. Roetzel, Temperature dependence of thermal conductivity enhancement for nanofluids, J. Heat Transfer 125 (2003) 567–574.
[39] N. Putra, W. Roetzel, S.K. Das, Natural convection of nanofluids, Heat Mass Transfer 39 (2003) 775–784.
[40] J. Koo, C. Kleinstreuer, A new thermal conductivity model for nanofluids, J. Nanopar. Res. 6 (2004) 577–588.
[41] C.H. Chon, K.D. Kihm, S.P. Lee, S.U.S. Choi, Empirical correlation finding the role of temperature and particle size for nanofluid (Al_2O_3) thermal conductivity enhancement, Appl. Phys. Lett. 87 (2005) 153107-1,3.
[42] Q. Li, Y. Xuan, Convective heat transfer performances of fluids with nano-particles, Proc. 12th Int. Heat Transfer Conference (2002) 483–488.
[43] S.E.B. Maı¨ga, C.T. Nguyen, N. Galanis, G. Roy, Heat transfer behaviours of nanofluids in a uniformly heated tube, Superlattices Microstruct. 35 (3–6) (2004) 543–557.
[44] S.E.B. Maı ¨ga, S.J. Palm, C.T. Nguyen, G. Roy, N. Galanis, Heat transfer enhancement by using nanofluids in forced convection flows, Int. J. Heat Fluid Flow 26 (2005) 530–546.
[45] G. Roy, C.T. Nguyen, P.-R. Lajoie, Numerical investigation of laminar flow and heat transfer in a radial flow cooling system with the use of nanofluids, Superlattices Microstruct. 35 (3–6) (2004) 497–511.
[46] D.A. Drew, S.L. Passman, Theory of Multicomponent Fluids, Springer, Berlin, 1999.
[47] Z.Ya.Kosakovskaya, L.A.Chernozatonskii, E.A.Fedorov, JETP Lett. (Pis'ma Zh. Eksp. Teor.) 55, 483 (1992).
[48] S.Iijima, T.Ichihashi, Nature (London) 363, 603 (1993).
[49] D.S.Bethune, C.H.Kiang, M.S.de Vries, G.Gorman, R.Savoy, J. Vasquez, R.Beyers, Nature (London) 363, 605 (1993).
[50] R.Saito, G.Dresselhaus, M.S.Dresselhaus, Physical Properties of Carbon Nanotubes (Imperial College Press, London 1998).
[51] J.Liu, A.G.Rinzler, H.Dai, J.H.Hafner, R.K.Bradley, P.J.Boul, A.Lu, T.Iverson, K.Shelimov, C.B.Huffman, F.Rodriguez-Macia, D.T.Colbert, R.E.Smalley, Science 280, 1253 (1998).
[52] W.Zhu, G.Kochanski, S.Jin, Science 282, 1471 (1998).
[53] A.G.Rinzler, J.H.Hafner, P.Nikolaev, L.Lou, S.G.Kim, D.Tomanek, D.T.Colbert, R.E.Smalley, Science 269, 1550 (1995).
[54] P.Chen, X.Wu, J.Lin, K.Tan, Science 285, 91 (1999).
[55] M.S.Dresselhaus, K.A.Williams, P.C.Eklund, MRS Bull. 24, (11), 45 (1999).
[56] B.I.Yakobson, C.J.Brabec, J.Bernholc, Phys. Rev. Lett. 76, 2511 (1996).
[57] M.M.J.Treacy, T.W.Ebbesen, J.M.Gibson, Nature 381, 678 (1996).
[58] M.Yu, O.Lourie, M.J.Dyer, K.Moloni, T.F.Kelly, R.S.Ruoff, Science 287, 637 (2000).
[59] H.J.Dai, J.H.Hafner, A.G.Rinzler, D.T.Colbert, R.E. Smalley, Nature 384, 147 (1996).
[60] Liu, M.-S.; Lin, M. C.-C.; Huang, I.-T.; Wang, C.-C., Int. Commun.Heat Mass Transfer, 32, 2005, 1202.
[61] Bönnemann, H.; Botha S. S.; Bladergroen B.; Linkov, V. M.; Appl. Organomet. Chem., 19, 2005, 768.

[62] Choi S U S, Zhang Z G, Yu W, Lockwood F E and Grulke E A 2001 Appl. Phys. Lett. 79 2252–4.
[63] Prasher R, Bhattacharya P and Phelan P E 2006 Brownian motion based convective conductive model for the effective thermal conductivity of nanofluids J. Heat Transfer 128 588–95
[64] Keblinski P, Phillpot S R, Choi S U S and Eastman J A 2002 Mechanisms of heat flow in suspensions of nanosized particles (nanofluids) Int. J. Heat Mass Transfer 45 855–63.
[65] Jang S P and Choi S U S 2004 Role of Brownian motion in the Enhanced thermal conductivity of nanofluids Appl. Phys. Lett. 84 4316–8.
[66] Buongiorno J 2006 Convective transport in nanofluids J. Heat Transfer 128 240–50
[67] Xie H, Lee H, Youn W and Choi M 2003 Nanofluids containing multiwalled carbon nanotubes and their enhanced thermal conductivities J. Appl. Phys. 94 4967–71.
[68] Wen D and Ding Y 2004 Effective thermal conductivity of aqueous suspensions of carbon nanotubes (carbon nanotubes nanofluids) J. Thermophys. Heat Transfer 18 481–5.
[69] Assael M J, Chen C-F, Metaxa I and Wakeham W A 2004 Thermal conductivity of suspensions of carbon nanotubes in water Int. J. Thermophys. 25 971–85.
[70] Vander Wal R L, Tomasek A J, Pamphlet M I, Taylor C D and ThompsonW K 2004 Analysis of HRTEM images for carbon nanostructure quantification J. Nanopart. Res. 6 555–68.
[71] Prasher R, EvansW, Meakin P, Fish J, Phelan P and Keblinski P 2006 Effect of aggregation on thermal conduction in colloidal nanofluids Appl. Phys. Lett. 89 143119–3.
[72] Buyevich, Y. A.; Fluid Dynamics in Fine Suspension Flow. In Advances in the Flow and Rheology of Non-Newtonian Fluids, Part B. 1st ed. Edited by Siginer, D. A.; De Kee, D.; Chhabra, R. P.; Amsterdam, The Netherlands: Elsevier, 1999, 1237-1297.
[73] Kwak, K.; Kim, C.; Kor.-Austr. Rheol. J., 17, 2005, 35.
[74] Xuan, Y.; Li, Q.; Int. J. Heat Fluid Flow, 21, 2000, 58.
[75] P.D.Mangalgiri, Composite materials for aerospace applications, Bull. Mater. Sci., 22, 3 (1999), 657-664.
[76] J.Njuguna, K.Pielichowski, Polymer Nanocomposites for Aerospace Applications, Adv. Eng. Mat.,5, 11 (2003), 769-778.
[77] B. J. Ash, A. Eitan, L. S. Schadler Polymer Nanocomposites with Particle and Carbon Nanotube Fillers Dekker Encyclopedia of Nanoscience and Nanotechnology 2917-2930. DOI: 10.1081/E-ENN 120009067
[78] Bueche, A.M. Filler reinforcement of silicone rubber. J. Polym. Sci. 1957, 25, 139–149.
[79] Kuriakose, B.; De, S.K.; Bhagawan, S.S.; Sivaramkrishnan, R.; Athithan, S.K. Dynamic mechanical properties of thermoplastic elastomers from polypropylene–natural rubber blend. J. Appl. Polym. Sci. 1986, 32, 5509–5521.
[80] Sumita, M.; Shizuma, T.; Miyasaka, K.; Shikawa, K.J. Effect of reducible properties of temperature, rate of strain, and filler content on the tensile yield stress of nylon 6 composites filled with ultrafine particles.Macromol. Sci.-Phys. 1983,B22,599–616.
[81] Sumita, M.; Tsukumo, Y.; Miyasaka, K.; Ishikawa, K. Tensile yield stress of polypropylene composites filled with ultrafine particles. J. Mater. Sci. 1983, 18, 1758–1764.
[82] Li, T.; Chen, Q.; Schadler, L.S.; Siegel, R.W.; Mendel, J.; Irvin, G.C., Jr. Scratch behavior of nanophase Al2O3-filled gelatin films. Polym. Compos. 2002, 23 (6), 1076–1086.
[83] Ruan, S.L.; Gao, P.; Yang, X.G.; Yu, T.X. Toughening high performance ultrahigh molecular weight polyethylene using multiwalled carbon nanotubes. Polymer 2003, 44, 5643–5654.
[84] Ash, B.J.; Stone, J.; Rogers, D.F.; Schadler, L.S.; Siegel, R.W.; Benicewicz, B.C.; Apple, T. Investigations into the thermal and mechanical behavior of PMMA/alumina nanocomposites. Mater. Res. Soc. Symp. Proc. 2001, 661, KK2.10.1– KK2.10.6.
[85] Caseri, W. Nanocomposites of polymers and metals or semiconductors: Historical background and optical properties. Macromol. Rapid Commun. 2000, 21, 705–722.
[86] Siegel, R.W. Nanophase Materials. In Encyclopedia of Applied Physics; Trigg, G.L., Ed.; Weinheim: VCH Publishing, 1994; Vol. 11.
[87] Hergeth, W.; Steinau, U.; Bittrich, H.; Simon, G.; Schmutzler, K. Polymerization in the presence of seeds: Part IV. Emulsion polymers containing inorganic filler particles. Polymer 1989, 30, 254–258.
[88] Becker, C.; Mueller, P.; Schmidt, H. Optical and thermomechanical investigations on thermoplastic nanocomposites with surface modified silica nanoparticles. SPIE 1998, 3469, 88–98.
[89] Carotenuto, G.; Nicolais, L.; Kuang, X.; Zhu, Z. A method for the preparation of PMMA–SiO2 nanocomposites with high homogeneity. Appl. Compos. Mater. 1995, 2, 385–393.
[90] Wang, Z.; Pinnavaia, T.J. Hybrid organic–inorganic nanocomposites: Exfoliation of magadiite nanolayers in an elastomeric epoxy polymer. Chem. Mater. 1998, 10, 1820–1826.

[91] Becker, C.; Krug, H.; Schmidt, H. Tailoring of thermomechanical properties of thermoplastic nanocomposites by surface modification of nanoscale silica particles. Mater. Res. Soc. Symp. Proc. 1996, 435, 237–242.
[92] Ash, B.J.; Schadler, L.S.; Siegel, R.W. Glass transition behavior of alumina/polymethylmethacrylate nanocomposites. Mater. Lett. 2002, 55, 83–87.
[93] Ding, W.; Eitan, A.; Fisher, F.T.; Chen, X.; Dikin, D.A.; Andrews, R.; Brinson, L.C.; Ruoff, R.S. Direct observation of polymer sheathing in carbon nanotube—Polycarbonate composites. Nano Lett. 2003, 3 (11), 1593–1587.
[94] Chan, C.M.; Wu, J.; Li, J.X.; Cheung, Y.K. Polypropylene/calcium carbonate nanocomposites. Polymer 2002, 43, 2981–2992.
[95] Abboud, M.; Turner, M.; Duguet, E.; Fontanille, M. PMMA-based composite materials with reactive ceramic fillers: Part 1. Chemical modification and characterization of ceramic particles. J. Mater. Chem. 1997, 7, 1527.
[96] Wang, S.; Wang, M.; Lei, Y.; Zhang, L. Anchor effect of poly(styrene maleic anhydride)/TiO2 nanocomposites. J. Mater. Sci. Lett. 1999, 18, 2009–2012.
[97] Caris, C.; van Elven, L.; van Herk, A.; German, A. Polymerization of MMA (methyl methacrylate) at the surface of inorganic submicron particles. Br. Polym. J. 1989, 21, 133–140.
[98] Rong, M.Z.; Zhang, M.Q.; Zheng, Y.X.; Zeng, H.M.; Friedrich, K. Improvement of tensile properties of nano-SiO2/PP composites in relation to percolation mechanism. Polymer 2001, 42, 3301–3304.
[99] von Werne, T.; Patten, T. Atom transfer radical polymerization from nanoparticles: A tool for the preparation of well-defined hybrid nanostructures and for understanding the chemistry of controlled/'living' radical polymerizations from surfaces. J. Am. Chem. Soc. 2001, 123, 7497–7505.
[100] Weimer, M.W.; Chen, H.; Giannelis, E.P.; Sogah, D.Y. Direct synthesis of dispersed nanocomposites by in situ living free radical polymerization using a silicate-anchored initiator. J. Am. Chem. Soc. 1999, 121, 1615–1616.
[101] Tsubokawa, N.; Kogure, A.; Maruyama, K.; Sone, Y.; Shimomura, M. Graft polymerization of vinyl monomers from inorganic ultrafine particles initiated by azo groups introduced onto the surface. Polym. J. 1990, 22, 827–833.
[102] Caruso, F. Nanoengineering of particle surfaces. Adv. Mater. 2001, 13, 11–22.
[103] Qian, D.; Dickey, E.C.; Andrews, R.; Rantell, T. Load transfer and deformation mechanisms in carbon nanotube–polystyrene composites. Appl. Phys. Lett. 2000, 76 (20), 2868–2870.
[104] Dalton, A.B.; Bayrne, H.J.; Coleman, J.N.; Curran, S.; Davey, A.P.; McCarthy, B.; Blau, W. Optical absorption and fluorescence of multi-walled nanotube– polymer composites. Synth. Met. 1999, 102, 1176–1177.
[105] Kahn, M.G.C.; Banerjee, S.; Wong, S.S. Solubilization of oxidized single-walled carbon nanotubes in organic and aqueous solvents through organic derivatization. Nano Lett. 2002, 2 (11), 1215–1218.
[106] Bower, C.; Kleinhammes, A.; Wu, Y.; Zhou, O. Intercalation and partial exfoliation of singlewalled carbon nanotubes by nitric acid. Chem. Phys. Lett. 1998, 288, 481–486.
[107] Nagasawa, S.; Yudasaka, M.; Hirahara, K.; Ichihashi, T.; Ijima, S. Effect of oxidation on single-wall carbon nanotubes. Chem. Phys. Lett. 2000, 328, 374–380.
[108] Chen, J.; Hamon, M.A.; Hu, H.; Chen, Y.; Rao, A.M.; Eklund, P.C.; Haddon, R.C. Solution properties of single-walled carbon nanotubes. Science 1998, 282, 95–98.
[109] Niyogi, S.; Hamon, M.A.; Hu, H.; Zhao, B.; Bhowmik, B.; Sen, R.; Itkis, M.E.; Haddon, R.C. Chemistry of single-walled carbon nanotubes. Acc. Chem. Res. 2002, 35, 1105–1113.
[110] Carrillo, A.; Swartz, J.A.; Gamba, J.M.; Kane, R.S.; Chakrapani, N.; Wei, B.; Ajayan, P. Noncovalent functionalization of graphite and carbon nanotubes with polymer multilayers and gold nanoparticles. Nano Lett. 2003, 3 (11), 1437–1440.
[111] Chen, J.; Liu, H.; Weimer, W.A.; Halls, M.D.; Waldeck, D.H.; Walker, G.C. Noncovalent engineering of carbon nanotube surfaces by rigid, functional conjugated polymers. J. Am. Chem. Soc. 2002, 124 (31), 9034–9035.
[112] Gong, X.; Liu, J.; Baskaran, S.; Voise, R.D.; Young, J.S. Surfactant-assisted processing of carbon nanotube/polymer composites. Chem. Mater. 2000, 12, 1049–1052.
[113] O'Connell, M.J.; Boul, P.; Ericson, L.M.; Huffman, C.; Wang, Y.; Haroz, E.; Kuper, C.; Tour, J.; Ausman, K.D.; Smalley, R.E. Reversible watersolubilization of single-walled carbon nanotubes by polymer wrapping. Chem. Phys. Lett. 2001, 342, 265–271.
[114] Czerw, R.; Guo, Z.; Ajayan, P.M.; Sun, T.-P.; Carroll, D.L. Organization of polymers onto carbon nanotubes: A route to nanoscale assembly. Nano Lett. 2001, 1 (8), 423–427.
[115] McCarthy, B.; Coleman, J.N.; Crezw, R.; Dalton, A.B.; in het Panhuis, M.; Drury, A.; Brenier, P.; Nagy, J.B.; Lahr, B.; Byrne, H.J.; Carroll, D.L.; Blau, W.J. A microscopic and spectroscopic study of

interactions between carbon nanotubes and a conjugated polymer. J. Phys. Chem., B 2002, 106 (9), 2210–2216.
[116] Hamon, M.A.; Hu, H.; Bhowmik, P.; Niyogi, S.; Zhao, B.; Itkis, M.E.; Haddon, R.C. End-group and defect analysis of soluble single-walled carbon nanotubes. Chem. Phys. Lett. 2001, 347, 8–12.
[117] Lin, Y.; Rao, A.M.; Sadanadan, B.; Kenik, E.A.; Sun, Y.-P. Functionalization of multiple-walled carbon nanotubes with aminopolymers. J. Phys. Chem., B 2002, 106 (6), 1294–1298.
[118] Hill, D.E.; Rao, A.M.; Allard, L.F.; Sun, Y.-P. Functionalization of carbon nanotubes with polystyrene. Macromolecules 2002, 35 (25), 9466–9471.
[119] Zhao, W.; Song, C.; Pehrsson, P.E. Water-soluble and optically PH-sensitive single-walled carbon nanotubes from surface modification. J. Am. Chem. Soc. 2002, 124 (42), 12418–12419.
[120] Liu, J.; Rinzler, A.G.; Dai, J.H.; Hafner, J.H.; Bradley, R.K; Boul, P.J.; Lu, A.; Iverson, T.; Shelimov, K.; Huffman, C.B.; Rodrigez-Macias, F.; Shon, Y.S.; Lee, T.R.; Colbert, D.T.; Smalley, R.E. Fullerene pipes. Science 1998, 280, 1253–1256.
[121] Hamon, M.A.; Chen, J.; Hu, H.; Chen, Y.; Itkis, M.E.; Rao, A.M.; Eklund, P.C.; Haddon, R.C. Dissolution of single-walled carbon nanotubes. Adv. Mater. 1999, 11 (10), 834–840.
[122] Baker, S.E.; Cai, W.; Lasseter, T.L.; Weidkamp, K.P.; Hamers, R.J. Covalently bonded adducts of deoxyribonucleic acid (DNA) oligonucleotides with single-wall carbon nanotubes: Synthesis and hybridization. Nano Lett. 2002, 2 (12), 1413–1417.
[123] Huang, W.; Fernando, S.; Allard, L.F.; Sun, Y.-P. Solubilization of single-walled carbon nanotubes with diamine-terminated oligomeric poly(ethylene glycol) in different functionalization reactions. Nano Lett. 2003, 3 (4), 565–568.
[124] Huang, W.; Taylor, S.; Fu, K.; Lin, Y.; Zhang, D.; Hanks, T.W.; Rao, A.M.; Sun, Y.-P. Attaching proteins to carbon nanotubes via diimide-activated amidation. Nano Lett. 2002, 2 (4), 311–314.
[125] Banerjee, S.; Wong, S.S. Synthesis and characterization of carbon nanotube–nanocrystal heterostructures. Nano Lett. 2002, 2 (3), 195–200.
[126] Mickelson, E.T.; Huffman, C.B.; Rinzler, A.G.; Smalley, R.E.; Hauge, R.H.; Margrave, J.L. Fluorination of single-wall carbon nanotubes. Chem. Phys. Lett. 1998, 296, 188–194.
[127] Ying, Y.; Saini, R.K.; Liang, F.; Sadana, A.K.; Billups, W.E. Functionalization of carbon nanotubes by free radicals. Org. Lett. 2003, 5 (9), 1471–1473.
[128] Holzinger, M.; Votrowsky, O.; Hirsch, A.; Hennrich, F.; Kappes, M.; Weiss, R.; Jellen, F. Sidewall functionalization of carbon nanotubes. Angew. Chem., Int. Ed. 2001, 40 (21), 4002–4005.
[129] Banerjee, S.; Wong, S.S. Structural characterization, optical properties, and improved solubility of carbon nanotubes functionalized with Wilkinson's catalyst. J. Am. Chem. Soc. 2002, 124, 8940–8948. 55. Georgakilas, V.; Kordatos, K.; Prato, M.; Guldi, D.M.; Holzinger, M.; Hirsch, A. Organic functionalization of carbon nanotubes. J. Am. Chem. Soc. 2002, 124 (5), 760–761.
[130] Dyke, C.A.; Tour, J.M. Solvent-free functionalization of carbon nanotubes. J. Am. Chem. Soc. 2003, 125, 1156–1157.
[131] Velasco-Santos, C.; Martı´nez-Herna´ndez, A.L.; Lozada-Cassou, M.; Alvarez-Castillo, A.; Castan˜o, V.M. Chemical functionalization of carbon nanotubes through an organosilane. Nanotechnology 2002, 13, 495–498.
[132] Bahr, L.J.; Tour, J.M. Highly functionalized carbon nanotubes using in situ generalized diazonium compounds. Chem. Mater. 2001, 13 (11), 3823–3824.
[133] ……..
[134] Ajayan, P.M.; Braun, P.; Schadler, L.S. Nanocomposite Science and Technology; Wiley-VCH Verlag GmbH & Co. KgaA: Weinheim, Germany, 2003.
[135] Hussain, M.; Nakahara, A.; Nishijima, S.; Niihara, K. Fracture behavior and fracture toughness of particulate filled epoxy composites. Mater. Lett. 1996, 27, 21–25.
[136] Sumita, M.; Tsukihi, H.; Miyasaka, K.; Ishikawa, K. Dynamic mechanical properties of polypropylene composites filled with ultrafine particles. J. Appl. Polym. Sci. 1984, 29, 1523–1530.
[137] Ou, Y.; Yang, F.; Yu, Z. A new conception on the toughness of nylon 6/silica nanocomposite prepared via in situ polymerization. J. Polym. Sci., B, Polym. Phys. 1998, 36, 789–795.
[138] Petrovic, Z.S.; Zhang, W. Glassy and elastomeric polyurethanes filled with nano-silica particles. Mat. Sci. Forum 2000, 352, 171–176.
[139] Petrovic, Z.S.; Javni, I.; Waddon, A.; Banhegyi, G. Structure and properties of polyurethane–silica nanocomposites. J. Appl. Polym. Sci. 2000, 76, 133–151.
[140] Zhang, J.; Wang, X.; Lu, L.; Li, D.; Yang, X. Preparation and performance of high-impact polystyrene (HIPS)/nano-TiO2 nanocomposites. J. Appl. Polym. Sci. 2003, 87, 381–385.
[141] Ash, B.J.; Rogers, D.F.; Wiegand, C.J.; Schadler, L.S.; Siegel, R.W.; Benicewicz, B.C.; Apple, T. Mechanical properties of Al2O3/polymethylmethacrylate nanocomposites. Polym. Compos. 2002, 23, 1014–1025.

[142] Zhang, Q.; Archer, L.A. Poly(ethylene oxide)/silica nanocomposites: Structure and rheology. Langmuir 2002, 18, 10435–10442.
[143] Sternstein, S.S.; Zhu, A.-J. Reinforcement mechanism of nanofilled polymer melts as elucidated by nonlinear viscoelastic behavior. Macromolecules 2002, 35, 7262–7273.
[144] Payne, A.R. The dynamic properties of carbon black-loaded natural rubber vulcanizates. J. Appl. Polym. Sci. 1962, 6, 368–372.
[145] Zhang, M.Q.; Rong, M.Z.; Yu, S.L.; Wetzel, B.; Friedrich, K. Effect of particle surface treatment on the tribological performance of epoxy based nanocomposites. Wear 2002, 253, 1086–1093.
[146] Hwang, D.K.; Moon, J.H.; Shul, Y.G.; Jung, K.T.; Kim, D.H.; Lee, D.W. Scratch resistant and transparent UV-protective coating on polycarbonate. J. Sol-Gel Sci. Technol. 2003, 26, 783–787.
[147] Ng, C.B.; Schadler, L.S.; Siegel, R.W. Synthesis and mechanical properties of TiO2–epoxy nanocomposites. J. Nanostruct. Mater. 1999, 12 (1–4), 507–510.
[148] Li, T.; Chen, Q.; Schadler, L.S.; Siegel, R.W. Scratch behavior of nanoparticle Al2O3-filled gelatin films. Polym. Compos. 2002, 23, 1076–1086.
[149] Gall, K.; Dunn, M.L.; Liu, Y.; Finch, D.; Lake, M.; Munshi, N.A. Shape memory polymer nanocomposites. Acta Mater. 2002, 50, 5115–5126.
[150] Iisaka, K.; Shibayama, K. Mechanical alphadispersion and interaction in filled polystyrene and polymethylmethacrylate. J. Appl. Polym. Sci. 1978, 22, 3135–3143.
[151] Avella, M.; Errico, M.E.; Martuscelli, E. Novel PMMA/CaCO3 nanocomposites abrasion resistant prepared by an in situ polymerization process. Nano Lett. 2001, 1, 213–217.
[152] Arrighi, V.; McEwen, I.J.; Qian, H.; Serrano Prieto, M.B. The glass transition and interfacial layer in styrene–butadiene rubber containing silica nanofiller. Polymer 2003, 44, 6259–6266.
[153] Tsagaropoulos, G.; Eisenberg, A. Direct observation of two glass transitions in silica-filled polymers. Implications for the morphology of random ionomers. Macromolecules 1995, 28, 396–398.
[154] Long, D.; Lequeux, F. Heterogeneous dynamics at the glass transition in van der Waals liquids, in the bulk and in thin films. Eur. Phys. J., E 2001, 4, 371.
[155] Mattsson, J.; Forrest, J.A.; Borgesson, L. Quantifying glass transition behavior in ultrathin freestanding polymer films. Phys. Rev., E. 2000, 62, 5187–5200.
[156] Merkel, T.C.; Toy, L.G.; Andrady, A.L.; Gracz, H.; Stejskal, E.O. Investigation of enhanced free volume in nanosilica-filled poly(1-trimethylsilyl-1- propyne) by 129Xe NMR spectroscopy. Macromolecules 2003, 36, 353–358.
[157] Zhong, J.; Wen, W.Y.; Jones, A.A. Enhancement of diffusion in a high-permeability polymer by the addition of nanoparticles. Macromolecules 2003, 36, 6430–6432.
[158] Kyprianidou-Leodidou, T.; Margraf, P.; Caseri, W.; Suter, U.W.; Walther, P. Polymer sheets with a thin nanocomposite layer acting as a UV filter. Polym. Adv. Technol. 1997, 8, 505–512.
[159] Nussbaumer, R.J.; Caseri, W.R.; Smith, P.; Tervoort, T. Polymer–TiO2 nanocomposites: A route towards visually transparent broadband UV filters and high refractive index materials. Macromol. Mater. Eng. 2003, 288, 44–49.
[160]. Weibel, M.; Caseri, W.; Suter, U.W.; Kiess, H.; Wehrli, E. Polymer nanocomposites with 'ultrahigh' refractive index. Polym. Adv. Technol. 1991, 2, 75–80.
[161] Zimmermann, L.; Weibel, M.; Caseri, W.; Suter, U.W.; Walther, P. Polymer nanocomposites with 'ultralow' refractive index. Polym. Adv. Technol. 1993, 4, 1–7.
[162] Dirix, Y.; Darribere, C.; Heffels, W.; Bastiaansen, C.; Caseri, W.; Smith, P. Optically anisotropic polyethylene–gold nanocomposites. Appl. Opt. 1999, 38, 6581–6586.
[163] Ash, B.J. Investigation into the Thermal and Mechanical Behavior of Alumina/Polymethylmethacrylate Nanocomposites. Ph.D. Thesis; Rensselaer Polytechnic Institute, 2003; 108–113.
[164] Roy, S.; Das, D.; Chakravorty, D.; Agrawal, D.C. Magnetic properties of glass–metal nanocomposites prepared by the sol–gel route and hot pressing. J. Appl. Phys. 1993, 74, 4746–4749.
[165] Morup, S.; Tronc, E. Superparamagnetic relaxation of weakly interacting particles. Phys. Rev. Lett. 1994, 72, 3278–3281.
[166] Banerjee, P.; Mandel, B.M. Conducting polyaniline nanoparticle blends with extremely low percolation thresholds. Macromolecules 1995, 28, 3940–3943.
[167] Hong, J.I.; Schadler, L.S.; Siegel, R.W.; Martensson, E. Rescaled electrical properties of ZnO/LDPE nanocomposites. Appl. Phys. Lett. 2003, 82, 1956–1958.
[168] Gonsalves, K.E.; Merhari, L.; Wu, H.; Hu, Y. Organic–inorganic nanocomposites: Unique resists for nanolithography. Adv. Mater. 2001, 13, 703–714.
[169] F. Findik, N. Tarim. Ballistic impact efficiency of polymer composites. Composite Structures 61 (2003) 187–192.

[170] Middleton DH. Composite materials in aircraft structures. Essex: Longman Scientific and Technical Ltd.; 1990.
[171] Engineering guide to composite materials. New York: American Society for Metals; 1989.
[172] D.Brown, C.Miller, M.Schumacher, K.Werner, S.-T. Crino. Improving Special Operations Aircraft Survivability through Better Ballistic Protection System Proceedings of the 2009 IEEE Systems and Information, Engineering Design Symposium, University of Virginia, Charlottesville, VA, USA, April 24, 2009.
[173] Treacy, M.M.J.; Ebbesen, T.W.; Gibson, J.M. Exceptionally high young's modulus for individual carbon nanotubes. Nature 1996, 381 (6584), 678– 680.
[174] Gao, G.H.; Cagin, T.; Goddard, W.A. Energetics, structure, mechanical and vibrational properties of single-walled carbon nanotubes. Nanotechnology 1998, 9 (3), 184–191.
[175] Lu, J.P. Elastic properties of carbon nanotubes and nanoropes. Phys. Rev. Lett. 1997, 79 (7), 1297–1300.
[176] Sanchez-Portal, D.; Artacho, E.; Soler, J.M.; Rubio, A.; Ordejon, P. Ab initio structural, elastic, and vibrational properties of carbon nanotubes. Phys. Rev., B 1999, 59, 12677–12688.
[177] Yakobson, B.I.; Barber, C.J.; Bemhole, J. Nanomechanics of carbon tubes: Instabilities beyond linear response. Phys. Rev. Lett. 1996, 76 (14), 2511–2514.
[178] Zhou, X.; Zhou, J.J.; Ou-Yang, Z.C. Strain energy and Young's modulus of single-wall carbon nanotubes calculated from electronic energy-band theory. Phys. Rev., B 2000, 62 (20), 13692–13696.
[179] Popov, V.N.; Van Doren, V.E.; Balkanski, M. Elastic properties of single-walled carbon nanotubes. Phys. Rev., B 2000, 61 (4), 3078–3084.
[180] Belytschko, T.; Xiao, S.P.; Schatz, G.C.; Ruoff, R.S. Atomistic simulations of nanotube fracture. Phys. Rev., B 2002, 65 (23), 235430/1–8.
[181] Yu, M.F.; Lourie, O.; Dyer, M.J.; Moloni, K.; Kelly, T.F.; Ruoff, R.S. Strength and breaking mechanism of multiwalled carbon nanotubes under tensile load. Science 2000, 287, 637–640.
[182] Yu, M.F.; Files, B.S.; Arepalli, S.; Ruoff, R.S. Tensile loading of ropes of single wall carbon nanotubes and their mechanical properties. Phys. Rev. Lett. 2000, 84 (24), 5552–5555.
[183] Krishnan, A.; Dujardin, E.; Ebessen, T.W.; Yanilos, P.N.; Treacy, M.M.J. Young's modulus of single-walled nanotubes. Phys. Rev., B 1998, 58, 14013.
[184] Lourie, O.; Wagner, H.D. Evaluation of Young's modulus of carbon nanotubes by micro-Raman spectroscopy. J. Mater. Res. 1998, 13 (9), 2418–2422.
[185] Thostenson, E.T.; Ren, Z.F.; Chou, T.W. Advances in the science and technology of carbon nanotubes and their composites: A review. Compos. Sci. Technol. 2001, 61 (13), 1899–1912.
[186] Schadler, L.S.; Giennaris, S.C.; Ajayan, P.M. Load transfer in carbon nanotube epoxy composites. Appl. Phys. Lett. 1998, 73 (26), 3842–3844.
[187] Sandler, J.; Werner, P.; Shaffer, M.S.P.; Demchuk, V.; Altsta¨dt, V.; Windle, A.H. Carbon-nanofibrereinforced poly(ether ether ketone) composites. Compos., Part A 2002, 33, 1033–1039.
[188] Jin, Z.; Pramoda, K.P.; Goh, S.H.; Xu, G. Poly(vinylidene fluoride)-assisted melt-blending of multi-walled carbon nanotube/poly(methyl methacrylate) composites. Mater. Res. Bull. 2002, 37, 271–278.
[189] Jia, Z.; Wang, Z.; Xu, C.; Liang, J.; Wei, B.; Wu, D.; Zhu, S. Study on poly(methyl methacrylate) carbon nanotube composites. Mater. Sci. Eng., A 1999, 271, 395–400.
[190] Park, C.; Ounaies, Z.; Watson, K.A.; Crooks, R.E.; Smith, J., Jr.; Lowther, S.E.; Connell, J.W.; Siochi, E.J.; Harrison, J.S.; St. Clair, T.L. Dispersion of single wall carbon nanotubes by in situ polymerization under sonication. Chem. Phys. Lett. 2002, 364, 303–308.
[191] Geng, H.Z.; Rosen, R.; Zheng, B.; Shimoda, H.; Fleming, L.; Liu, J.; Zhou, O. Fabrication and properties of poly(ethylene oxide) and functionalized carbon nanotubes. Adv. Mater. 2002, 14 (19), 1387–1390.
[192] Kimura, T.; Ago, H.; Tobita, M.; Ohshima, S.; Kyotani, M.; Yumura, M. Polymer composites of carbon nanotubes aligned by a magnetic field. Adv. Mater. 2002, 14 (19), 1380–1383.
[193] Haggenmueller, R.; Gommans, H.H.; Rinzler, A.G.; Fischer, J.E.; Winey, K.I. Aligned single-wall carbon nanotubes in composites by melt processing methods. Chem. Phys. Lett. 2000, 330, 219–225.
[194] M. Wong, M. Paramsothy, X. J. Xu, Y. Ren, S. Li and K. Liao. Physical interactions at carbon nanotube-polymer interface. Polymer, Volume 44, Issue 25, December 2003, Pages 7757-7764.
[195] C. Bower, R. Rosen, L. Jin, J. Han and O. Zhou. Appl Phys Lett 74 22 (1999), pp. 3317–3319.
[196] B.H. Chang, Z.Q. Liu, L.F. Sun, D.S. Tang, W.Y. Zhou, G. Wang, L.X. Qian, S.S. Xie, J.H. Fen and M.X. Wan. J Low Temp Phys 119 1/2 (2000), pp. 41–48.
[197] Z. Jia, Z. Wang, C. Xu, J. Liang, B. Wei, D. Wu and S. Zhu. Mater Sci Engng A 271 (1999), pp. 395–400.
[198] H.D. Wagner, O. Lourie, Y. Feldman and R. Tenne. Appl Phys Lett 72 2 (1998), pp. 188–190.

[199] O. Lourie and H.D. Wagner. Appl Phys Lett 73 24 (1998), pp. 3527–3529.
[200] D. Qian, E.C. Dickey, R. Andrew and T. Rantell. Appl Phys Lett 76 20 (2000), pp. 2868–2870.
[201] X.J. Xu, M.M. Thwe, C. Shearwood and K. Liao. Appl Phys Lett 81 15 (2002), pp. 2833–2835.
[202] H.D. Wagner. Chem Phys Lett 361 (2002), pp. 57–61.
[203] K. Liao and S. Li. Appl Phy Lett 79 25 (2001), pp. 4225–4227.
[204] V. Lordi and N. Yao. J Mater Res 15 12 (2000), pp. 2770–2779.
[205] C.A. Cooper, S.R. Cohen, A.H. Barber and H.D. Wagner. Appl Phys Lett 81 20 (2002), pp. 3873–3875.
[206] L.S. Schadler, S.C. Giannaris and P.M. Ajayan. Appl Phys Lett 73 26 (1998), pp. 3842–3844.
[207] P.M. Ajayan, L.S. Schadler, S.C. Giannaris and A. Rubio. Adv Mater 12 10 (2000), pp. 750–753.
[208] T. A. Hassan, V. K. Rangari, S. Jeelani. Synthesis, processing and characterization of shear thickening fluid (STF) impregnated fabric composites. Materials Science and Engineering A 527 (2010) 2892–2899.
[209] H.A. Barnes, J. Rheol. 33 (2) (1989) 329.
[210] R.L. Hoffmann, Trans. Soc. Rheol. 16 (1972) 155.
[211] R.L. Hoffmann, J. Colloid Interface Sci. 46 (1974) 491.
[212] R.L. Hoffmann, Sci. Technol. Polym. Colloids 2 (1983) 570.
[213] W.H. Boersma, J. Laven, H.N. Stein, J. Colloid Interface Sci. 149 (1992) 10.
[214] H.M. Laun, R. Bung, S. Hess, W. Loose, O. Hess, K. Hahn, E. Hadicke, R. Hingmann, F. Schmidt, P. Lindner, J. Rheol. 36 (1992) 743.
[215] J.W. Bender, N.J. Wagner, J. Colloid Interface Sci. 172 (1995) 171.
[216] J.W. Bender, N.J. Wagner, J. Rheol. 40 (1996) 899.
[217] T.N. Phung, J.F. Brady, J. Fluid Mech. 313 (1996) 181.
[218] J.R. Melrose, J.H. van Vliet, R.C. Ball, Phys. Rev. Lett. 77 (1996) 4660.
[219] R.S. Farr, J.R. Melrose, R.C. Ball, Phys. Rev. 55 (1997) 7203.
[220] J.F. Brady, G. Bossis, Annu. Rev. Fluid Mech. 20 (1988) 111.
[221] B.J. Maranzano, N.J. Wagner, J. Chem. Phys. 117 (2002) 22.
[222] G. Bossis, J.F. Brady, J. Chem. Phys. (1989) 911866.
[223] C.G. Albert, TAPPI 34 (1951) 453.
[224] B. Alince, P. Lepoutre, TAPPI 6 (1983) 57.
[225] G.N.M. Choi, Ph.D. Thesis, Ann Arbor, MI, 1983.
[226] E.J.W. Verwey, J.H. de Boer, Rec. Truu. Chim. 57 (1939) 383.
[227] Z. Andreja, L. Romano, Z. Miha, TAPPI 30 (1997) 67.
[228] R. Srinivasa, Raghavan, S.A. Khan, J. Colloid Interface Sci. 185 (1997) 57.
[229] Y.S. Lee, E. Wetzel, N.J. Wagner, J. Mater. Sci 38 (2003) 2825.
[230] T. A. Hassan, V. K. Rangari, S. Jeelani. Sonochemical synthesis and rheological properties of shear thickening silica dispersions. Ultrasonics Sonochemistry 17 (2010) 947–952.
[231] S. Lee, E. Wetzel, N. Wagner, J. Mater. Sci. 38 (2003) 2825.
[232] R. Egres Jr., M. Decker, C. Halbach, S. Lee, J. Kirkwood, K. Kirkwood, N. Wagner, Army Sci. Conf. (2004).
[233] S. Lee, E. Wetzel, R. Egres Jr., N. Wagner, Army Sci. Conf. (2002).
[234] C. Sauter, M.A. Emin, H.P. Schuchmann, S. Tavman, Ultrason. Sonochem. 15 (2008) 517.
[235] M. Toan, N. Tsing, T. Tsung, H. Chang, J. Vac. Sci. Technol., B 27 (2009) 1586.
[236] M.H. Choi, I.J. Chung, D.J. Lee, Chem. Mater. 12 (2000) 2977.
[237] I.G. Eskin, Ultrason. Sonochem. 8 (2001) 319.
[238] K. Suslick, Sci. Am. (1989).
[239] K. Suslick, Modem Synth. Methods 4 (1986) l.
[240] P. Boudjouk, J. Chem. Educ. 63 (1986) 427.
[241] K. Suslick, B. Edward, Flint Nature 330 (1987) 553.
[242] K. Suslick, VCH Publishers, Inc., 1988.
[243] L.A. Pe´rez-Maqueda, A. Duran, J.L. Pe´ rez-Rodrı´guez, Appl. Clay Sci. 28 (2005) 245.
[244] F. Franco, J.A. Cecila, L.A. Perez-Maqueda, J.L. Perez-Rodriguez, C.S. Gomes, Appl. Clay Sci. 35 (2007) 119.
[245] Holzinger M, Hirsch A, Bernier P, Duesberg GS, Burghard M. A new purification method for single-wall carbon nanotubes (SWNTs). Applied Physics A: Materials Science & Processing. 2000;70(5):599-602.
[246] Sumanasekera GU, Allen JL, Fang SL, Loper AL, Rao AM, Eklund PC. Electrochemical Oxidation of Single Wall Carbon Nanotube Bundles in Sulfuric Acid. The Journal of Physical Chemistry B. 1999;103(21):4292-4297.

[247] Rinzler AG, Liu J, Dai H, Nikolaev P, Huffman CB, Rodríguez-Macías FJ, et al. Large-scale purification of single-wall carbon nanotubes: process, product, and characterization. Applied Physics A: Materials Science & Processing. 1998;67(1):29-37.
[248] Wang Y, Iqbal Z, Malhotra SV. Functionalization of carbon nanotubes with amines and enzymes. Chemical Physics Letters. 2005;402(1–3):96-101.
[249] Kitamura H, Sekido M, Takeuchi H, Ohno M. The method for surface functionalization of single-walled carbon nanotubes with fuming nitric acid. Carbon. 2011;49(12):3851-3856.
[250] Mussi V, Biale C, Visentin S, Barbero N, Rocchia M, Valbusa U. Raman analysis and mapping for the determination of COOH groups on oxidized single walled carbon nanotubes. Carbon. 2010;48(12):3391-3398.
[251] Sayes CM, Liang F, Hudson JL, Mendez J, Guo W, Beach JM, et al. Functionalization density dependence of single-walled carbon nanotubes cytotoxicity in vitro. Toxicology Letters. 2006;161(2):135-142.
[252] Peng H, Alemany LB, Margrave JL, Khabashesku VN. Sidewall Carboxylic Acid Functionalization of Single-Walled Carbon Nanotubes. Journal of the American Chemical Society. 2003;125(49):15174-15182.
[253] Rosca ID, Watari F, Uo M, Akasaka T. Oxidation of multiwalled carbon nanotubes by nitric acid. Carbon. 2005;43(15):3124-3131.
[254] Yang Y, Xie X, Wu J, Yang Z, Wang X, Mai Y-W. Multiwalled Carbon Nanotubes Functionalized by Hyperbranched Poly(urea-urethane)s by a One-Pot Polycondensation. Macromolecular Rapid Communications. 2006;27(19):1695-1701.
[255] Shiren W, Zhiyong L, Tina L, Ben W, Chuck Z. Effective amino-functionalization of carbon nanotubes for reinforcing epoxy polymer composites. Nanotechnology. 2006;17(6):1551.
[256] Paiva MC, Zhou B, Fernando KAS, Lin Y, Kennedy JM, Sun YP. Mechanical and morphological characterization of polymer–carbon nanocomposites from functionalized carbon nanotubes. Carbon. 2004;42(14):2849-2854.
[257] Wang S. Functionalization of carbon nanotubes: characterization, modeling and composite applications. Florida State University, Department of Industrial and Manufacturing Engineering, 2006.
[258] Khare BN, Meyyappan M, Cassell AM, Nguyen CV, Han J. Functionalization of Carbon Nanotubes Using Atomic Hydrogen from a Glow Discharge. Nano Letters. 2001;2(1):73-77.
[259] Egres Jr. RG, Lee YS, Kirkwood JE, Kirkwood KM, Wetzel ED, Wagner NJ. "Liquid armor": protective fabrics utilizing shear thickening fluids. IFAI 4th International Conference on Safety and Protective Fabrics, October 26-27, 2004, Pittsburgh, PA.
[260] Wetzel ED, Wagner NJ. Stab Resistance of Shear thickening Fluid (STF)-Kevlar Composite for Body Armor Applications. 24th Army Science Conference, December 2, 2004, Orlando, FL.
[261] Decker MJ, Halbach CJ, Nam CH, Wagner NJ, Wetzel ED. Stab resistance of shear thickening fluid (STF)-treated fabrics. Composite Science and Technology 2007;67: 565-578.
[262] J. T. Tzeng, E. A. Schmidt. Advanced materials bring electromagnetic gun technology one step closer to the battlefield. Weapons and Materials Research Directorate, US Army Research Laboratory Aberdeen Proving Ground, MD. The AMPTIAC Quarterly, Volume 8, Number 4, 79-84.
[263] J.T. Tzeng, A Summary of materials and mechanics research for electromagnetic gun pulsed power applications, ARL-TR-2948, April 2003.
[264] P. Putman. Milestones in Cannon Launch to Space. LIFEBOAT FOUNDATION EM Launch Competitors' Guide, Chapter 1, March 2006.
[265] I.R. McNab, Early Electric Gun Research, IEEE Trans. Mag., vol. 35, no. 1, pp. 250–261, 1999.
[266] A. Egeland, Birkeland's Electromagnetic Gun: A Historical Review, IEEE Trans. Plasma Sci., vol. 17, no. 2, pp.73–82, 1989.
[267] G.V. Bull and C.H. Murphy, Paris Kanonen - the Paris Guns (Wilhelmgeschütze) and Project HARP, Verlag E.S. Mittler & Sohn, Herford, Germany,1988.
[268] E.F. Northrup, Zero to Eighty, Princeton, N.J: Scientific Publishing Co., 1937.
[269] K. Thom and J. Norwood, Theory of an Electromagnetic Mass Accelerator for Achieving Hypervelocities. NASA, Tech. Note D-886, 1961.
[270] H. Kolm and P. Mongeau, An alternative launching medium, IEEE Spectrum, vol. 19, no. 4, pp. 30–37, 1982.
[271] F. Winterberg, Magnetic Acceleration of a superconducting solenoid to hypervelocities, Plasma Physics, vol. 8, pp. 541–553, 1966.
[272] H.D. Fair, Electromagnetic Launch: A Review of the U.S. national Program, IEEE Trans. Mag., vol. 33, no. 1, pp.11–16, 1997.
[273] W. Ying, R. Marshall, and C. Shukang, Physics of Electric Launch, Science Press, Beijing, China, 2004.

[274] R. Marshall and W. Ying, Railguns: Their Science and Technology, China Machine Press, Beijing, China, 2004.
[275] R.A. Marshall, Railgunnery: Where Have We Been? Where Are We Going? IEEE Trans. Mag., vol. 37, no. 1, pp.440–444, 2001.
[276] P. Mongeau, Inductively commutated coilguns, IEEE Trans. Mag., vol. 27, no. 1, pp. 568–572, 1991.
[277] S.K. Ingram, Theoretical Analysis of a Collapsing Field Accelerator, IEEE Trans. Mag., vol. 29, no. 1, pp.675–679, 1993.
[278] M. Cowan, E.C. Cnarre, B.W. Duggin, R.J. Kaye, and T.J. Tucker, The Reconnection Gun, IEEE Trans. Mag., vol. Mag-22, no. 6, pp. 1429-1434, 1986.
[279] M. Cowan, M.M. Widner, E.C. Cnare, B.W. Duggin, R.J. Kaye, and J.R. Freeman, Exploratory Development of the Reconnection Launcher 1986–1990, IEEE Trans. Mag., vol. 27, no. 1, pp. 563–567, 1991.
[280] S.-S. Gao and C.-W. Sun, The Test and Analysis of a 3-Stage Reconnection Coilgun, IEEE Trans. Mag., vol. 35, no. 1, pp. 142–147, 1999.
[281] R.F. Post and D.D. Ryutov, The Inductrack: A Simpler Approach to Magnetic Levitation, IEEE Trans. Appl. Superconductivity, vol. 10, no.1, pp. 901–904, 2000.
[282] R.F. Post, Maglev: A New Approach, Scientific American, vol. 282, pp. 82–87, 2000.
[283] K. Halbach, Application of Permanent Magnets in Accelerators and Electron Storage Rings, Journal of Applied Physics, vol. 57, pp. 3605–3608, 1985.
[284] M.R. Palmer, R.X. Lenard, A Revolution in Access to Space Through Spinoffs of SDI Technology, IEEE Trans. Mag., vol. 27, no. 1, pp. 11–20, 1991.
[286] F. Kuznik, Battle of the Big Shots,Air and Space, pp. 55–61, Aug./Sept. 1993.
[287] J.A. Morgan and E.Y. Robinson, A Long Shot for Satellite Launch, Aerospace America, vol. 36, no. 4, pp. 32–39, 1998.
[288] Haghmaram R and Shoulaie A. Study of Traveling wave Tubular Linear Induction Motors. International Conference on power System Technology, POWERCON 2004, November 21-24, 2004, Singapore.
[289] Lell P, Igenbergs E, Kuczera H. An electromagnetic accelerator. Journal of Physiscs E 1983;16: 325-330.
[290] McNab IR. Launch to space with an electromagnetic railgun. IEEE Transaction on magnetic, 2003;39: 295-304.
[291] Schmidt E and Bundy M. Ballistic Launch to Space. International symposium on Ballistics, November 14-18, 2005, Vancouver BC, Canada.
[292] Shope S, Alexander J, Gutierrez W, Kaye R, Kniskern M, Long F, Smith D, Turman B, Marder B, Hodapp Jr. A, and Waverik R. Results of a study for a long range coilgun naval bombardment system. Sandia National Laboratories, Albuquerque, NM 87185.
[293] Purcell EM, editor Mc Graw-Hill book Company – Electricity and Magnetism. U.S.A.; 1965.
[294] Micheli D, Apollo C, Pastore R, and Marchetti M. Ballistic characterization of nanocomposite materials by means of “Coil Gun” electromagnetic accelerator. XIX International Conference on Electrical Machines - ICEM 2010, Rome, Italy.
[295] Micheli D, Pastore R, Apollo C, and Marchetti M.Coil Gun electromagnetic accelerator for aerospace material anti-ballistic application. ISSN: 1826-4697, (2011).